Analysis and Modeling of the Hybrid Vessel's Electrical Power System

A study on Power Quality, Short-Circuit Currents and Protection & Coordination

Matthijs Mosselaar

TU Delft

Alewijnse WeConnect.

Analysis and Modeling of the Hybrid Vessel's Electrical Power System

A study on Power Quality, Short-Circuit Currents and Protection & Coordination

by

Matthijs Mosselaar

to obtain the degree of Master of Science
at the Delft University of Technology,
to be defended publicly on Wednesday August 30, 2023 at 10:00 AM.

Student number:	4584600	
Project duration:	November 1, 2022 – August 30, 2023	
Thesis committee:	Prof.dr.ir. Marjan Popov,	TU Delft, supervisor
	Dr.ir. Aleksandra Lekić,	TU Delft, daily supervisor
	Dr.ir. Gautham Ram Chandra Mouli,	TU Delft
	Ir. Zoran Malbasic	Alewijnse, company supervisor

This thesis is confidential and cannot be made public until September 1, 2024.

TU Delft

Alewijnse WeConnect.

Preface

This thesis has been a collaboration between TU Delft and Alewijnse and marks the completion of my studies in Electrical Power Engineering at TU Delft. I want to thank Alewijnse for giving me the internship and thesis opportunity and I want to thank ir. Zoran Malbasic in particular for his invaluable expertise and support. From TU Delft I want to thank Prof.dr.ir. Marjan Popov and Dr.ir. Aleksandra Lekić for their excellent support and guidance during this whole year. Finally, I want to thank my parents for their unlimited support and confidence. I look forward to whatever challenges lie ahead.

Matthijs Mosselaar
Delft, August 2023

Abstract

Zero emission fuels and reducing emissions are important topics in all transport sectors and hybrid systems play a key role in the transition towards full decarbonization. This thesis studies the components that are found in hybrid maritime electrical power systems and their influence on power quality, short-circuit currents and protection & coordination. In order to help system integrators such as Alewijnse in the design of these hybrid systems, two typical models of actual vessels are created in simulation software ETAP. Both systems are low-voltage, high-power systems, based on either an AC or DC busbar.

Rules and standards related to power quality and short-circuit currents are studied as well as practical protection strategies. For the AC model, various studies have been successfully simulated including a load flow study, transient stability study including peak shaving and virtual generator simulations for the battery, a protection & coordination study and a harmonic study. Some challenges with ETAP regarding DC grid simulations are discussed, but is also demonstrated how to use the formulas and standard approximation function from the IEC 61660 to calculate short-circuit currents and I^2t values and how to use these results in the protection & coordination study.

Keywords: vessel, hybrid, simulation, power quality, short-circuit current, protection, ETAP

Contents

List of Figures

List of Tables

Nomenclature

Abbreviation	Definition
AC	Alternating Current
AFE	Active Front End
BMS	Battery Management System
CCT	Critical Clearing Time
CSI	Current-Source Inverter
DC	Direct Current
DNV	Det Norske Veritas
DP	Dynamic Positioning
EN	European Norm
EMC	Electromagnetic Compatibility
EMS	Energy Management System
ETAP	Electrical Transient Analyzer Program
HVAC	Heating, Ventilation and Air Conditioning
IEC	International Electrotechnical Commission
IEEE	Institute of Electrical and Electronics Engineers
IGBT	Insulated-Gate Bipolar Transistor
MCCB	Moulded-Case Circuit Breaker
PE	Protected Earth
PS	Port side
PMS	Power Management System
PTI	Power Take In
PTO	Power Take Off
PWM	Pulse-Width Modulation
RMS	Root Mean Square
SB	Starboard side
SC	Short-Circuit
SCR	Silicon Controlled Rectifier
TCC	Time Current Curve
THD	Total Harmonic Distortion
UDM	User-Defined Model
VFD	Variable Frequency Drive
VSI	Voltage-Source Inverter

1 Introduction

The Getting to Zero Coalition is an alliance of over 200 organizations within the maritime, energy, infrastructure and finance sectors. Their goal is to get commercially viable deep sea zero emission vessels powered by zero emission fuels into operation by 2030 for a path towards full decarbonization by 2050. [1] Hybrid ships and vessels play a key role in this transition and it is important to fully understand these hybrid power systems.

1.1. Electrical power systems in vessels

Traditionally, a maritime power system is built up from a main busbar to which the main generators and the heavy loads are connected. The voltage level of the systems is usually 690 or 400V and the main busbar may be split in two busbars (port side and starboard side) that can be connected. The frequency is either 50 or 60Hz. From the main busbar, the power can be further distributed on a lower voltage level of 400 or 230V. Often, there is also an emergency generator that can be connected to the main busbar, either directly or through another busbar. The Power Management System (PMS) on a vessel controls the power balance and maintains the voltage and frequency. The Energy Management System (EMS) on a vessel analyzes the energy usage on a vessel and tries to maximize the energy generated from the minimum amount of fuel. It also tries to maximize the useful work obtained from the minimum amount of generated energy.

The amount of power that is installed on a vessel depends on the anticipated load profile. Some vessel types such as dredging vessels may require over 30 MW of power to be installed on the vessel. This is because dredging operations require a lot of power, but also because of redundancy requirements. An overview of different vessel types and their installed power is given in table 1.1. Classifiers like DNV, Bureau Veritas or Lloyd's Register determine rules and regulations for every aspect of a vessel. Together with relevant IEC and IEEE norms, their rules and regulations form the basic constraints of any design that is part of a vessel.

Table 1.1: An overview of installed power in different vessel types

Vessel type	**Vessel name**	**Total power installed (kW)**
Cable laying vessel	Ndurance	7500
Construction support vessel	Boka Northern Ocean	16000
Cutter suction dredger	Artemis	24662
Flexible fallpipe vessel	Nordnes	17363
Heavy transport vessel	Boka Vanguard	28500
Offshore installation vessel	Aeolus	19688
Side stone dumping vessel	HAM 602	4129
Split hopper barge	Jan Blanken	3239
Suction dredger	Sliedrecht 27	7207
Superyacht	Infinity	2871
Trailing suction hopper dredger	Vox Máxima	31309
Water injection dredger	Sagar Manthan	2106

The electrical components that can be found in a typical maritime electrical power system are shown in figure 1.1a or 1.1b. Figure 1.1a shows an electrical power system that is based on an AC bus and figure 1.1b shows an electrical power system that is based on a DC bus. At the top of figure 1.1a there are the Diesel Engine Synchronous Generators, acting as the main power source of the system. They are connected with a cable to a busbar or rail where all loads are connected as well. To protect the system in case of a fault, all components run through Circuit Breakers that can isolate components by opening and creating a physical separation.

On the bottom of the busbar to the left there is a bidirectional AC/DC converter connecting a battery through a fuse and another (DC) cable. A fuse is also a protective element, but if it is used to isolate a fault, it has to be replaced. More information about protective elements can be found in sections 3.2 and 3.4. Next to the battery, there is an induction motor connected through a Variable Frequency Drive, and to the right there is a transformer (T) to step down the voltage to create another busbar that more loads can be connected to.

The components of the DC system are very similar to the components of the AC system, with the main difference being that there are more converters involved. The extra converters are typically unidirectional as power can only go from a generator to the grid and not back for example. The component in figure 1.1b on the bottom left between the fuse and the cable is a DC/DC converter. The converter connecting the motor is a motor inverter, the combination of an inverter and a Variable Frequency Drive.

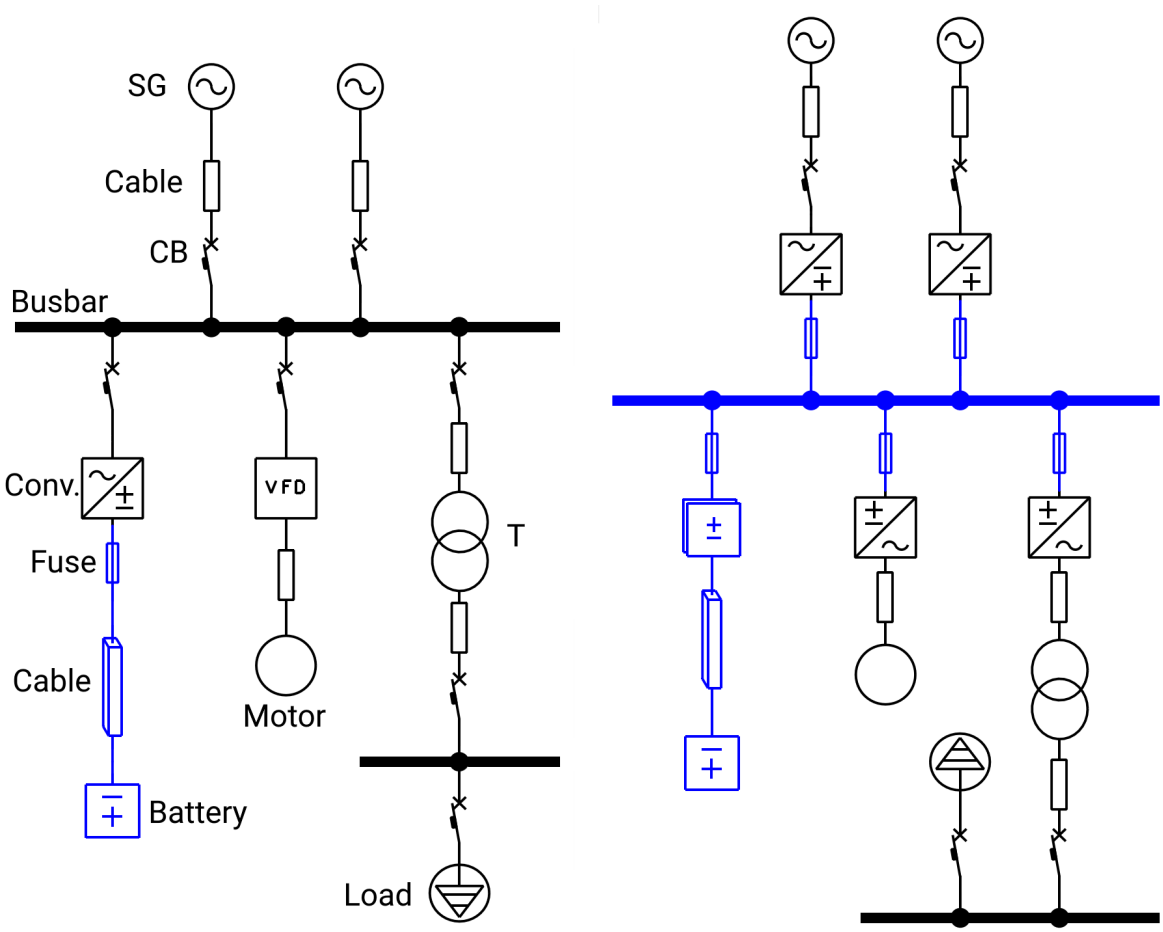

(a) Typical AC single line diagram

(b) Typical DC single line diagram

Figure 1.1: Two typical circuits

A component not directly shown in figure 1.1 is the filter that is required when using converters. The effects of all these components on power quality and short-circuit currents will be discussed in more detail in the following chapters.

1.2. Hybrid systems in vessels

Conventionally, the vast majority of the vessels listed in table 1.1 are diesel-powered. However, in the past decade, the hybrid propulsion concept has begun to grow in popularity. When a battery is added to the power system of the vessel, it can be used to save fuel by running the generators at a more efficient setpoint. When the overall power consumption is low, the battery can be charged and when there is a peak in demand, the battery can be discharged. This is called *peak shaving*. If the size of the battery is big enough, it can also be used as the only source of power, acting like a virtual generator. In operations such as Dynamic Positioning where the position and heading of the vessel should be maintained, it is critical to maintain power in case of an unexpected shutdown of the main generator. Traditionally, this is done by running a second generator, but a battery acting as a *spinning reserve* can also be used. These and various other applications of a battery are shown in figure 1.2.

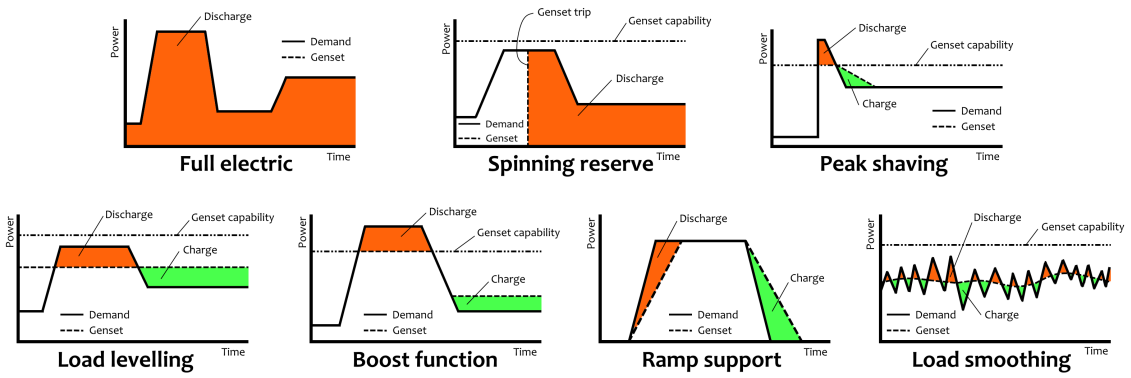

Figure 1.2: Different battery applications

Saving fuel is certainly not the only advantage of hybrid systems in vessels, mainly as the return on investment time will strong depend on the fuel price. If the fuel price is too low, it is not economically viable to install a battery at all. A big advantage however, independent from the fuel price, is a reduction in maintenance cost over the lifetime of a generator. Reference [2] shows a relation between the loading of a generator and the minimum time between overhaul, showing that an average loading between 50% and 80% results in the highest minimum time between overhaul. Since the overhaul cost is 50% of the investment cost of the generator, this can result in a significant cost saving as well.

Hybrid systems are not only interesting for newly built vessels, as a battery can be added to older vessels as well. This is typically done during a *refit*, which happens halfway through the vessel's expected lifetime. A refit can include repairing, fixing, restoring, renewing, mending, and renovating the vessel, depending on its needs. As long as there is space on the vessel to fit the battery and its converter, it should be possible to convert a regular (diesel) vessel to a hybrid vessel. When the vessel has an AC main busbar, the battery can be connected through a bidirectional inverter. When the vessel has a DC main busbar, the battery can be connected either directly or through a DC/DC converter, just like other DC components.

1.3. Power Management System (PMS)

The Power Management System (PMS) on a vessel controls the power balance and maintains the voltage and frequency. To do this, the PMS monitors all generators and engines that are connected. It manages the power build up and deloading of generators, the load sharing between generators, and it has the ability to connect or disconnect generators. When connecting or disconnecting a generator, the PMS manages synchronization as well as black out start up. The PMS also has the ability to switch off non-critical loads in case of an overload.

Traditionally, multiple operating modes are defined in the PMS. Two typical modes are *Auto mode* and *Dynamic Positioning (DP)*. In Auto mode, generators are automatically connected and disconnected depending on the requested power and priority. The bustie splitting the main busbar in port side and

starboard side (if applicable) may be open or closed. This will usually depend on the potential short-circuit current. In case of a failure on a generator, the next generator in the priority list will be connected. In DP mode, it is mission critical that the position of the vessel is maintained. This means that the bow thrusters must be powered at all times. In order to provide redundancy, the bustie is opened such that a fault on one side will not cause the entire system to shut down. Additional generators are connected on each side to prevent a blackout in case of a generator fault.

When a battery is added, the PMS needs to be updated, as well as the EMS. The PMS will need to communicate with the EMS that will need to communicate with the Battery Management System (BMS), in order to optimize battery usage and minimize the payback period. In auto mode, the overall power consumption is generally not very high and it will be important to run the generators as efficiently as possible, or not at all. The generator is most efficient on higher loading percentages as is also shown in figure 1.3. The usage of the generator can be increased by charging the battery. When the battery is full, the generator can be shut down and the battery is used to power the system until it is almost empty again. This is also called *deep cycling*. If the power demand is high, the battery can be used for peak shaving or load levelling to keep the generator in its most fuel efficient region.

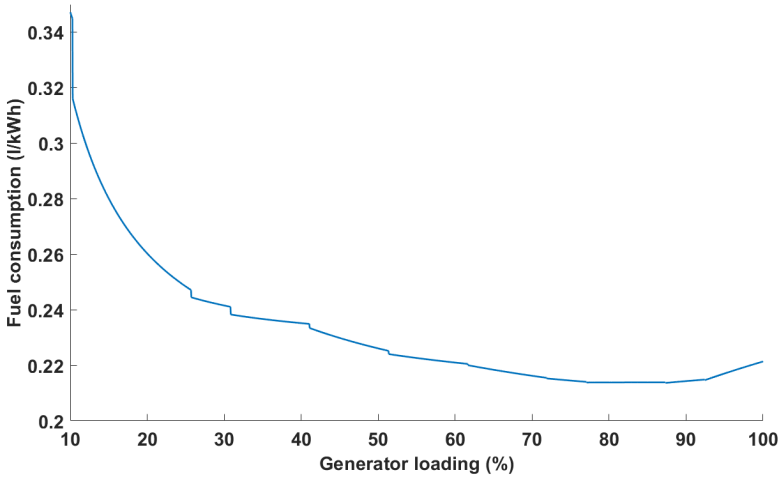

Figure 1.3: Generator fuel efficiency

Because of the redundancy requirements for DP, it is not possible to turn off all generators and use the battery as the only source. It is however possible to use one generator and have the battery act as a virtual generator that will kick in immediately if the generator shuts down unexpectedly. By doing this, there is no need to run a second generator when the overall power demand is low, which increases the efficiency of the main generator. The battery can only be used as a virtual generator if it is big enough and charged enough to provide the power required by the system for a certain amount of time. Usually this is for 15-20 minutes.

1.4. Objective and scope

This thesis will focus on creating and simulating two typical versions of a hybrid power system model in ETAP simulation software. The first model uses an AC main busbar and the main objective is to analyze the energy flow and the influence of electrical components on the power quality of the system. Furthermore, short-circuit situations and selectivity are studied, with a particular interest of the contribution of the battery and its converter. The system is a low-voltage, high-power microgrid including a lithium-ion battery.
The second model uses a DC main busbar and the main objective here is to study short-circuit situations and selectivity. This system is also a low-voltage, high-power system including a lithium-ion battery and a connection to an AC distribution busbar.

1.5. Related research

For the first model, related research includes reference [3], [4] and [5] discussing power quality in AC and DC microgrid buildings and power quality in the iron and steel industry. For the maritime industry, reference [6] and [7] discuss about the power quality of maritime microgrids, but none of these references include a battery in their model.

Reference [8] and [9] focus on short-circuit protection issues and the calculation of short-circuit currents in DC systems, but on the medium-voltage level. Reference [10] talks about selectivity in offshore and marine DC distribution systems and uses fuses to achieve selectivity. This is however an integrated system and it is interesting to see if this method can work using components from different manufactures. This system also doesn't include a battery. Other ways to achieve selectivity are by using semi-conductor DC breakers, but the price of these breakers is often disregarded. Reference [11] suggests that since all components connected to the DC busbar use a controllable switching device, selectivity can be achieved through a combination of fuses and the controlled turn-off of these switching devices.

1.6. Research questions

Next to the objective of creating and simulating two typical hybrid vessels, the following research questions are to be answered:

- What are the rules and standards related to power quality, harmonics and short-circuit calculations in hybrid AC and DC grids?
- What is the theoretical harmonic influence of various electrical components?
- What is the theoretical short-circuit contribution of various electrical components?
- What is the best approach for achieving selectivity in hybrid AC and DC grids?

These questions will form the theoretical basis that will allow for a successful design and analysis of the hybrid AC and DC electrical power systems.

1.7. Alewijnse Company Netherlands

Alewijnse is a systems integrator from the Netherlands with over 130 years of experience in Maritime and Industry. Their Maritime sector can be divided in three segments: Yachting, Dredging, offshore & transport and Naval & governmental. As a systems integrator, Alewijnse creates many solutions for automation, drive systems, navigation & communication, power distribution, Audio/Video & IT and more. Alewijnse also has offices in Romania, France and Vietnam and also collaborates with TU Delft on research topics like this thesis.

1.8. Outline

This thesis starts with an overview on power quality in chapter 2 and short-circuit currents and selectivity in chapter 3. These chapters cover the theoretical background required to get a good fundamental understanding of the vessel's electrical power system and to answer the research questions. Chapter 4 covers the analysis and modeling of the hybrid electrical power system based on an AC bus and chapter 5 covers the analysis and modeling of the hybrid electrical power system based on a DC bus. Finally in chapter 6 the research questions are answered and limitations and recommendations are discussed.

2

Power Quality

The term power quality refers to a wide variety of electromagnetic phenomena that characterize the voltage and current at a given time and at a given location on the power system. [12] The IEEE 1159 describes the recommended practice for monitoring electric power quality and will be used investigate the power quality of power grids. The standard uses the electromagnetic compatibility approach to describe power quality phenomena which has been accepted by the international community in in International Electrotechnical Commission (IEC) standards. In the IEC 61000-2-5:2017, the IEC classifies electromagnetic phenomena into several groups. Some examples of these electromagnetic phenomena are shown in figure 2.1.

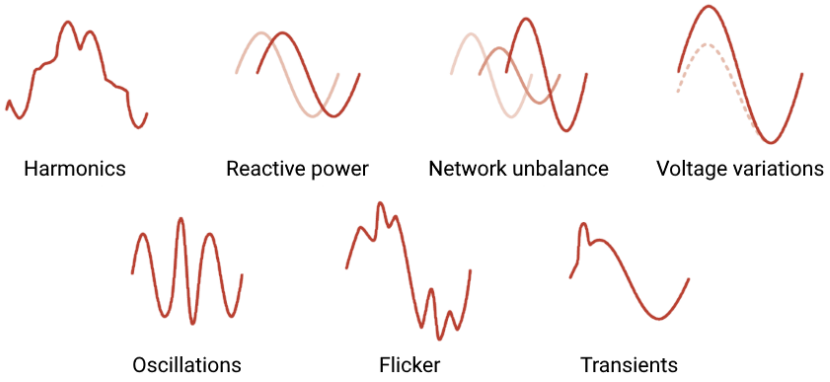

Figure 2.1: Power quality issues

Other norms that are related to power quality are the IEEE 519, IEC 60533:2015 and the EN 50160 standards. The IEEE 519 is the IEEE Standard for Harmonic Control in Electric Power Systems, the IEC 60533:2015 is the standard for electromagnetic compatibility (EMC) in ships with a metallic hull and the EN 50160 talks about voltage disturbances and voltage characteristics in public distribution systems. Harmonics are the main focus regarding power quality and will be discussed in more detail in section 2.1. Voltage quality is briefly discussed in section 2.2.

2.1. Harmonics

The Fourier theorem states that almost any periodic function can be represented by a sum of sines and cosines. Each wave in this sum is and integer multiple of the original function's fundamental frequency, and each sum can have a different amplitude and phase. For power systems in Europe, this fundamental frequency is 50Hz, and a periodic voltage waveform can be mathematically expressed as:

$$V(t) = V_0 + \sum_{h=1}^{N} V_h sin(h2\pi f_0 t + \theta_h) \tag{2.1}$$

Where V_0 is the DC offset, h the harmonic integer, V_h the amplitude, f_0 the (50Hz) fundamental frequency and θ_h the phase.

One indication of how distorted a waveform is, is the Total Harmonic Distortion (THD). The THD is the ratio of the RMS value of the combined harmonics (the non-fundamental frequencies) and the RMS value of the fundamental waveform. This value is usually a percentage and can be expressed as:

$$THD = \frac{\sqrt{\sum_{h=2}^{N} (V_h)^2}}{V_1} \tag{2.2}$$

For three-phase power systems, harmonic orders can be divided into positive, negative and zero sequence components.

Positive sequence components consist of three phasors that are equal in magnitude, are displaced by 120° in phase and have the same phase sequence as the original phasors (ABC). This is the case for the 1st, 4th, 7th, 10th, etc. harmonic.

Negative sequence components consist of three phasors that are equal in magnitude, are displaced by 120° in phase and have the opposite phase sequence as the original phasors (ACB). This is the case for the 2nd, 5th, 8th, 11th, etc. harmonic. Because of the opposite phase sequence, a negative sequence harmonic rotates in the opposite direction from the fundamental in an induction motor. This reverse rotation can cause a reduced forward torque of the motor.

Zero sequence components consist of three phasors that are equal in magnitude and have zero phase displacement from each other. This is the case for the 3rd, 6th, 9th, 12th, etc. harmonic. [13]
Because vessels typically have an IT earthing system compared to a more typical TN-S earthing system, in theory there should be no zero sequence harmonics. In practice however, all systems will have a small amount of zero sequence harmonics because of common-mode coupling between phases due to capacitive and inductive coupling. Earthing systems will be covered in more detail in section 2.3.

There are also harmonics that are not integer multiples of the fundamental frequency. These are called inter-harmonics, or sub-harmonics when their frequency is lower than the fundamental frequency. [14] Interharmonics generally appear in electrical networks with non-linear loads such as static frequency converters, cycloconverters, arc furnaces and adjustable speed drives. Interharmonics cause additional losses of active power, accelerate the aging of insulation and decrease the reliability of the supply of electrical power. [15]

2.1.1. Harmonic standards

The IEEE 519 [16] is the IEEE Standard for Harmonic Control in Electric Power Systems. It describes that, harmonic measurements shall be made at least up to the 50th order. The measurement windows used by digital instruments employing Discrete Fourier Transform techniques shall be approximately 200 ms, which means 10 cycles in a 50 Hz system. With this window width, spectral components have to be available every 5 Hz. A harmonic component magnitude is considered to be the combination of the center frequency (50, 100, 150, .. Hz) and the two adjacent 5 Hz values. These three values are combined into a single RMS value.
Very short time harmonic measurements are assessed over a three-second interval based on an aggregation of 15 consecutive 10 cycle windows, according to the following formula:

$$F_{n,vs} = \sqrt{\frac{1}{15} \sum_{i=1}^{15} F_{n,i}^2} \tag{2.3}$$

Short time harmonic measurements are assessed over a 10-minute interval based on an aggregation of 200 consecutive very short time values, according to the following formula:

$$F_{n,sh} = \sqrt{\frac{1}{200} \sum_{i=1}^{200} F_{(n,vs),i}^2} \tag{2.4}$$

In both formula 2.3 and 2.4, *F* represents an RMS voltage or current, *n* represents the harmonic order and *i* is a counter.

The IEEE 519 has defined harmonic limits for both voltages and currents as some level of voltage distortion is generally acceptable. The limits given by the IEEE 519 apply only at the Point of Common Coupling. The Point of Common Coupling is defined as the point on a public power supply system, electrically nearest to a particular load, at which other loads are, or could be, connected. The PCC is a point located upstream of the considered installation and is visualized in figure 2.2. Harmonic voltages and currents at other locations could be found to be significantly that the limits at the PCC due to lack of diversity, cancellation, and other phenomena that tend to reduce the combined effects of multiple harmonic sources. [16]

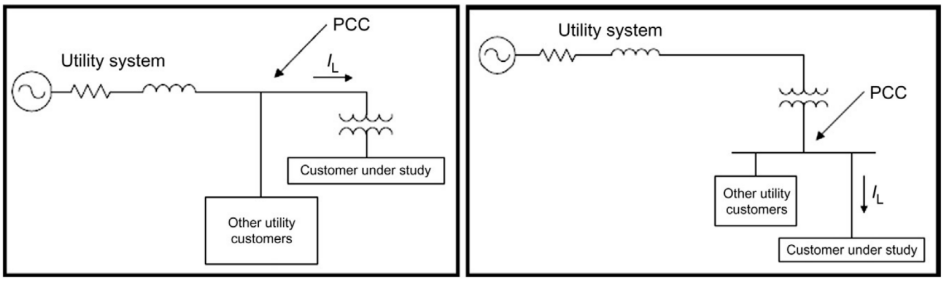

Figure 2.2: Point of Common Coupling (PCC) [17]

Voltage distortion limits are given in table 2.1 and line-to-neutral voltage harmonics shall be less than 1.5 times the values for very short time (equation 2.3) measurements and less than the given values for short time (equation 2.4) measurements. Current distortion limits are also given by the IEEE 519, but if the installation has a distributed energy resource or inverter-based resource that generates more than 10% of the annual average load demand, current limits from the IEEE 1547 standard apply. Note that for voltage distortion limits in vessels, only the first requirement for systems less than 1kV is of interest.

Table 2.1: Voltage distortion limits according to the IEEE 519

Bus voltage V at PCC	Individual harmonic (%) h≤50	Total harmonic distortion THD (%)
$V \leq 1.0\ kV$	5.0	8.0
$1\ kV < V \leq 69\ kV$	3.0	5.0
$69\ kV < V \leq 161\ kV$	1.5	2.5
$161\ kV < V$	1.0	1.5

Classifiers each have their own requirements for voltage distortion limits:

- DNV follows the IEE 519 exactly and states that no single harmonic should be greater than 5% and the THD may not exceed 8%
- Lloyds states that the maximum THD is 8% of the fundamental for all frequencies up to 50 times the supply frequency and no voltage at a frequency above 25 times the supply frequency is to exceed 1.5%
- Bureau Veritas states that the single harmonic distortion may not exceed 5% of the nominal voltage up to the 15^{th} harmonic of the nominal frequency, decreasing to 1% at the 100^{th} harmonic and the THD may not exceed 8%

2.1.2. Harmonics of Synchronous Generators

The IEC 60034 [18] describes the standard for rotating electrical machines and also sets rules for the harmonic content of the generated line-to-line open-circuit voltage. It states that all generators above 500 kVA must have a Total Harmonic Distortion of less than 5%. Reference [19] describes the effects and causes of harmonics in rotating machines. Harmonics can increase copper and iron losses resulting in heating and can also generate pulsating torques. Harmonics are mainly caused by not-perfectly sinusoidally distributed winding slots, resulting in a distorted magnetomotive force (mmf).

The influence of the geometry of the machine is also discussed in reference [20] and [21]. Measurements of the Total Harmonic Distortion performed by [20] are shown in figure 2.3. Machines 1-4 are four pole 72 stator slot generators with ratings from 5 to 10 MVA. Machines 5-8 are four pole 60 stator slot generators with ratings from 12 to 20 MVA. THD values range between 0.62% and 1.57%.

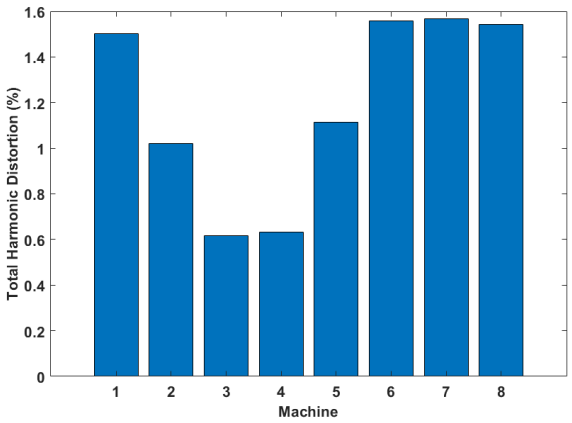

Figure 2.3: THD of different Synchronous generators [20]

The winding pitch on a generator also has a big influence on the harmonics. Specifically 2/3rd and 5/6th pitch wounded generators are optimized to reduce certain harmonics. A 2/3rd pitch wounded generator is optimized to reduce the triplen harmonics and have a lower impedance for the 3^{rd} harmonic and for unbalanced loading. This reduction in the 3^{rd} harmonic comes usually at the cost of the 5^{th} and 7^{th} harmonic. A 5/6th pitch wound generator is optimized to have a lower impedance for the 5^{th} and 7^{th} harmonic and is more suited in situations where the starpoint is not connected to a solid ground. [22]

2.1.3. Harmonics of Variable Frequency Drives and Inverters

A variable-frequency controller is part of a variable-frequency drive (VFD) and is used to control an AC (induction) motor. A variable frequency controller consists of three parts: a rectifier, a DC link and an inverter. A cycloconverter can vary the frequency without using a DC link.

The two main frequency controllers that use a DC link are either a Voltage-source Inverter (VSI) or a Current-source Inverter (CSI). Out of these two, the Voltage-source Inverter is most popular nowadays. The VSI can furthermore use either a diode front end or an active front end and both require a different solution for harmonic compensation. A frequency controller based on a VSI and using a diode front end is displayed in figure 2.5. The difference between the diode- and active front end is that the active front end uses IGBTs instead of diodes. Using IGBTs reduces the harmonics when used in combination with an LCL filter and allows for four-quadrant operation. This means that it is able to handle regenerative power. The structure and implementation of the LCL filter is shown in figure 2.4. The capacitors are connected in a delta configuration and the filter also includes capacitors connected against ground potential. [23]

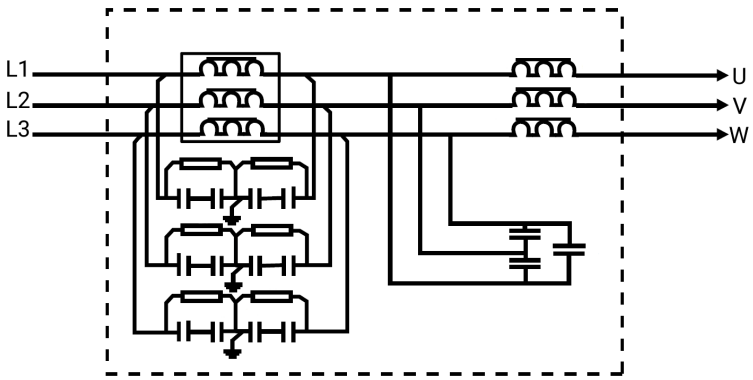

Figure 2.4: LCL filter implementation according to a drive manufacturer [23]

The rectifier in figure 2.5 is called a 6-pulse diode front-end rectifier. To improve the harmonics generated by this rectifier, multiple 6-pulse rectifiers can be combined using phase-shift transformers such that harmonics from one set are cancelled by the harmonics from the other set. This will not completely cancel out all harmonics, but will give a significant improvement to the THD. Figure 2.6 compares typical current waveforms of 6/12/18 pulse diode rectifiers and their harmonic spectrum. For the 6-pulse rectifier, the THD of the input current measured by reference [24] was 36%. For the 12-pulse rectifier it was 8.5% and 4.5% for the 18-pulse rectifier. In practice, due to non-ideal behaviour of the transformer, there will be slight angle phase errors causing the harmonics to not be perfectly cancelled.

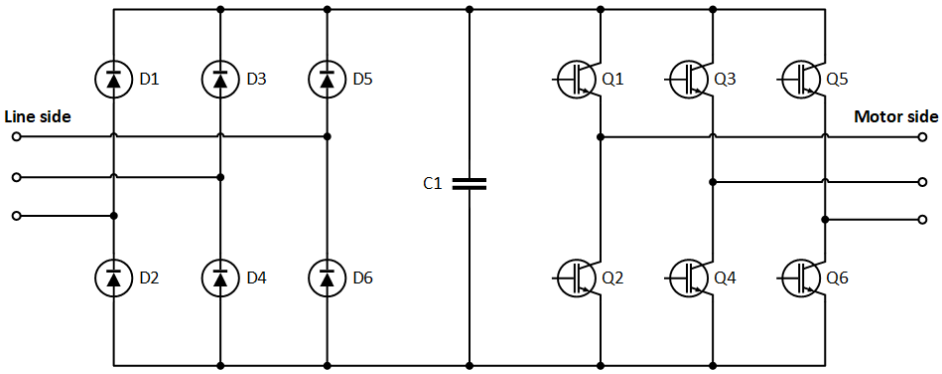

Figure 2.5: Frequency controller schematic

To further improve the harmonics of a diode front-end rectifier, usually only a line reactance or an LC filter is used.

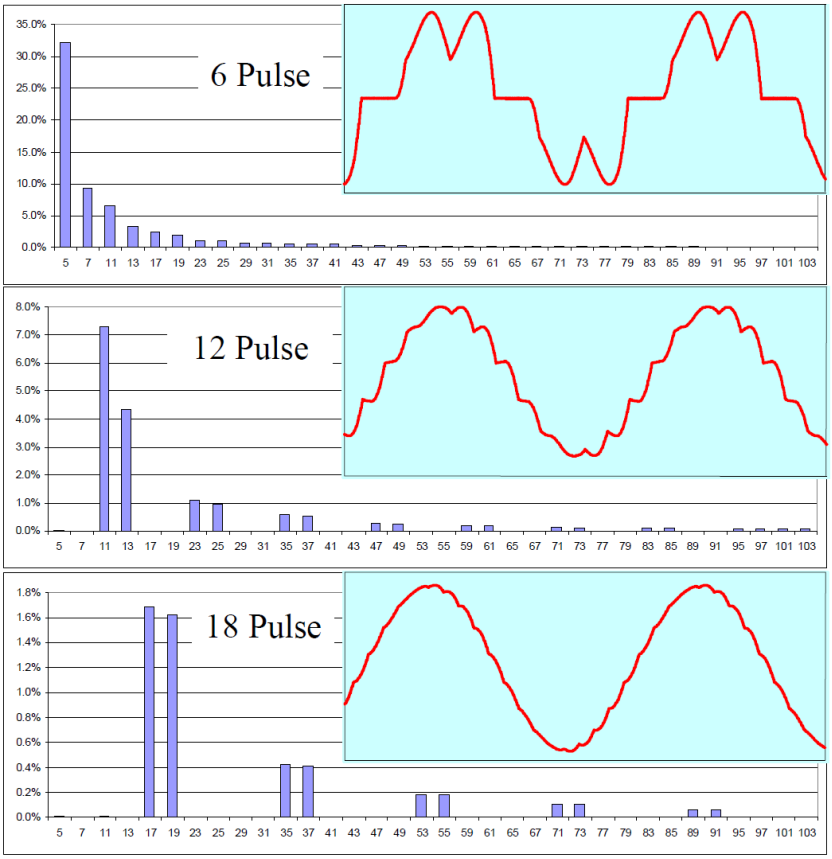

Figure 2.6: Typical current waveforms and harmonic spectra for 6/12/18 pulse diode rectifiers [24]

Diode rectifiers are normally used with Voltage Source Inverters, and thyristor-based rectifiers (also called Silicon Controlled Rectifier, SCR) are normally used with Current Source Inverers. The SCR provides an adjustable DC current for the CSI, which on its term converts the DC current to a three-phase AC PWM current. SCR rectifiers have to use gatedriver circuits which increase the risk of a fault in drive components. Another disadvantage is related to the input power factor which varies greatly with the firing angle which is a function of the load. [24]

Active Front End (AFE) VFDs use pretty much the same hardware on the rectifier side as on the inverter side. Both sides have active switches with anti-parallel diodes that allow a reverse current flow due to an inductive load. The anti-parallel diodes are not shown in figure 2.5. An AFE can eliminate certain harmonic orders through the pulse pattern that is provided to the IGBTs. Two main types of control are sinusoidal Pulse Width Modulation and Space Vector Modulation.
As the switching frequency increases, lower harmonic orders are eliminated almost entirely. However, the harmonic distortion is still there, it is just shifted towards higher frequencies. [25] A 6-pulse AFE can reduce the THD to 5% or less, but will require an LCL filter to reduce the higher-order harmonics. [26]

An LCL filter as shown before is a third order low-pass filter consisting of two inductors and a capacitor that is either star or delta connected. The values of the individual filter components will depend on the switching frequency, the required ripple current on the converter side, the desired ripple current reduction and the resonant frequency. Reference [27] and [28] describe how the parameters of the LCL filter can be designed.

2.1.4. Filters & Harmonic reduction

The L, LC and LCL filters have already been mentioned as ways to reduce harmonics, but generally, filters can be divided into two categories: passive and active harmonic filters.
All previously mentioned filters are examples of a passive harmonic filters, but there are other passive filters as well such as the single-tuned, double-tuned and c-type filters. These are shown in figure 2.7

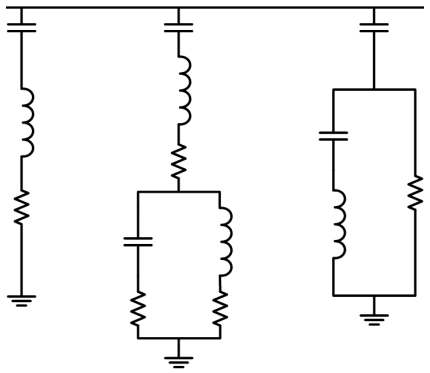

Figure 2.7: Left to right: single tuned, double tuned and damped c-type filters

The single- and double tuned filters are usually used to filter specific frequencies, while a damped filter, such as the c-type filter, is used to filter a wide range of frequencies. In applications where there is only a small harmonic producing load, it is often possible to use one single-tuned filter to eliminate problematic harmonic currents. It can be tuned near the 5^{th} harmonic for example. In large applications, multiple tuned filters and a damped filter is often used. In most cases, it is common to tune single-tuned filter banks to slightly below the frequency of the harmonic to be removed. This is usually because of the temperature sensitivity of the electrical components. [29]

Active harmonic filters work similar to the principle of a noise-cancelling headphone. Its goal is to actively improve the line current by injecting a compensation current. It uses a fast response digital signal processor that creates a harmonic spectrum using the Fast Fourier Transform. It then uses an IGBT based harmonics generator to generate a harmonic spectrum with opposite phase to cancel it out. The cost of an active filter is much higher compared to a passive one, but it can be more effective and can also improve the power factor and improve an unbalance in loading. The active harmonic filter is connected in parallel with the load that needs compensation.

2.1.5. Harmonic Distortion in vessels

When designing the electrical power system of a vessel, a THD calculation is performed to understand the THD levels on the vessel during different loading scenarios. The load balance of a vessel defines active power sources and loads based of several operation modes. For each of these operation modes, the harmonic spectrum is calculated and this calculation for several vessels that have been designed in the past is summarized in figure 2.8 and 2.9.

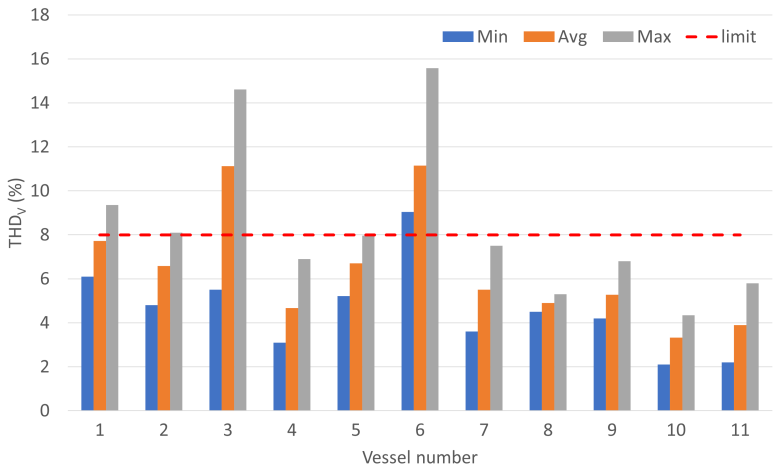

Figure 2.8: Voltage distortion calculation of several vessels

Figure 2.8 shows the voltage harmonic distortion for 11 different vessels. Based on the operating modes for these vessels, a minimum, average and maximum THD is specified. The class and IEEE limit of 8% is also shown in the graph and the maximum calculated THD of vessel 1, 2, 3 and 6 exceeds this limit. The THD of vessels 3 and 6 is particularly bad as the average is above the limit as well. Figure 2.9 shows the current distortion of the first six vessels, as the calculations for the other five vessels were not available.

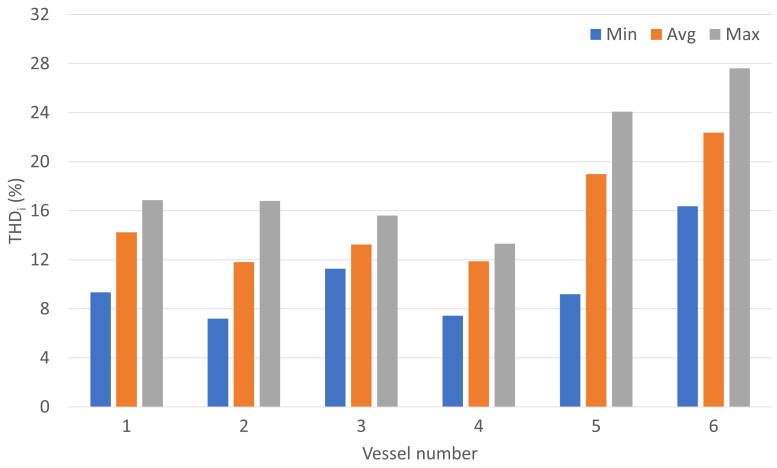

Figure 2.9: Current distortion calculation of several vessels

Big sources for harmonic distortion were found to be the battery energy storage system (if the vessel had one), the HVAC and the converters without an active front-end. These calculations are done for a worst-case scenario and the actual THD is likely to be lower. In the design of the main switchboard can be accounted for the space and connection required for an active harmonic filter, if it turns out to be necessary.

2.2. Voltage Quality

Voltage quality is concerned with the deviation of the voltage from the ideal. The ideal voltage is a single-frequency sine wave of constant frequency and magnitude. The EN 50160 describes the characteristics of the supply voltage. Examples of voltage problems are fluctuations, dips, interruptions and imbalance. Voltage fluctuations mean that the amplitude and frequency of the sine wave are not consistent over multiple periods. During a voltage dip, the amplitude of the sine wave is reduced by 10% or more for a period longer than 10ms. During a voltage interruption, the amplitude of the sine wave is reduced by more than 95% for a period longer than 10ms. Voltage imbalance means that here is a difference in the sine wave amplitude between the phases. Figure 2.10 shows a visual presentation of some of these definitions.

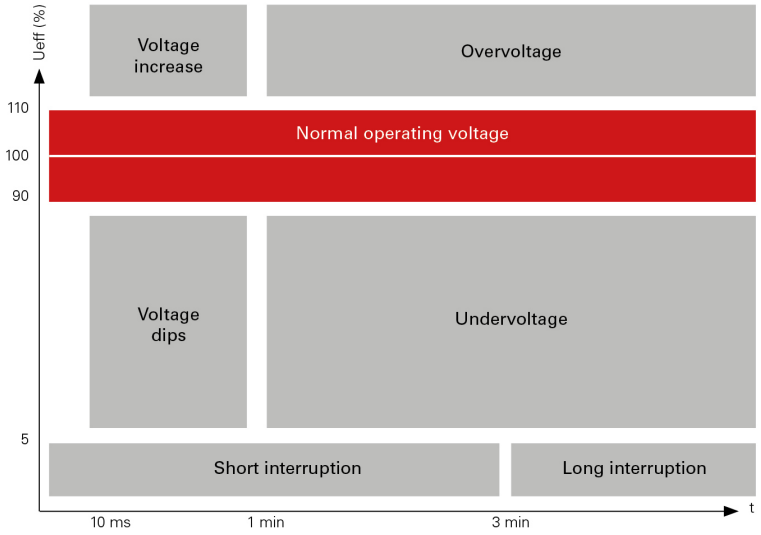

Figure 2.10: Voltage quality definitions [30]

Classifiers each have their own requirements concerning the supply voltage quality. DNV describes the following:

- a maximum of ±2.5% of nominal AC system voltage for main power distribution
- a maximum of ±3.5% of nominal AC system voltage for emergency power distribution
- a maximum of -15% to +20% of nominal AC voltage during a transient state
- after a transient condition has been initiated, the voltage in a main distribution AC system shall not differ from nominal system voltage by more than ±3% within 1.5. For an emergency distribution system it is ±4% within 5s
- for DC voltage, a tolerance from +30% to -25% for equipment connected to battery during charging
- for DC voltage, a tolerance from +20% to -25% for equipment connected to battery not being charged
- a maximum voltage cyclic variation of 5% and a maximum voltage ripple of 10%

Bureau Veritas specifies:

- a variation between +6% and -10% for AC distribution systems
- a variation of ±20% for transient conditions with a recovery time of 1.5s
- a variation of ±10% for DC distribution systems
- a maximum voltage cyclic variation of 5% and a maximum voltage ripple of 10%

The specifications of Lloyd's Registrar are identical to those of Bureau Veritas.

2.3. Earthing

There are five major earthing systems that can be distinguished and each one is shown in figure 2.11. In a TN earthing system, one of the points in the generator or transformer is connected with earth. Usually this is the star point. The conductor that connects exposed metallic parts of the consumer's electrical installation is called Protective Earth (PE). The conductor that connects to the star point in a three-phase system, or that carries the return current in a single-phase system is call the neutral (N).

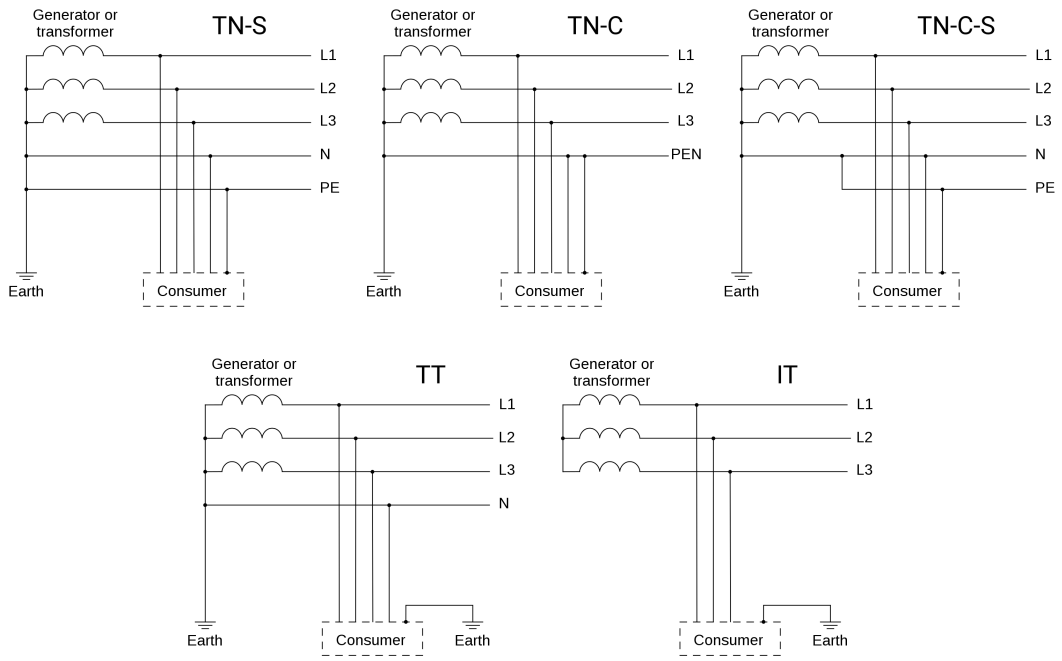

Figure 2.11: Comparison of different earthing systems

In a TN-S system, the PE and N are separate conductors. This is an earthing system that is commonly used in yachts. In a TN-C system, there is a combined PEN conductor for the PE and N. In a TN-C-S system, part of it uses a combined PEN conductor, but at some point, for example at the entry of a building, the PEN conductor will split off in separate PE and N conductors.

In a TT system, the generator or transformer is directly connected to earth, but there is no PE conductor. Instead, the consumer is (separately) connected to earth as well and the earth's mass will serve as the return path. In an IT system, the installation is either isolated from earth, or the neutral point is connected to earth through a high impedance. Exposed conductive parts are earthed, either individually or collectively. This is an earthing system that is commonly used in work vessels.

3

Short-circuit currents and protection

3.1. Short-circuit calculations in AC grids

In vessels, short-circuit calculations are important to determine the size of circuit breakers and fuses. Components from the typical circuit in figure 1.1a that will contribute to the short-circuit current are the generators, the VFD and the converter. Asynchronous motors that are directly connected (not through a VFD) will also contribute to the short-circuit current. Cables will not contribute to the short-circuit current and will actually reduce it as their impedance goes up for the high frequency short-circuit current. This is similar for the transformer as a higher short-circuit impedance ($U_k\%$) will reduce the fault current during a fault on the load side.

3.1.1. IEC 61363 standard

For calculating short-circuit currents, there are two main IEC standards, the IEC 60909 and the IEC 61363. The IEC 61363 outlines procedures for calculating short-circuit currents that may occur on a marine or offshore AC electrical installation and is the standard that will be followed. The calculation procedures are for a three-phase symmetrical short-circuit condition i.e. three-phase conductors shorted together, or shorted to the ship's hull and for which the short-circuit occurs on all three poles simultaneously. [31] The short-circuit current is a complex time-dependent function occurring in each phase. The current contains both a.c. and d.c. components typically as shown in figure 3.1. In this figure, I''_k is the initial symmetrical short-circuit current, i_p is the peak short-circuit current, I_k is the steady-state short-circuit current, i_{dc} is the decaying component of the short-circuit current and A is the initial value of the aperiodic component.

The majority of marine/offshore electrical systems are operated with the neutral point insulated from the hull or connected to it through an impedance. In such systems, the highest value of short-circuit current is the three-phase short circuit. If the neutral point is directly connected to the hull, then the line-to-line to ship's hull, or line-to-ship's hull short circuit may produce a higher current. [31]

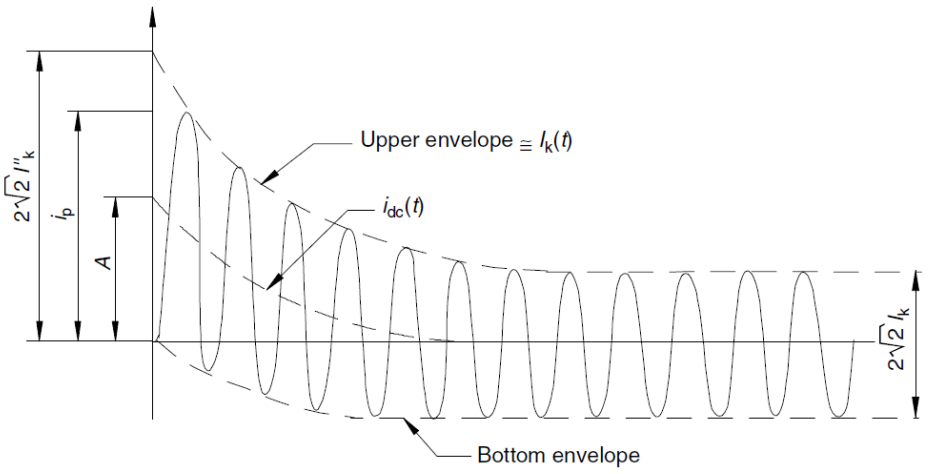

Figure 3.1: Three-phase short-circuit current curve [31]

Synchronous machine

For a synchronous machine, the current i_k in figure 3.1 is defined by equation 3.1. From this, it is common to calculate three functions. $I_{ac}(T)$ describes the a.c. component, $i_{dc}(t)$ describes the d.c. component and i_p describes the maximum possible peak value. These equations are equations 3.2 and 3.3 and are calculated at $t = T/2$ to get the peak value. The currents are calculated using the Stator resistance, Synchronous reactance, Transient Reactance and Subtransient Reactance and their corresponding time constants taken from the datasheet of the generator.

$$i_k(t) = \sqrt{2} I_{ac}(t) + i_{dc}(t) \tag{3.1}$$

$$I_{ac}(t) = (I''_{kd} - I'_{kd})e^{-t/T''_d} + (I'_{kd} - I_{kd})e^{-t/T'_d} + I_{kd} \tag{3.2}$$

$$i_{dc}(t) = \sqrt{2}(I''_{kd} - I_0 sin(\Phi_0)e^{-t/T_{dc}} \tag{3.3}$$

Asynchronous motor

For asynchronous motors, there are two configurations: direct-online and through a converter. The short-circuit current curve looks different compared to the generator, as can be seen in figure 3.2. Here, i_{OM} is the no-load current, i_{pM} is the peak short-circuit current, A is the initial value of the aperiodic component i_{dc}, I''_M is the initial symmetrical short-circuit current and i_{dcM} is the decaying (aperiodic) component of the short-circuit current. These currents can all be calculated from the stator and rotor resistances and reactances and their time constants. For the peak value, the equations are again evaluated at time $t = T/2$.

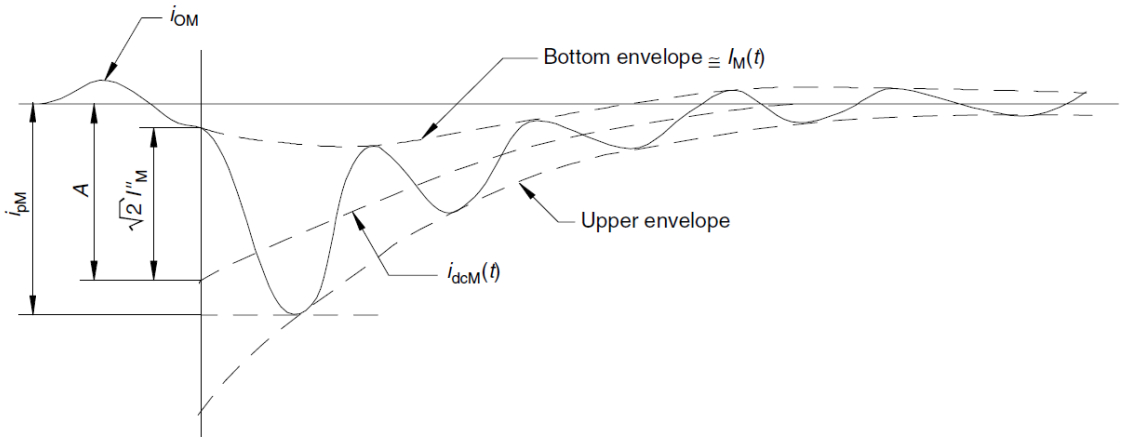

Figure 3.2: Short-circuit current curve of an asynchronous motor [31]

When the motor is connected through a converter, the evaluation method changes significantly. The short-circuit current evaluation depends heavily on knowledge of the converter control system characteristics and protective functions of the converter such as current-limiting devices, static switches and any other devices that will limit the short-circuit current. Even when all information is available, an accurate calculation is complicated due to the switching action of the solid-state components. If no information from the manufacturer is available, the IEC 61363 describes a method to predict the short-circuit current.

To predict the short-circuit current of a converter-connected motor, assumptions are made and the motor-converter can be represented as the system impedance diagram in figure 3.3. R_{aM} and L''_M are properties of the motor, R_{dc} and L_{dc} are the resistance and inductance of the DC part of the converter, R_{com} and L_{com} are the resistance and inductance of the commutation coils and R_c and L_c are the resistance and inductance of converter. L''_M is scaled by a factor f_e/f_r where f_e is the lowest frequency of the converter and f_r is the rated network frequency.

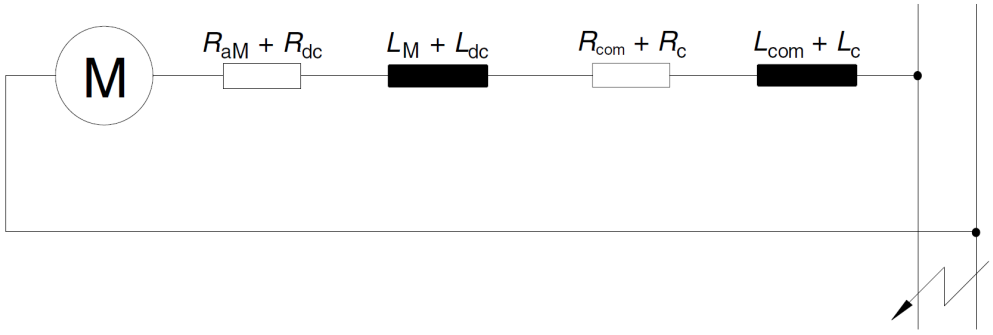

Figure 3.3: System impedance diagram of a converter fed motor [31]

Transformer
As mentioned before, a transformer does not contribute to the short-circuit current and will actually attenuate it. The IEC 61363 provides equations to calculate the equivalent resistance, transient reactance and subtransient reactance of the transformer. The positive-sequence resistance, reactance and impedance can also be calculated using the rated ohmic voltage u_{rR}, the rated line-line voltage U_r, the rated power S_{rT}, and the rated short-circuit voltage u_{rk}. These equations are equation 3.4 through 3.6.

$$R_T = u_{rR}\frac{U_r^2}{100}S_{rT} \qquad R_T = \frac{P_{cu}}{3I_{rT}^2} \tag{3.4}$$

$$X_T = \sqrt{Z_T^2 - R_T^2} \tag{3.5}$$

$$Z_T = u_{rk}\frac{U_r^2}{100}S_{rT} \tag{3.6}$$

Cables
Cables will attenuate the short-circuit current as well. The cable impedance comprise a resistance and reactance. For short-circuit currents, the temperatures rise of the cables should be considered as this can influence the cable impedance.

3.2. AC protection devices

Protection devices are devices that can disconnect a fault current. In maritime systems, the moulded-case circuit breaker is often used. Another device that can be encountered in an AC system is a fuse. The basics of both devices will be covered.

3.2.1. Moulded-case circuit breaker

When a circuit breaker interrupts a high current, an arc is generated. Circuit breakers use various mediums to safely extinguish this arc, such as air, oil, SF6 or vacuum. A moulded-case circuit breaker uses air as the dielectric medium to break a fault current. The breaker typically has a thermal element for overcurrent situations and a magnetic element for short-circuit conditions. A bimetalic contact is involved in the overcurrent protection which allows the current to flow under normal conditions, but will engage the tripping mechanism under overload conditions. An electromagnetic coil is involved in the short-circuit protection. Under normal conditions, only a small electromagnetic field is generated by the coil which is not strong enough to engage the tripping mechanism. During a short-circuit however, a strong magnetic field is generated that is strong enough to engage the tripping mechanism.

The moulded-case circuit breaker (MCCB) can also have an electronic or a microprocessor release. Instead of the thermal magnetic element, the breaker will have a separate power electronics circuit or microprocessor controller that monitors the current flow and engages the tripping mechanism. The electronic MCCB using the power electronics circuit has the main advantage that the tripping performance is not affected by the ambient temperature. The microprocessor MCCB allows for fine tuning and more flexibility in the tripping characteristics.

The arc chamber contains the tripping mechanism which contains the mechanical moving contact. When the tripping mechanism is engaged, the contacts move away creating an air gap, and in the case of a short-circuit current, also an arc. When the contacts open, a blow of air blows the arc upwards and into an arch chute which increases the arc resistance and extinguishes it more rapidly.

3.2.2. Fuse

Compared to the circuit breaker, the fuse is a simpler device as it does not contain a moving tripping mechanism. This also means that the fuse is a single-use device that has to be replaced after interrupting a fault current. Instead of a moving mechanism, there is a special fuse element that melts and opens in case of an overcurrent. Fuses exist for many applications, in ranges from milliamps to kiloamps.

Fuse operation depends primarily on the balance between the rate of heat generated within the element and the rate of heat dissipated to external connections and surrounding atmosphere. For current values up to the fuse's continuous current rating, its design ensures that all the heat generated is dissipated without exceeding the pre-set maximum temperatures of the fuse element. Under conditions of sustained overloads, the rate of heat generated is greater than that dissipated, causing the fuse element temperature to rise. Once the temperature reaches the element material melting point, it will start arcing and "burn back" until the circuit is opened. The time it takes for the element to melt and open decreases with increasing current levels. [32]

The time it takes from the initiation of the arc to the arc being extinguished, is called the arcing time. The sum of the pre-arcing and arcing time is the total clearing time. The terms pre-arcing energy and arcing energy are also used to correspond to the times. The energy will be proportional to the integral of the square of the current multiplied by the time the current flows and is notated as I^2t, where I is the RMS value of the current and t the time in seconds.

3.3. Short-circuit calculations in DC grids

Components from the typical circuit in figure 1.1b that will contribute to the short-circuit current are the converters and a capacitor bank or battery that is connected to the DC bus directly. A DC motor that is connected to the DC bus will also contribute to the short-circuit current. Similar to a short-circuit on an AC grid, the cables will reduce the short-circuit current because of their impedance. Of course, all AC components that are connected through converters still need protection implemented on the AC side in case of a fault there.

3.3.1. IEC 61660 standard

For calculating short-circuit currents in DC grids, there is only one available standard. The IEC 61660 describes a method for calculation short-circuit currents in DC auxiliary systems in power plants and substations. It accounts for rectifiers in three-phase AC bridge connection for 50 Hz, stationary lead-acid batteries, smoothing capacitors and DC motors with independent excitation. [33] For DC short-circuit currents, the IEC 61660 defines some typical short-circuit currents and a standard approximation function that covers different current variations. Figure 3.4 shows two typical DC short-circuit diagrams.

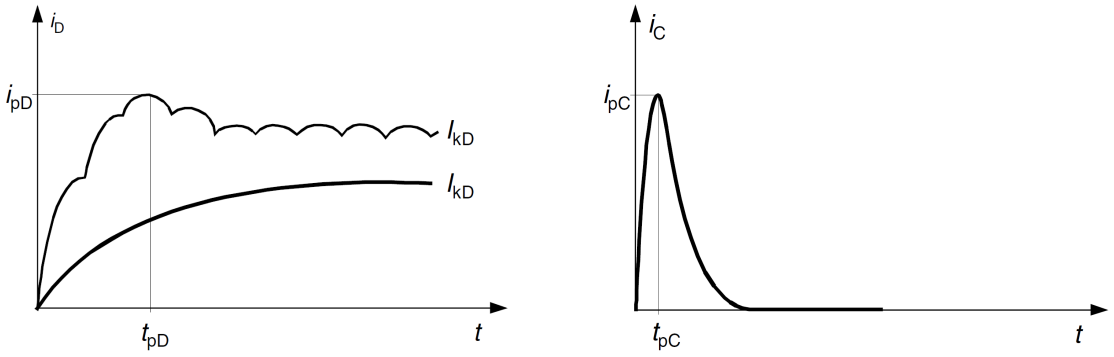

(a) Rectifier without and with smoothing reactor

(b) Capacitor

Figure 3.4: Typical DC short-circuit diagrams [33]

For the rectifier in figure 3.4a, i_{pD} is the peak short-circuit current and I_{kD} is the quasi steady-state short-circuit current. The equivalent circuit for the rectifier in this situation is given in figure 3.5. Here, R_N and L_N are the equivalent resistance and inductance of all resistances and inductances on the AC side of the rectifier. Likewise, $\frac{cU_n}{\sqrt{3}}$ is the equivalent voltage source on the AC side. R_{DBr} and L_{DBr} represent all resistances and inductances on the DC side of the rectifier.

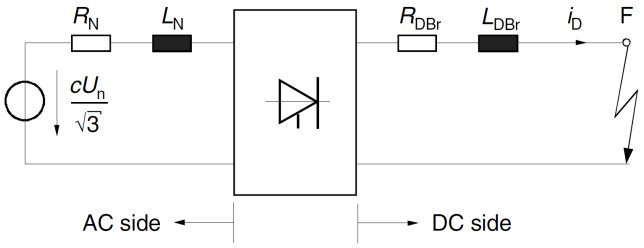

Figure 3.5: DC short-circuit rectifier equivalent circuit [33]

For the capacitor in figure 3.4b, i_{pC} is the peak short-circuit current. The equivalent circuit for the capacitor in this situation is given in figure 3.6. Here, R_{CBr} is a combination of the DC resistance of the capacitor, the resistance of the conductor in the capacitor branch and the resistance of the rest of the circuit. L_{CBr} is the combination of the inductance of the conductor in the capacitor branch and the inductance of the rest of the circuit.

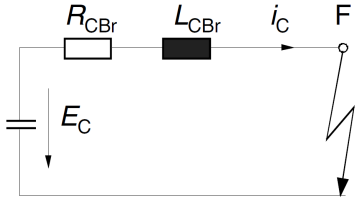

Figure 3.6: DC short-circuit capacitor equivalent circuit [33]

The current i_{pC} in figure 3.4b is defined by equation 3.7 where κ_C depends on R_{CBr}, L_{CBr} and C. The standard provides an equation for this. The standard also provides an equation to calculate the time to peak t_{pC}. The standard approximation function of figure 3.7 can be used to describe the current as a function of time.

$$i_{pC} = \kappa_C \frac{E_C}{R_{CBr}} \tag{3.7}$$

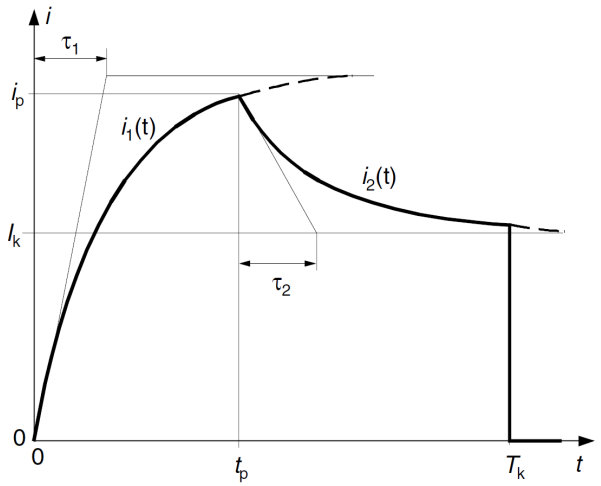

Figure 3.7: Standard approximation function [33]

The time constants from figure 3.7 depend on the factors k_{1C} and k_{2C}, which depend on $\frac{1}{\delta}$ and ω_0 which again depend on the C, L_{CBr} and R_{CBr}.

The problem with the IEC 61660, as reference [34] mentions as well, is that the standard only includes radial DC grids and does not consider a more complex system, such as meshed DC grids or a hybrid AC/DC microgrid. The standard dates from 1997 and does not provide any calculations for Lithium-Ion batteries, only for Lead-Acid batteries. The short circuit current curve of a Lithium-Ion battery is similar to that of a capacitor [35], but what if the battery is connected using a DC/DC converter? There is currently no standard that clearly describes the contribution of all modern day components and educated guesses have to be made instead.

3.4. DC protection devices

A regular circuit-breaker cannot interrupt a DC current because the current does not naturally pass through zero. Fuses are one of the only protection devices suitable for interrupting DC current. There are semiconductor based DC circuit breakers, but these devices are still expensive and cannot be used for every component.

3.4.1. Semiconductor based DC circuit breakers

Semiconductor, or solid-state circuit breakers replace the electromechanical contact with semiconductor switches in order to disconnect the current. Because of the high switching speeds of semiconductor devices, a semiconductor-based breaker can in theory interrupt a fault current in a matter of tens to hundreds of microseconds. This also means that there is little to no arc as there is not enough time for the current to rise to high enough levels. A big disadvantage is that the DC breaker brings high on-state losses compared to conventional breakers. There are also hybrid circuit breakers that combine the electromechanical breaker and the semiconductor switches, but these breakers are largely still in the research and development phase.

3.4.2. Fuse

The principle of the DC fuse is exactly the same as the AC fuse discussed in section 3.2.2. The main difference is that extinguishing the fuse arc is not assisted by a reducing voltage or the zero crossing of an AC current. The inductance in a DC circuit limits the rate of current rise. The time required for the current to reach 63 percent of the final value is called the time constant τ and is often referred to in terms of L/R. For long operating times (>1 second), the heating effect of an AC current is the same as DC current. However, depending on the DC time constant, it can take more DC current for a fuse to melt compared to an AC current. [32]

3.5. Selectivity

Selectivity in electrical power systems is fundamental in reducing the problems caused by abnormal operating conditions or actual faults in the system. A good protection system must be able to discriminate between abnormal but tolerable situations and fault situations within its zone, avoiding unwanted trips causing interruptions in healthy parts of the system. It should also act as rapidly as possible to limit any damage. [36]

Four selectivity techniques can be defined out of which time-current selectivity is most often realized. In general, a time characteristic is intended as a trip characteristic where, as the current increases, the trip time of the circuit breaker decreases. Time-current selectivity adjusts the protections such that the load-side protection, for all possible overcurrent values, trips more rapidly than the supply-side circuit breaker. A typical trip characteristic can be seen in figure 3.8.

Current selectivity is based on the observation that the closer the fault point is to the power supply of the installation, the higher the short-circuit current is. It is therefore possible to set instantaneous protections to different current values. A big downside is that redundancy, which guarantees fault elimination in case of another breaker failing, is not possible. Time selectivity fixes this by also defining a trip time: certain current value will make the protection trip after a defined time delay. The delayed trip thresholds must take tolerances and circulating currents into account.

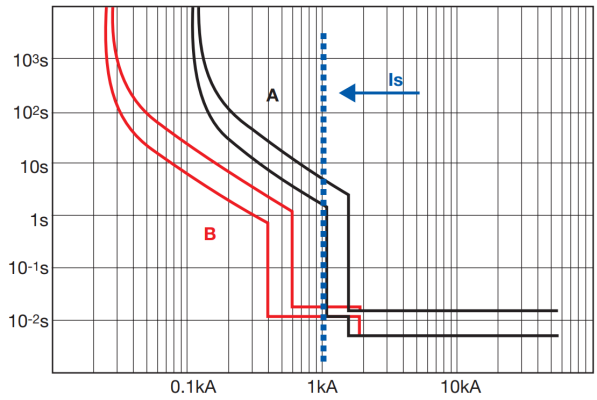

Figure 3.8: Typical trip characteristic of a circuit breaker [36]

Zone selectivity is realized through current measuring devices which, once a threshold has been detected as having been exceeded, allows fault zone to be identified after which the power supply to it can be cut off. Two ways to do this is by sending all information to a supervision system which identifies which protection needs to intervene, or by communication directly between protection devices. [36]

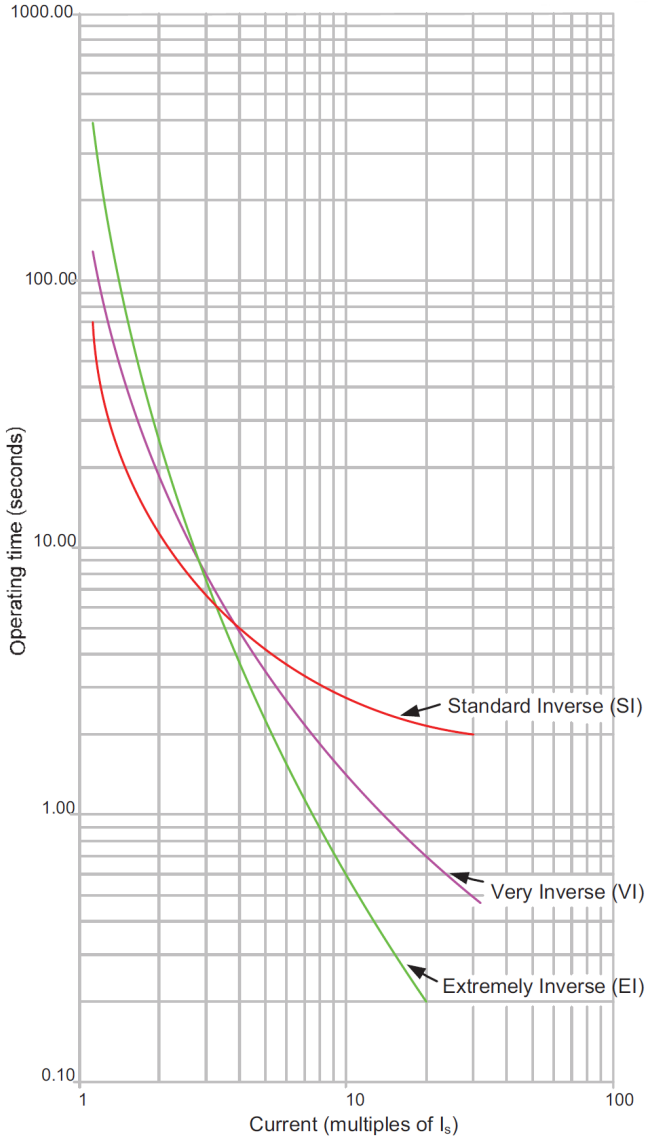

Figure 3.9: IEC 60255 standard characteristics [37]

For time-current selectivity, the IEC 60255 has defined four standard characteristics and three of them are shown in figure 3.9. These curves can be adjusted by changing the Time Multiplier Setting which moves the curve up and down. Almost all relays have an instantaneous setting as well that will trip the breaker as soon as possible after the current has reached a certain (short-circuit) level. Overcurrent relays are normally also provided with definite time characteristics which is mainly used to lower operating times at lower current values. It has a set current and time value for which it operates and can be seem more as an overcurrent protection. If the current is higher than the set current for longer then the set time, it will trigger.

Although by using a current setting that is only just above the maximum load current in the circuit a certain degree of protection against overloads as well as faults may be provided, the main function of overcurrent protection is to isolate primary system faults and not to provide overload protection.
The time interval that must be allowed between the operation of two relays close to each other, in order to achieve accurate selectivity, is called the *grading margin*. If the grading margin is insufficient, more than one relay will operate for a fault leading to unnecessary loss of supply. The grading margin depends on factors such as the interrupting time of the circuit breaker and timing, overshoot or current transformer errors. [37]

The Time Current Curve gives a graphical representation of the selective coordination of overcurrent devices in an electrical system. An example is shown in figure 3.10 and it shows two circuit breaker curves in blue and violet, and a fuse curve in red. Furthermore it shows a transformer damage curve in orange and three cable damage curves in green. A generator decrement curve indicating the fault current during subtransient, transient and sustained periods of the fault condition, is usually also included.

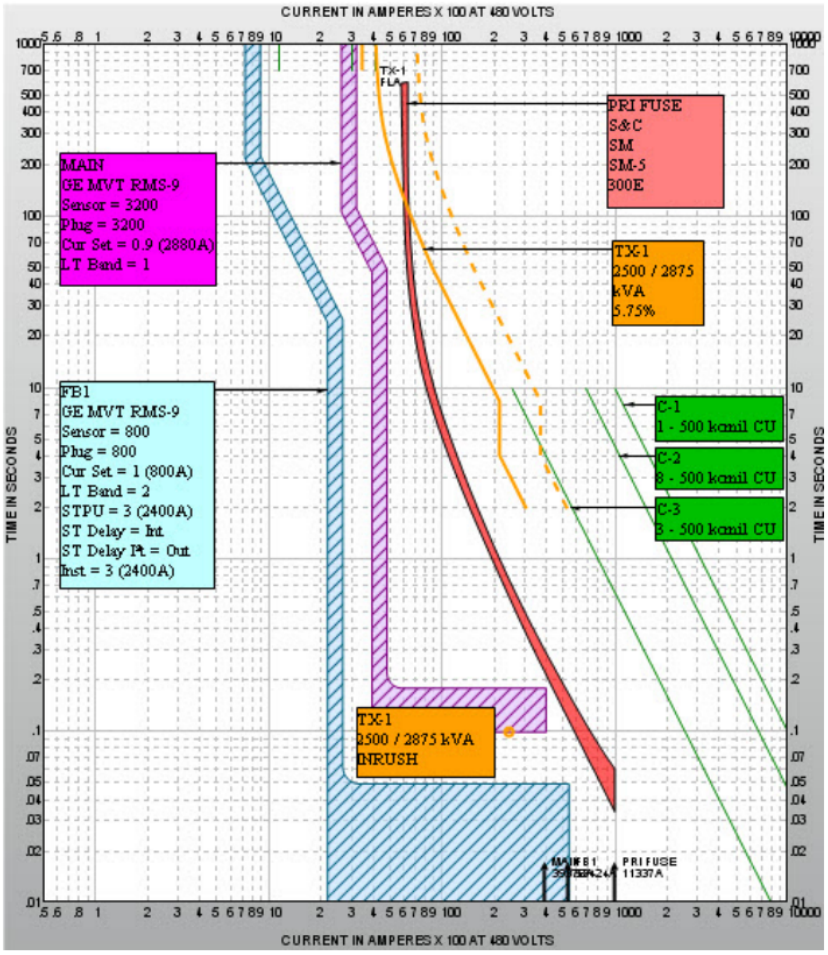

Figure 3.10: Typical Time Current Curve Plot [38]

4

Hybrid AC grid simulation

4.1. Single Line Diagram

As part of the power quality and energy flow analysis, two hybrid power systems will be analyzed. The first system is a traditional - non-hybrid system that has been converted. The simulation will take place in simulation software ETAP version 22.5.0. ETAP has the ability to a simulate load flow and transient stability simulation, as well as the ability to perform short-circuit calculations according to the IEC standards discussed in section 3.1. ETAP also has the capability to study selectivity and harmonic distortion. All of this will be covered in this chapter.

The first system is based on an AC bus and is shown in figure 4.1. The system can be divided in three parts according to the three different sections of the propulsion busbar. The port side (PS) and starboard side (SB) are identical and have two different size 690V generators acting as the main power source. Each side has a propulsion thruster and a bow thruster, and a transformer powering the 440V distribution busbar. To convert the system to a hybrid system, a 1500 kWh battery is added on both sides. Specifications of the generators and the loads have been listed in tables 4.2 through 4.5. The middle part of the propulsion busbar only has a single generator and a retractable bow thruster connected to it.

The circuit breakers connecting the three parts can be closed to create a single propulsion busbar. However, in this case only three generators may be running in parallel continuously to limit the short circuit current. When a fourth generator is connected, the circuit breaker (tie breaker) will open to divide the busbar again. In DP mode, all generators are connected and both tie breakers will open to limit the short circuit current, but ensure redundancy. These situations can be represented in an operational matrix such as table 4.1.

Table 4.1: Operational matrix first system

Operational modi	**Required power**	**Generator configuration**							**Total available power**
		DG#01	**DG#02**	**TB1**	**DG#05**	**TB2**	**DG#03**	**DG#04**	
Auto	5761 kW	1	1	1	0	1	1	0	7032 kW
		1	1	1	0	1	0	1	6384 kW
		1	0	1	0	1	1	1	6384 kW
		0	1	1	0	1	1	1	7032 kW
DP	6992 kW	1	1	0	1	0	1	1	10.244 kW

With the batteries added to the system, this operational system will need to be revised in order to take into account the new functionalities as described in section 1.3.

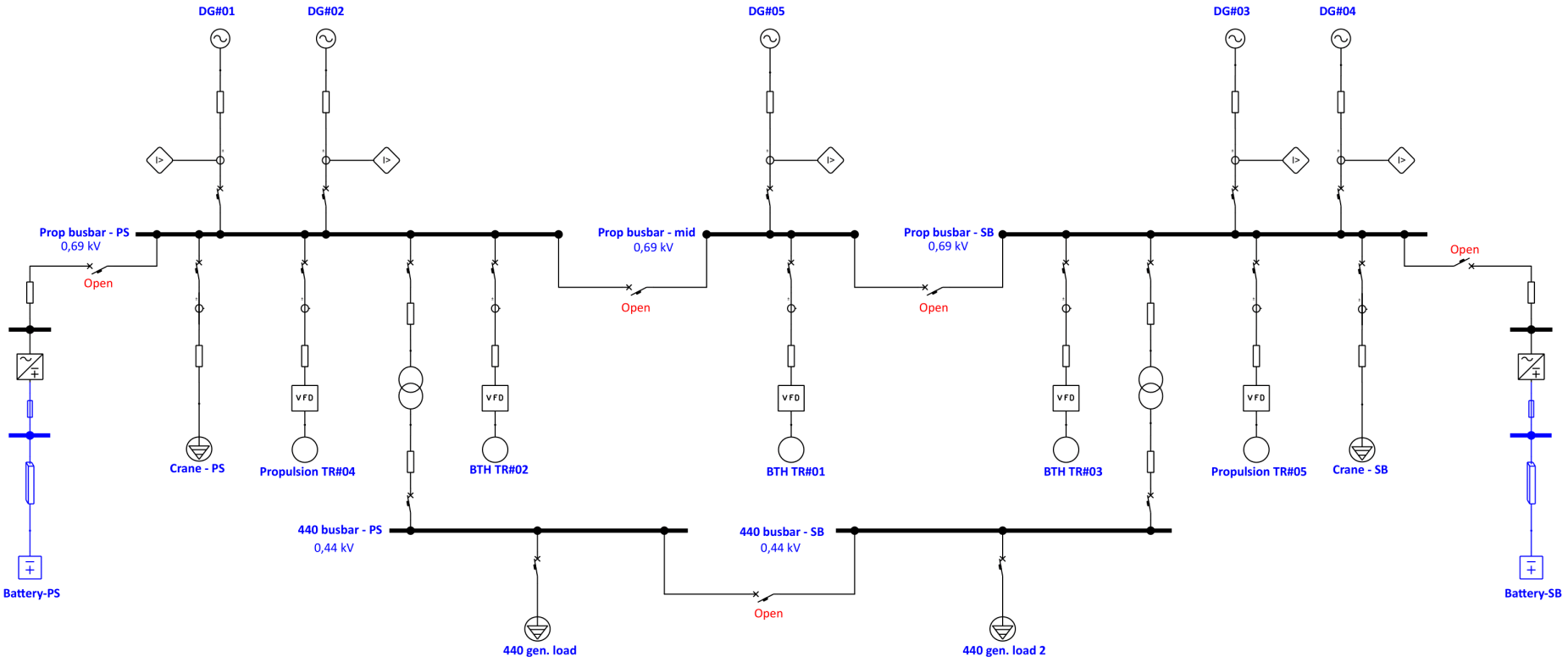

Figure 4.1: Single line diagram AC grid

4.2. Generator specifications

The general specifications of the generators and loads in the Single Line Diagram from figure 4.1 are shown in table 4.2 through 4.5. More specific simulation parameters are given in section A.1.

Table 4.2: Specification of generators DG#01 and DG#04

DG#01, DG#04		
Rated power	2395	kVA
Rated power	1916	kW
Voltage	690	V
Current	2004	A
Frequency	60	Hz
Power factor	0.80	
Poles	10	
Speed	720	rpm
Winding resistance per phase	1.02	mΩ

Table 4.3: Specification of generators DG#02 and DG#03

DG#02, DG#03		
Rated power	3213	kVA
Rated power	2570	kW
Voltage	690	V
Current	2688	A
Frequency	60	Hz
Power factor	0.80	
Poles	10	
Speed	720	rpm
Winding resistance per phase	0.7	mΩ

The four generators DG#01 through DG#04 are 10 pole synchronous machines that will be running at 720rpm in the 60Hz system. Generator DG#05 only has 4 poles and will be running at 1800rpm in the 60Hz system. The two inverters connecting the batteries are rated at 1500kW and define the maximum charge and discharge rate of the batteries. The three bow thrusters are rated at 1000kW at 0.85 power factor and the two propulsion thrusters are rated at 2100kW at 0.85 power factor. At half load all power factors of the thrusters drop to 0.75. The cranes are modeled as lumped loads with a 20% static part and 80% motor part with a 0.75 power factor. This results in a 746.7kVA load. The 440 gen. loads are also modeled as lumped loads, but with a 65% static and 35% motor part at 0.90 power factor.

Table 4.4: Specification of generator DG#05

DG#05		
Rated power	1713	kVA
Rated power	1370	kW
Voltage	690	V
Current	1433	A
Frequency	60	Hz
Power factor	0.80	
Poles	4	
Speed	1800	rpm
Winding resistance per phase	1.46	mΩ

Table 4.5: Specification of the different loads

Loads		
Inverters	1500	kW
Batteries	1500	kWh
Crane - PS, Crane - SB	560	kW
BTH TR#01	1000	kW
BTH TR#02	1000	kW
BTH TR#03	1000	kW
Propulsion TR#04	2100	kW
Propulsion TR#05	2100	kW
Transformers	1500	kVA
440 gen. loads	800	kVA

The exciter used for the generators is shown in figure 4.2. The block diagram describes the terminal voltage of the synchronous machine (in p.u.) and its relation to the field voltage of the synchronous machine. The system is based on the IEEE AC4 excitation system model. Specific parameters can be found in appendix A.

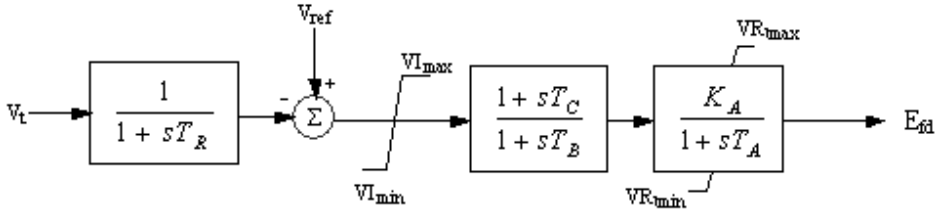

Figure 4.2: Exciter block diagram

Figure 4.3 shows the governor system used for the generators. In ETAP, this system is listed as the Diesel Engine (DT) governor-turbine system. It uses the generator speed and real power output as inputs, and outputs the turbine/engine mechanical power. The governor is set to operate in isochonous mode such that the speed and thus the system frequency will always be constant. The specific parameters of the governor can also be found in appendix A.

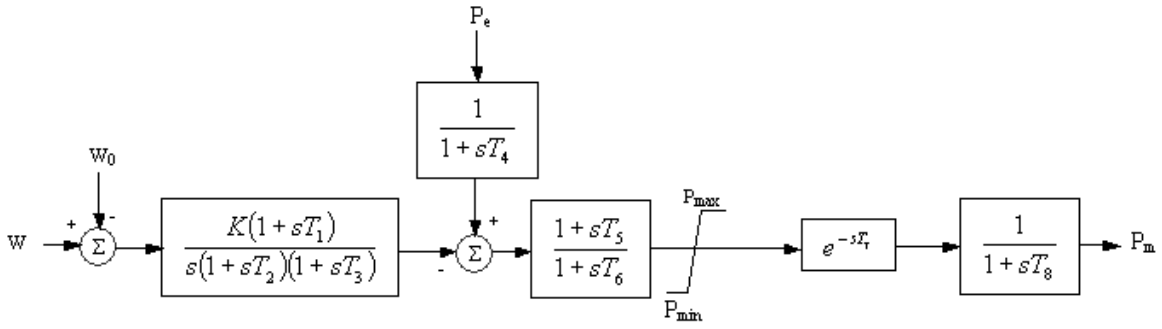

Figure 4.3: Governor block diagram

4.3. Load flow study

To get an idea of bus voltages and the loading of the generators, a load flow study is performed. In the first situation, the vessel is simulated to be in DP mode, meaning both circuit breakers connecting the three propulsion busbars are open. The circuit breaker between the two 440 busbars is open as well and both batteries connected, but are used as a stand-by virtual generator. In this simulation, the loading is even higher than the required power from table 4.1. The results of the simulation are shown in tables 4.6, 4.7 and 4.8.

Table 4.6: Load flow results busbars - full load, no battery

Bus ID	Voltage (V)	MW Loading	Mvar Loading
Prop busbar - PS	689.3	4.006	1.836
Prop busbar - mid	689.7	0.864	0.313
Prop busbar - SB	689.4	4.007	1.836
440 busbar - PS	438.8	0.717	0.347
440 busbar - SB	438.9	0.718	0.348

Table 4.6 shows the busbar voltages and loading. The symmetry between the port side and starboard side is clearly visible as the bus voltage and loading is equal. At maximum, the bus voltage on the 690V level deviates 1%. On the 440V level, the bus voltage deviates 2.7%.

Table 4.7 shows the generator loading during the given study case. The generator loading is again equal on the port side and starboard side due to the symmetry of the power system. Generator DG#01 through DG#04 all operate at a 90.9% power factor. DG#05 operates at a 94% power factor and is only loaded for 63% in this study case.

Table 4.7: Load flow results generators - full load, no battery

Generator ID	MW	Mvar	Amp (A)	PF (%)	Loading (%)
DG#01	1.755	0.804	1615	90.92	91.6
DG#02	2.256	1.033	2076	90.92	87.8
DG#03	2.256	1.034	2076	90.91	87.8
DG#04	1.754	0.804	1615	90.91	91.6
DG#05	0.864	0.313	769.4	94.01	63.1

Table 4.8 shows the loads and their power. All loads are operating according to the power factor specified in their datasheet and in section 4.2.

Table 4.8: Load flow results loads - full load, no battery

Load ID	MW	Mvar	Amp (A)	PF (%)
BTH TR#01	829	513.8	816.1	85
BTH TR#02	829	513.8	816.1	85
BTH TR#03	829	513.8	816.1	85
Propulsion TR#04	1744.5	1053.6	1708	85.6
Propulsion TR#05	1744.5	1053.6	1708	85.6
Crane - PS	557.1	470.6	618.2	76.39
Crane - SB	557.2	470.7	618.1	76.39
440 gen. load	717.5	347.5	1049	90
440 gen. load 2	717.7	347.6	1049	90

In the second situation, a peak shaving scenario is depicted where the middle busbar and the starboard busbar are connected, and DG#02 and DG#04 are turned off. In this situation, both batteries are providing power. The circuit breaker between the port side and the middle busbar is still open, just like the circuit breaker between the two 440 busbars. Tables 4.9 and 4.10 show the result of this simulation.

Table 4.9: Load flow results busbars - peak shaving

Bus ID	Voltage (V)	MW Loading	Mvar Loading	Amp Loading (A)
Prop busbar - PS	689,3	2,152	1,163	2049
Prop busbar - mid	689,4	0,864	0,313	769,8
Prop busbar - SB	689,4	3,016	1,477	2812
440 busbar - PS	438,8	0,717	0,347	1049
440 busbar - SB	438,9	0,718	0,348	1049

Table 4.9 shows the busbar voltages and loading. The port side and starboard side are no longer symmetrically loaded, except for the 440 busbars as nothing changed there. The voltage on the 690V level still deviates a maximum of 1%, and a maximum of 2.7% for the 440V level.

Table 4.10 shows the loading and powers of the two connected generators and both the inverters. In this situation, the inverters are set to provide a fixed amount of (active) power. This also results in the negative power factor. If the batteries were charging, the power factor would be positive.

Table 4.10: Load flow results generators - peak shaving

Generator ID	MW	Mvar	Amp (A)	PF (%)	Loading (%)
DG#01	1,655	1,164	1693	81,8	86,4
DG#03	2,221	1,478	2232	83,26	86,4
INV-PS	0,5	0	417,8	-100	35
INV-SB	0,8	0	667,4	-100	53,5

4.4. Transient stability study

In the transient stability study, the system is modeled in time domain and four cases are simulated:

- Motor starting through a Variable Frequency Drive
- Peak shaving, keeping the generator loading at a maximum of 80%
- DP-mode, a sudden loss of a generator and the battery will provide whatever power the generator was providing
- Three-phase short circuit, investigating system stability and the Critical Clearing Time of the generators

4.4.1. Motor starting

In the motor starting study case, both generators are connected and the battery is disconnected. At $t = 0$s, different loads are already running and the system is in steady-state condition. At $t = 2$s, propulsion thruster TR#04 is started using a variable frequency drive. Over the course of 10 seconds, the VFD gradually increases the voltage and speed to 100% using a constant V/Hz of 11.5.

Figure 4.4a shows the acceleration torque and the slip of the induction motor. Because the speed of the motor is increasing, there must be an acceleration torque. After the motor has reached its final speed at $t = 12$s, the torque drops to 0. The slip starts at 100% and quickly drops to a value close to zero. At the end of the simulation the slip settles at 0.79%. Figure 4.4b shows the mechanical power, electrical power and reactive power of the induction motor. The motor is set to be loaded at 80% of its rated value. Figure 4.4c shows the bus voltage, terminal voltage and terminal current of the induction motor. The bus voltage drops slightly, but the voltage and current increase gradually.

Figure 4.4d shows the speed of the two generators supplying power to the system. As the motor suddenly stops accelerating after it has reached its rated speed, there is a spike in the generator speed that quickly resolves. Figure 4.4e shows the active and reactive power of the generators supplying power to the system and figure 4.4f shows the generator exciter voltage and current.

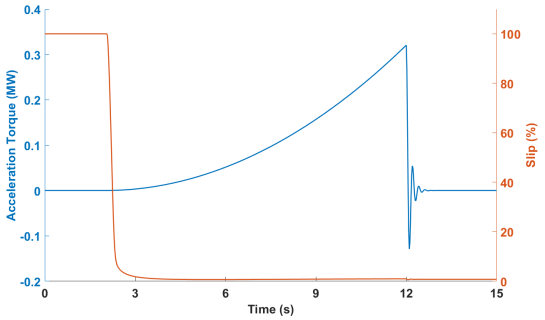

(a) Induction Motor Acceleration Torque and Slip

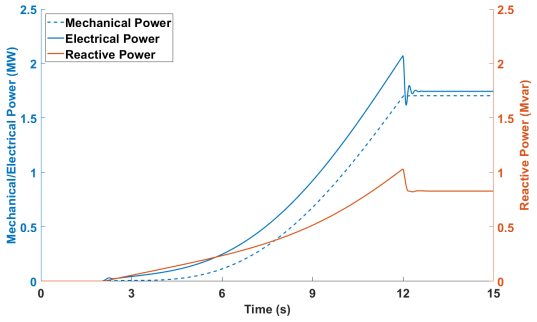

(b) Induction Motor Powers

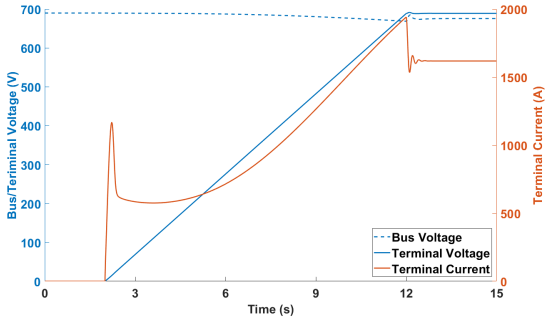

(c) Induction Motor Voltages and Current

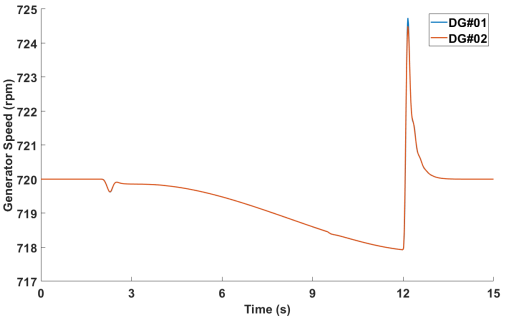

(d) Generator speeds

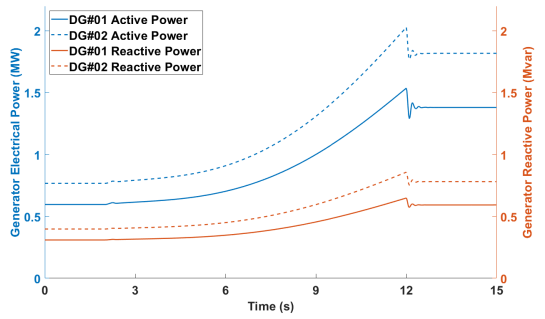

(e) Generators active and reactive power

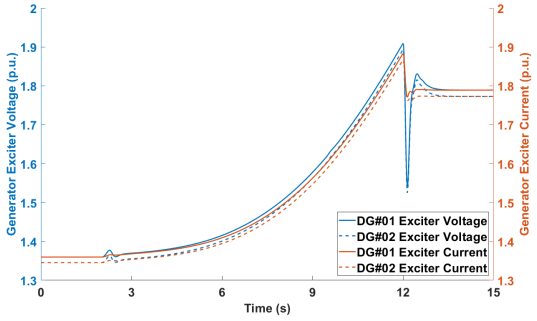

(f) Generator exciter voltages and currents

Figure 4.4: Simulation results for the motor starting simulation

4.4.2. Peak Shaving

In the peak shaving study case, the goal is to show the peak shaving capability of the inverter. Peak shaving is realized through an ETAP User-Defined Model (UDM) for the inverter that monitors the power of the generators throughout the simulation. If the power were to rise above 80%, the inverter is told to supply the difference, keeping the loading steady at 80%. For DG#01, 80% means 1.5MW and for DG#02, 80% means 2.0MW. The output power of the inverter is limited according to its rating. The inverter is also set to provide reactive power if it were to go above 1Mvar or 1.5Mvar for generator DG#01 and DG#02 respectively.

To simulate this, only generator DG#01 is connected and it is loaded slightly under 1.5MW. Then, at $t = 5$s, a lumped load is increased and later decreased, taking the loading of the generator above 1.5MW. Figures 4.5a and 4.5b show the inverter during this event. Slightly after $t = 5$s, when the generator power has reached 1.5MW, the inverter starts to provide power according to the increasing load. Only at the very end of the load ramp does the reactive power of the generator go above 1Mvar. Figures 4.5c and 4.5d show the mechanical power, electrical power, reactive power and speed of the connected generator. As can be seen, the active power of the generator does not go above 1.5MW and the reactive power does not go above 1Mvar. The generator speed is also very stable during this event.

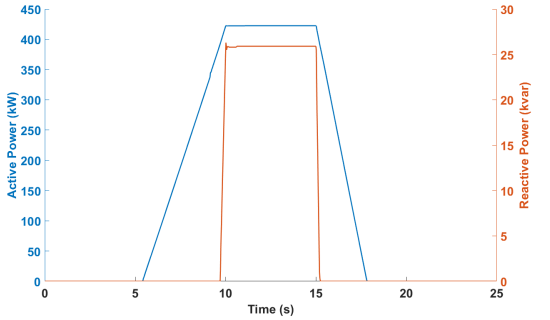

(a) Inverter active and reactive power

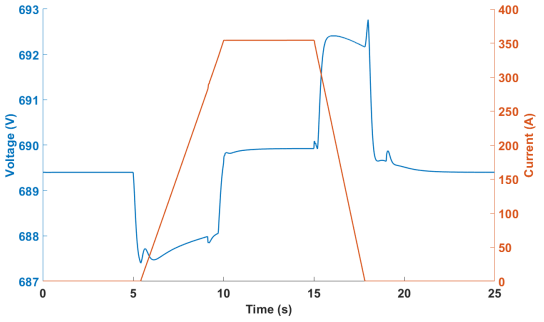

(b) Inverter voltage and current

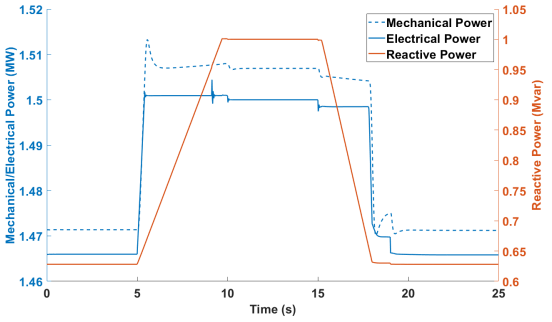

(c) Generator active and reactive powers

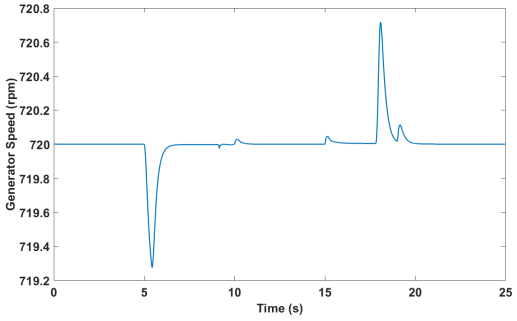

(d) Generator speed

Figure 4.5: Simulation results for the peak shaving simulation

4.4.3. DP-Mode

In the DP-mode simulation, a sudden loss of a generator is simulated by opening the circuit breaker that connects the generator to the main busbar. The inverter is then set to provide whatever power the generator that got disconnected was providing, up to its rated limit. This is again done through a UDM that monitors power of the generators and stores a delayed value, such that it can provide that value in case of a sudden loss of power.

In this simulation, both DG#01 and DG#02 are connected, and DG#02 will suddenly disconnect. Figure 4.6a shows the inverter active and reactive power and figure 4.6b shows the inverter voltage and current. As soon as the generator disconnects at $t = 2$s, the inverter starts providing power. Figures 4.6c and 4.6d show the power and speed of the generators in this situation. After a short spike in the power request from the unaffected generator, the power level goes back to the original level. Because the disconnected generator becomes unloaded, its speed increases to a constant value.

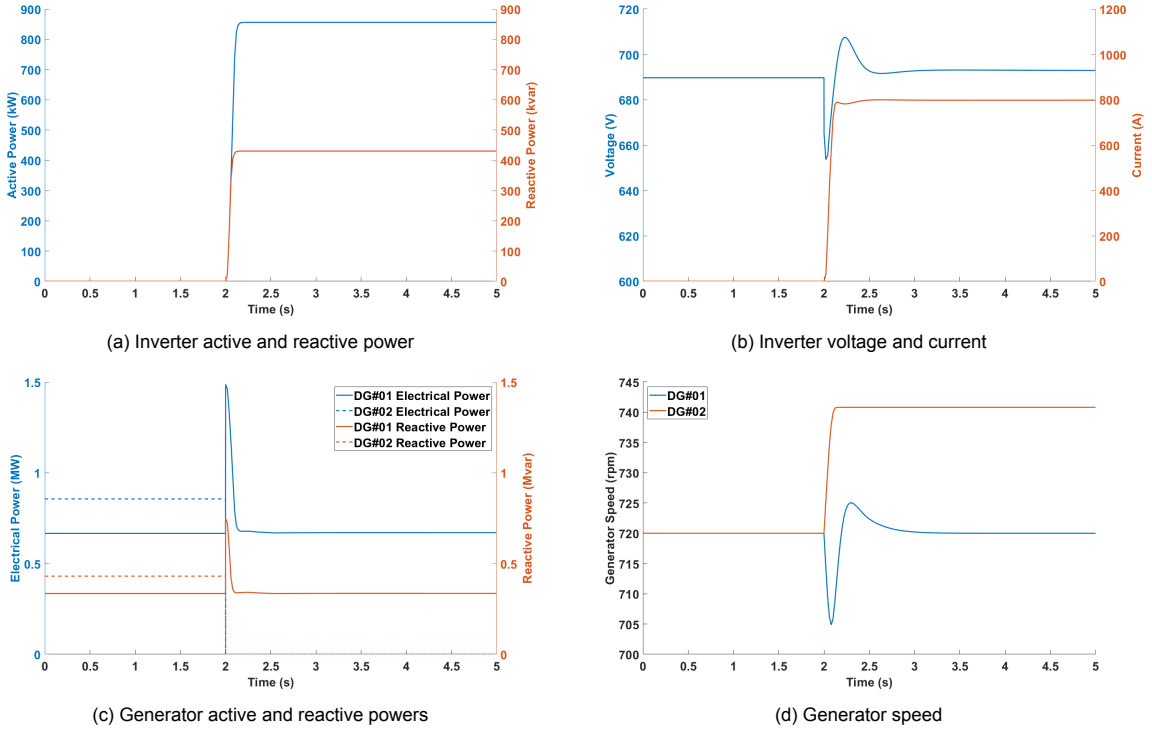

(a) Inverter active and reactive power

(b) Inverter voltage and current

(c) Generator active and reactive powers

(d) Generator speed

Figure 4.6: Simulation results for the DP-mode simulation

4.4.4. Short-Circuit stability

The short-circuit stability simulation simulates a short-circuit condition on the main busbar and focuses on the Critical Clearing Time (CCT) of the generators. As highlighted in section B.5, if the power angle of a generator rises above 90°, the generator can lose synchronism and shut down. Usually when the CCT is calculated, an (infinite) grid is used as a reference for the power angle, but since this is not applicable, another generator will be used as reference.

In all cases, the applied fault is a worst-case fault where the generators are loaded at 90% and the fault is a short-line fault at only 1% cable distance. At first, an extended fault of 1 second is applied that will for sure result in loss of synchronism that will be indicated by a steep drop in the power angle. Then it is investigated at what time the power angle goes above 90 degrees and that time will be used as an indicator to find the exact time for which the power angle will stay below 90 degrees.

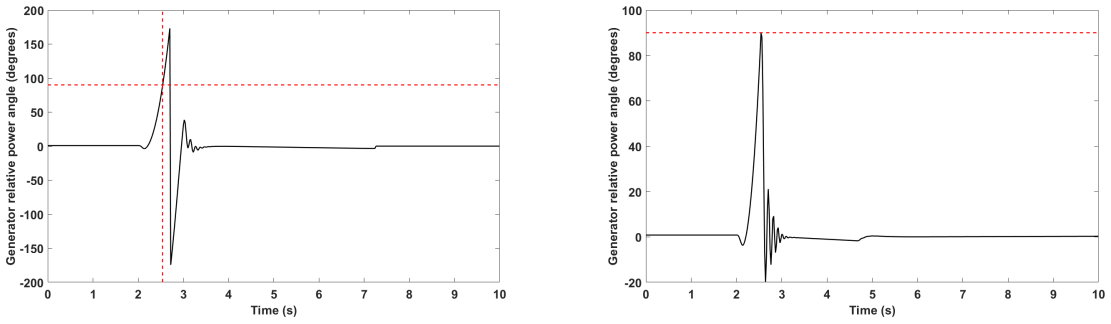

(a) Relative Power Angle DG#01 during extended fault

(b) Relative Power Angle DG#01, fault cleared after 542ms

Figure 4.7: Power angels for DG#01, CTT = 542ms

Figure 4.7 shows the simulation results for generator DG#01. The reference generator in this case is generator DG#02 and the critical clearing time is 542ms. This means that the fault has to be cleared within 542ms in order for the generator to remain stable and connected to the system. This clearing time is also inspected in section 4.6 where a protection and coordination study is done.

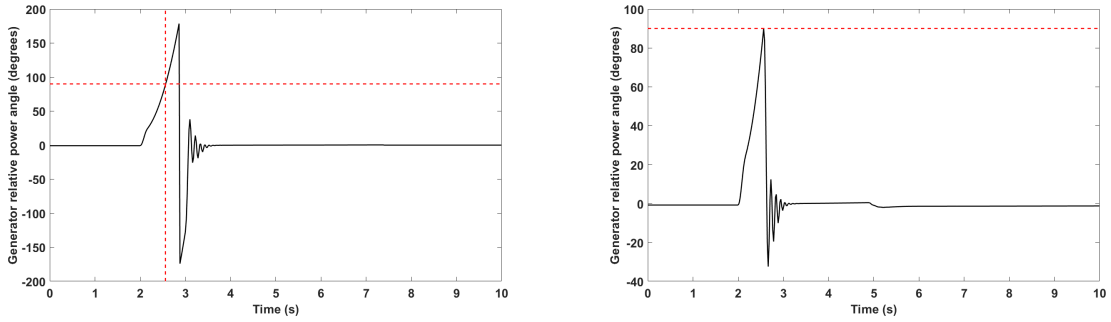

(a) Relative Power Angle DG#02 during extended fault

(b) Relative Power Angle DG#02, fault cleared after 564ms

Figure 4.8: Power angels for DG#02, CTT = 564ms

Figure 4.8 shows the simulation result for generator DG#02 where DG#01 is used as the reference generator. For this machine, the critical clearing time is 564ms. Figure 4.9 shows the simulation result for generator DG#05 where DG#01 is again used as the reference generator. For this machine, the critical clearing time is 574ms.

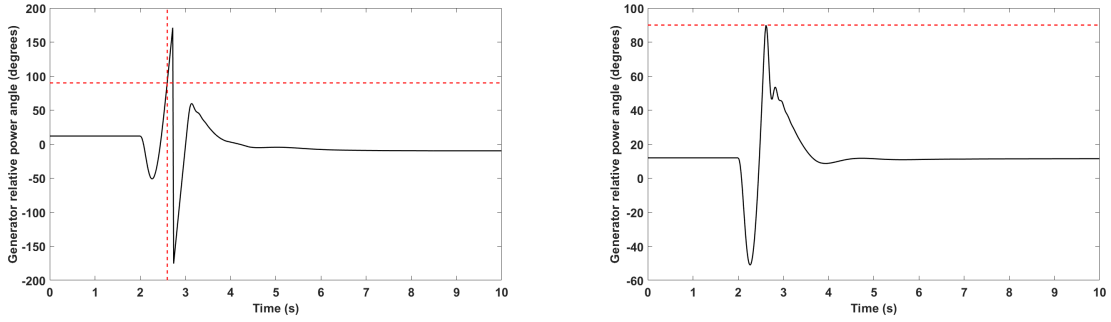

(a) Relative Power Angle DG#05 during extended fault

(b) Relative Power Angle DG#05, fault cleared after 574ms

Figure 4.9: Power angels for DG#05, CTT = 574ms

4.5. Short-circuit calculations

Theoretical short-circuit calculations can be performed through the equations in section 3.1.1. First, short-circuit currents are calculated for the generators including their connecting cables. These results are shown in table 4.11. The results of the simulated short-circuit currents using the IEC 61363 calculation tool in ETAP are shown in table 4.12.

Table 4.11: Calculated generator short-circuit currents

	DG#01	DG#02	DG#05
$I_{ac}(t)$	13.759 kA	17.971 kA	12.773 kA
$i_{dc}(t)$	16.311 kA	21.076 kA	15.458 kA
$i_p(t)$	35.769 kA	46.490 kA	33.521 kA

Table 4.12: Simulated generator short-circuit currents

	DG#01	DG#02	DG#05
Iac(t)	11.231 kA	14.710 kA	11.662 kA
idc(t)	16.265 kA	21.264 kA	14.867 kA
ip(t)	32.148 kA	42.067 kA	31.359 kA

All values that are used for the theoretical calculation are taken from the datasheets, just like the values for the simulation. The short-circuit currents i_p are a sum of the AC I_{ac} and DC i_{dc} components. When comparing table 4.11 and 4.12, there is a distinct difference between the two. One possible explanation for this difference could be that ETAP uses open-circuit time constants in its simulation model and short-circuit time constants are used for the theoretical calculation. The datasheets of generators DG#01 and DG#02 only provide short-circuit time constants and their time constants have been converted for the simulation model. The datasheet of generator DG#05 provides both open-circuit and short-circuit time constants and its simulated short-circuit current is closer to the theoretical value compared to the other two generators. This means a conversion error could be a contributing factor to the difference seen between theoretical and simulated results, but a much larger sample size of generators is needed to prove this.

A second explanation for the difference can possibly be found in the AC part of the short-circuit calculation. Looking at equation 3.2 specifically, there is the term I_{kd} which represents the steady-state short-circuit current which is generally obtained from the manufacturer. The datasheet value of this current is used in the theoretical calculation, but ETAP calculates this value based on the system impedance at the time of the fault.

Further contribution to the short-circuit current comes from the variable frequency drives and the two lumped loads in the simulation. Impedance values for a short-circuit model of the VFDs as discussed in section 3.1.1 are not available, but the short-circuit contribution is typically set at 150% of the nominal current. This same short-circuit contribution is also used in the simulation software.

The cranes are modeled as lumped loads with a 20% static part and 80% motor part. The motor part of the lumped load will contribute to the short-circuit current. ETAP shows a contribution of 4.831kA and using the IEC 61363 with the same X/R ratio, a contribution of 4.488kA is calculated.

4.6. Protection & coordination study

In the protection and coordination study, it is made sure that the system is able to selectively trip circuit breakers to protect its components during a fault condition. Important aspects for this study are the decrement curves of the generators and the Time Current Curves of the circuit breakers. The decrement curves of the generators, as received from the manufacturer are shown in figure 4.10a and shows the current output of the machine considering a 3-phase fault at or near its terminals. The curve shows a time-current relation and the circuit breaker protecting the generator has to operate on the left side of this curve in order to prevent damage.

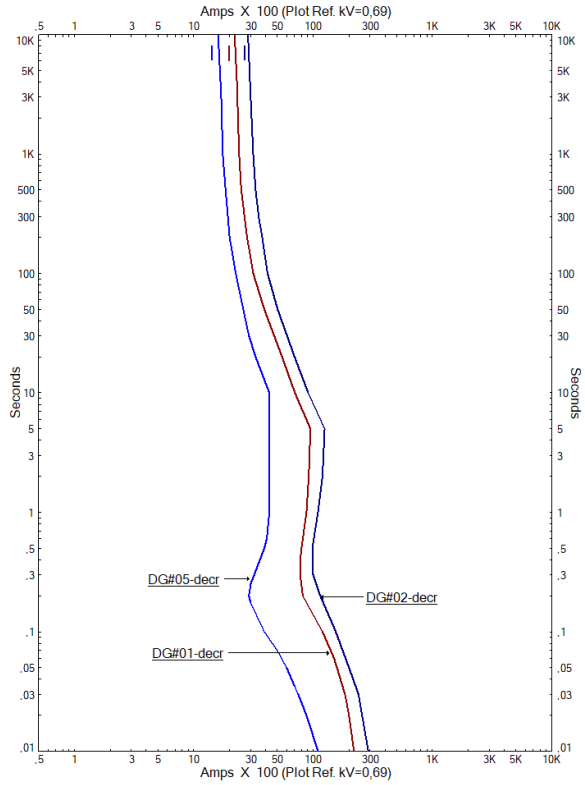

(a) Generator decrement curves
x-axis has to be multiplied by 100

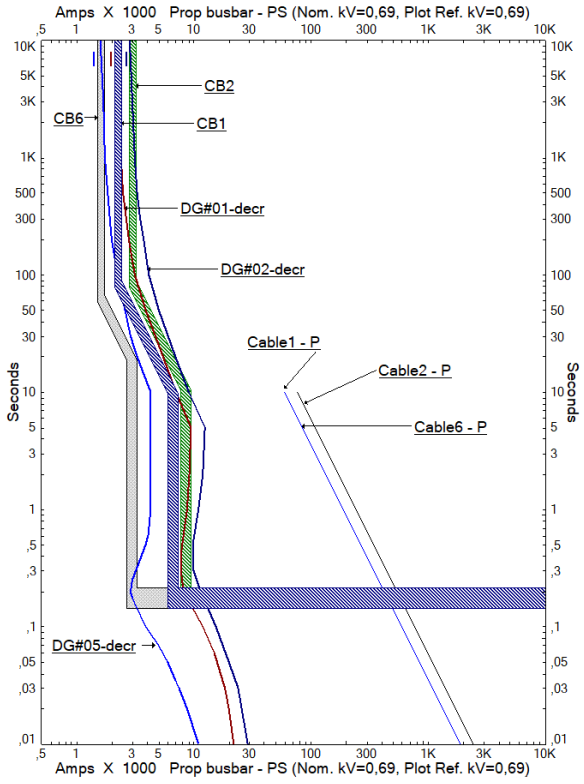

(b) Added circuit breaker and cable curves
x-axis has to be multiplied by 1000

Figure 4.10: Generator, circuit breaker and cable curves

The following short-circuit locations are considered:

- A short-circuit at the generator
- A short-circuit at the PS main busbar
- A short-circuit at the crane load
- A short-circuit at the mid busbar when the tiebreakers are closed
- A short-circuit at the 440V busbar

4.6.1. Short-circuit at the generator

In case of a short-circuit fault between the generator and the generator circuit breaker, it is important that the circuit breaker is opened as soon as possible to prevent damage to the generator and instability to the system as discussed in the previous section. However, it also important that only the generator circuit breaker switches off. If the breaker detects a fault, but it's somewhere else in the system, the breaker should wait for another breaker to clear the fault. If another breaker does not clear the fault within a specific time, the breaker should still open.

In practice this means that if a fault occurs between generator DG#01 and its breaker, the breaker will see a fault current in the direction of the generator. The breaker will then send a lock-signal to the other breakers that are contributing to the fault. This will start a delay where, if the fault is not cleared within this time, the breakers that received the lock-signal will open anyway. In the case where the three propulsion busbar sections are connected, if the breaker connecting the port side and the mid busbar receives a lock-signal, it will pass on the lock signal to the other active breakers that are contributing to the fault current.

ETAP's Sequence-of-Operation does not have the ability to implement lock-signals, but it does verify that all breakers detect the fault and are able to switch off quickly. Without implementing the lock signals, ETAP shows that all circuit breakers detecting the fault will open after 216ms, which is within the critical clearing time of all generators. This also shows why no instantaneous tripping is implemented, but only (directional) short- and long-time. Since the fault current will depend on the exact location and the loading of the generators, it would be very difficult to set a current threshold for all breakers for all situations. The protection systems needs a bit of time to send out lock-signals to maintain selectivity and prevent a black-out.

4.6.2. Short-circuit at the PS main busbar

In case of a short-circuit fault at port side main busbar, it is important that all circuit breakers on the port side that are contributing to the fault current, open. If the three propulsion busbar section are connected, the breaker between the port side and mid should open as well and it should send a lock-signal to the other breakers that are contributing to the fault current.

4.6.3. Short-circuit at the crane load

In case of a short-circuit fault at the crane load, the situation is similar to section 4.6.1. The crane load breaker will detect a fault current in the direction of the load and sends a lock signal to the other breakers contributing to the fault current. This will make sure that only the load gets disconnected and that the disruption in the rest of the system is minimal.

4.6.4. Short-circuit at the mid main busbar

In case of a short-circuit fault at the mid main busbar, DG#05 has to be switched off and both circuit breakers connecting the main busbar have to open. Both breakers will detect a fault current in the direction of the busbar and send lock signals to the breakers contributing to the fault current on the port and starboard side busbars.

4.6.5. Short-circuit at the 440V busbar

In case of a short-circuit fault at the 440V busbar, the situation will depend on if the two 440V busbars are connected and which transformer from the 690V side is supplying the 440V busbar. If the 440V busbars are connected and the port side transformer is supplying the fault for example, when the fault

is on the starboard side, the circuit breaker connecting the two busbars will detect this and send a lock-signal to the transformer circuit breaker on the 440V side. If the fault is on the port side, the circuit breaker connecting the two busbars will still open, but it will not send a lock-signal to the transformer circuit breaker. As the circuit breaker did not receive a lock signal, it will send a lock-signal to the circuit breaker on the 690V side and clear the fault. The circuit breaker on the 690V side will then pass on the lock-signal to all breakers contributing to the fault current.

4.7. Harmonic study

In the harmonic study, a harmonic spectrum is added to the various components and ETAP is used to a harmonic load flow calculation that will calculate the combined Total Harmonic Distortion. For the generators there is no harmonic spectrum available for these specific models, but a spectrum from the type test of a different generator is used as a representative spectrum for all generators. This spectrum is shown in figure 4.11.

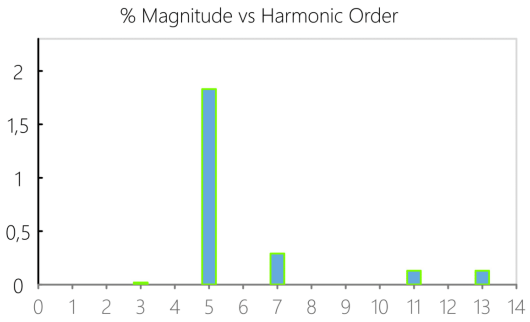

Figure 4.11: Generator harmonic spectrum

For the Variable Frequency Drives and the battery converter, there is also no spectrum available from the manufacturer, but a Matlab-based internal tool from Alewijnse is used to generate representative spectra for these components. The used spectra are shown in figure 4.12a and 4.12b.

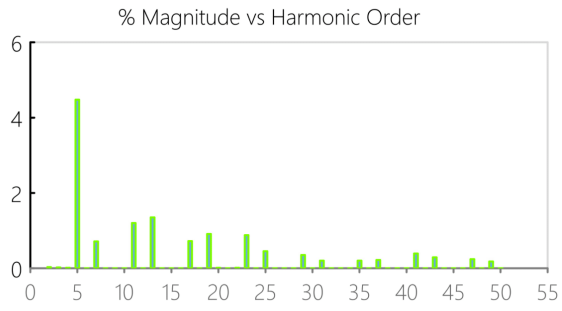

(a) Harmonic spectrum for variable frequency drives

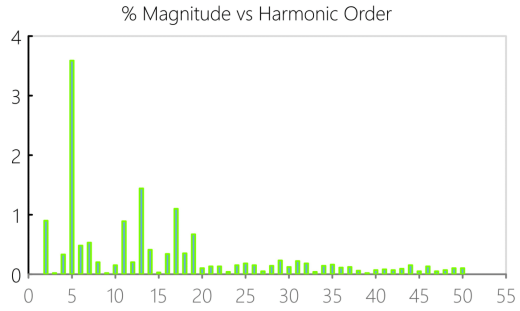

(b) Harmonic spectrum for battery converter

Figure 4.12: Harmonic spectra for the VFDs and battery converters

The harmonic analysis will also be done for different scenario's. In the first scenario, only one generator on the port side is active, the battery is being charged and the crane and 440V loads are active. Table 4.13 shows the simulation results in this situation. The voltage THD of the propulsion busbar is 1.24% and the current THD varies between 0.93 and 2.06%.

Table 4.13: THD_V and THD_i values for the first scenario

Bus/Branch	$\mathbf{THD_V}$ (%)	$\mathbf{THD_i}$ (%)
Generator DG#01	1.24	1.32
Inverter - PS		2.06
Crane - PS		0.93
Transformer - PS		1.11

In the second scenario, both generators are connected on the port side, as well as both thrusters, the crane and 440V loads. The simulation results for this scenario are shown in table 4.14. In this scenario the voltage THD is actually lower compared to the previous scenario at 0.93%. The current THD varies between 0.69 and 2.43% for this situation.

Table 4.14: THD_V and THD_i values for the second scenario

Bus/Branch	**THD_V (%)**	**THD_i (%)**
Generator DG#01	0.93	1.38
Generator DG#02		1.55
Crane - PS		0.69
Propulsion TR#04		2.00
Transformer - PS		0.79
BTH TR#02		2.43

The voltage THD can also be shown as its individual components. For the second scenario, the voltage spectrum is shown in figure 4.13.

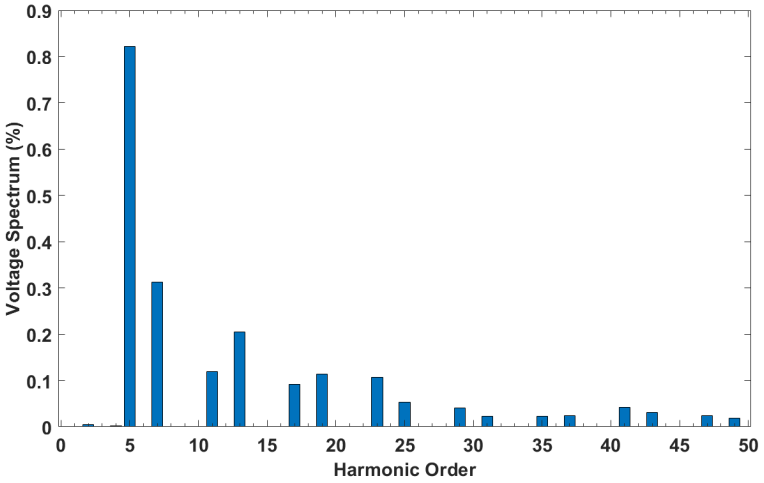

Figure 4.13: Propulsion busbar harmonic spectrum

Comparing the results from table 4.13 and 4.14 with the values from section 2.1.5, it is clear that the simulated values are much lower compared to the calculated values of section 2.1.5. Calculating the THD_V of the spectra used, the THD_V of the generator, VFD and converter is 1.85%, 5.17% and 4.45% respectively, so these do seem representative. In the simulation, the phase angles of the harmonic spectrum generated by Matlab was also used. If these phase angles are set to zero, the THD_V will increase from 0.93% to 2.21% for the second scenario.
For Alewijnse, it will be important to directly compare the result of their internal tool to the simulated value of ETAP. This should be done using the same component values and for components where the harmonic spectrum is provided by the manufacturer. This is outside the scope of this thesis.

5

Hybrid DC grid simulation

5.1. Single Line Diagram

The second system is based on a DC grid and is shown in figure 5.1. This system is in many ways similar to the AC grid system, but there are a couple of key differences. In this system, the main busbar is divided in only two sections. The port side and starboard side are not identical as there are only three generators that are all the same size. On the port side, there is one generator and the battery, one propulsion thruster, two smaller thrusters and the connection to the AC 400V distribution board. The port side also has the option to connect a shore connection instead of the generator, but this is not modeled.

On the starboard side, there are two generators, another battery that is the same as the battery on the port side, one propulsion thruster and one bow thruster and also the connection to the AC 400V distribution board. Both batteries are directly connected to the DC busbar without a DC/DC converter and all AC components are connected to the DC busbar with inverters and (motor) converters. In ETAP, all thrusters have to be modeled with both an inverter and a Variable Frequency Drive, but in the real system these two components are integrated. Other limitations of ETAP regarding the DC grid simulation were encountered as well and they will be mentioned in the section of the corresponding simulation study.

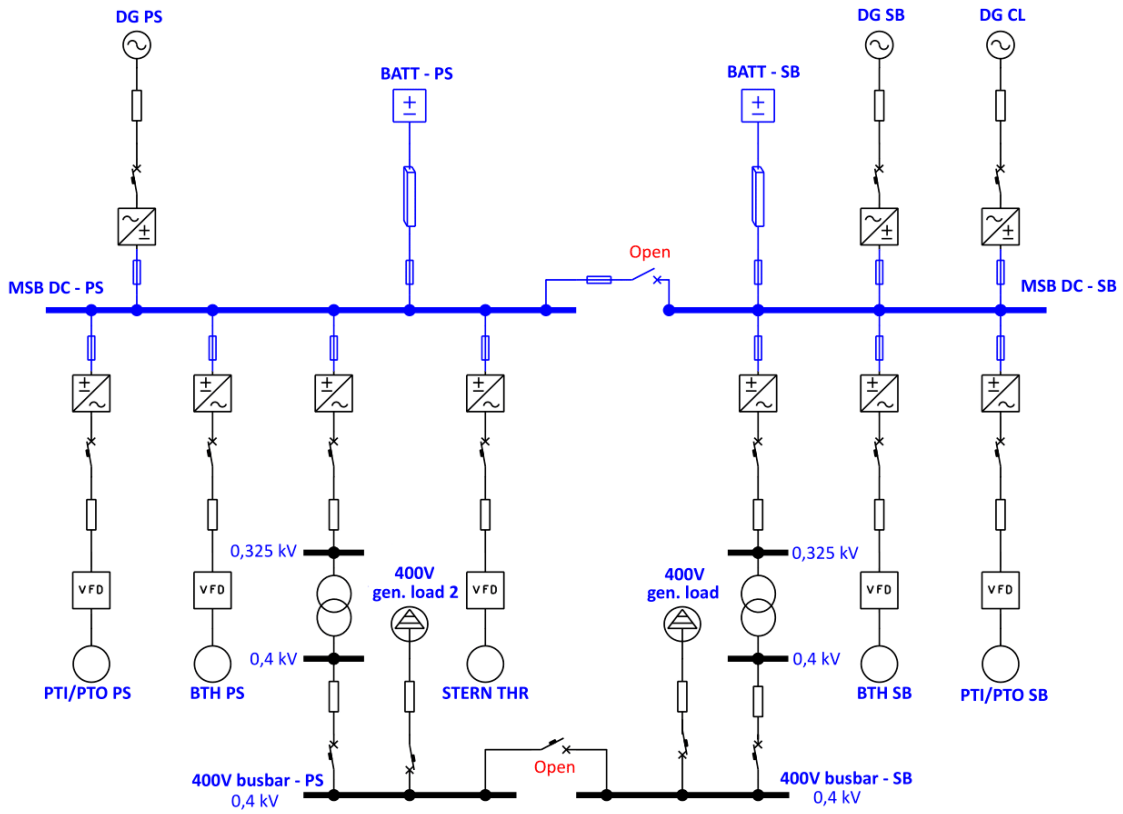

Figure 5.1: Single line diagram DC grid

5.2. Generator specifications

The general specifications of the generators and loads in the Single Line Diagram from figure 5.1 are shown in table 5.1 and 5.2. More specific simulation parameters are given in section A.3.

Table 5.1: Specification of DC grid generators

Generators		
rated power	582	kVA
rated power	465.6	kW
voltage	400	V
current	840	A
frequency	50	Hz
power factor	0.8	
poles	4	
speed	1500	rpm
winding resistance per phase	3.4	mΩ

Table 5.2: Specification of different DC loads

Loads		
Batteries	500	kWh
Generator converters	850	A
PTI/PTO thrusters	550	kW
PTI/PTO inverters	1150	A
Bow thrusters	200	kW
Stern thruster	200	kW
Bow and stern inverters	460	A
Transformers	600	kVA
transformer inverters	2060	A
400 gen. loads	400	kVA

All three generators are 4-pole synchronous machines that will be running at their 1500rpm to create a steady 50Hz for the generator converters. The generators are using the same excitation and governor as the generators in chapter 4. The converters are rated at 850A and will be able to cover the full load of the generators. The two batteries are directly connected to the busbar without any converters. The two propulsion PTI/PTO thrusters are rated at 550kW at 0.85 power factor and have an inverter rated at 1150A. The two bow thrusters and the stern thruster are all equal at 200kW at 0.85 power factor and have an inverter rated at 460A. The transformers are rated at 600kVA and have grid inverters rated at 2060A. Finally, the 400 gen. loads are modeled at 400kVA and have a 65% static and 35% motor part at 0.85 power factor.

5.3. Load flow study

To get an idea of bus voltages and the loading of the generators, a load flow study is performed. In ETAP it is possible to perform a hybrid AC/DC load flow study using the Time Domain Load Flow analysis in ETAP, but it is not possible to properly use the battery. The integrated BMS can only charge or discharge the battery based on a bus voltage or loading. This is useful in the case of renewable resources, but not for studying peak shaving for example. It is also not (yet) possible to create a custom BMS to implement this functionality. Because of this, the battery will be connected, but not used.

In the first situation, the vessel is simulated to be in DP mode, meaning the circuit breaker connecting the port side and starboard side is open. The circuit breaker between the two 400V busbars is open as well and so are the breakers for the propulsion thrusters. The results are shown in tables 5.3, 5.4 and 5.5.

Table 5.3: Load flow results busbars - full load, no battery

Bus ID	**Voltage (V)**	**kW Loading**	**kvar Loading**
MSB DC - PS	648.6	379.4	-
MSB DC - SB	649.4	317.0	-
400V busbar - PS	400.1	204.5	126.8
400V busbar - SB	398.6	202.9	125.8

Table 5.3 shows the busbar voltages and loading. The bus voltages all deviate less than 1% which makes sense as the battery is connected to the DC busbar, acting as a steady voltage source. The loading is very similar on the 440V busbars as the load is the same and the difference in loading between the DC busbars can be explained by the extra thruster being connected on the port side.

Table 5.4: Load flow results generators - full load, no battery

Generator ID	kW	kvar	Amp (A)	PF (%)	Loading (%)
DG PS	399.3	247.5	679.0	85.0	80.8
DG SB	166.9	103.4	283.5	85.0	33.8
DG CL	166.9	103.4	283.5	85.0	33.8

Table 5.4 shows the generator loading in the first situation. The generator on the port side is loaded at 80% as it is powering both the bow and stern thruster on its own. On the starboard side, both generators are sharing the load an are only loaded at 33.8%. The power factor for all generators is 85%.

Table 5.5 shows the loading of the thrusters and 400V generic loads. The thrusters are operating at a reduced power factor because their loading percentage is reduced.

Table 5.5: Load flow results loads - full load, no battery

Load ID	kW	kvar	Amp (A)	PF (%)
BTH PS	63.7	54.5	121.0	76.0
STERN TR	63.7	54.5	121.0	76.0
BTH SB	63.7	54.5	121.0	76.0
400V gen. load PS	204.5	126.8	346.6	85.0
400V gen. load SB	202.9	125.8	346.0	85.0

In the second situation, the DC and 440V busbars are connected and only the PTI/PTO propulsion thrusters are running. Table 5.6 shows the busbar voltages and loading in this situation. Similar to the previous situation, the voltage deviation is less than 1%. The overall load is shared between the three generators and the DC busbar loading is again directly related to the port side only having one generator connected and the starboard side having two generators connected.

Table 5.6: Load flow results busbars - full load, no battery

Bus ID	Voltage (V)	kW Loading	kvar Loading
MSB DC - PS	648.6	399.6	-
MSB DC - SB	648.6	799.2	-
400V busbar - PS	399.3	101.7	63.1
400V busbar - SB	399.3	101.7	63.1

Table 5.7 shows the loading of the generators and the loads in this situation. The load is shared between the three generators and all are loaded exactly the same. This is also the case for the propulsion thrusters and the 400V generic loads. The propulsion thrusters have a power factor of 80.6% as they're loaded at 70%.

Table 5.7: Load flow results generators - full load, no battery

Component ID	kW	kvar	Amp (A)	PF (%)	Loading (%)
DG PS	399.3	247.5	715.3	85.0	85.2
DG SB	399.3	247.5	715.3	85.0	85.2
DG CL	399.3	247.5	715.3	85.0	85.2
PTI/PTO PS	412.4	302.8	738.5	80.6	70
PTI/PTO SB	412.4	302.8	738.5	80.6	70
400V gen. load PS	101.7	63.1	173.1	85.0	30
400V gen. load SB	101.7	63.1	173.1	85.0	30

5.4. Transient stability study

In the transient stability study, the system is modeled in time domain, but again limitations in ETAP were encountered. The main limitation for this study is that it is not possible to study the DC part of the grid. The two AC parts (generators and loads) are two completely separate systems and there is no power balance between the two. To 'solve' this, the generators are connected to inverters instead of charger components. This is because the inverters have the option to create a custom User-Defined Model (UDM), just like section 4.4 for the AC grid. The model is programmed to restore the power balance and the DC part is ignored. It takes the power that is provided at the loads by the inverters and sets that as the power required for the generator. To show this, just one transient stability study will be simulated. In the future, more advanced capabilities can be programmed into the UDM, to show power sharing between the generators or even 'including' the battery, but these functionalities would be difficult to showcase in ETAPs current version and thus don't add much value to this thesis. ETAP can't directly showcase the parameters and variables used in the UDM.

The study case that will be simulated is a combination of a load ramp and a motor starting. The tie breaker connecting the busbars is open and only the propulsion thruster and 440V gen. load on the port side are connected. At $t = 0$s, the loading is 0, but immediately the 440V gen. load starts to ramp during 4 seconds. At $t = 10$s, the propulsion thruster is started through the variable frequency drive.

Figure 5.2a shows the acceleration torque and the slip of the induction motor. Because the speed of the motor is increasing, there must be an acceleration torque. After the motor has reached its final speed at $t = 20$s, the torque drops to 0. The slip starts at 100% and quickly drop to a value close to zero. At the end of the simulation the slip settles at 0.37%. Figure 5.2b shows the mechanical power, electrical power and reactive power of the induction motor. The motor is set to be loaded at 40% of its rated value. Figure 5.2c shows the speed of the generator. As the motor suddenly stops accelerating after it has reached its rated speed, there is a spike in the generator speed that quickly resolves. Figure 5.2d shows the active and reactive power of the generators.

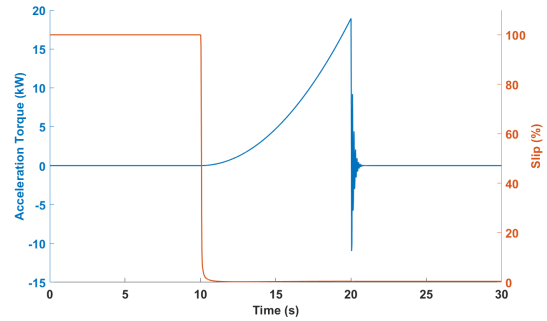

(a) Induction Motor Acceleration Torque and Slip

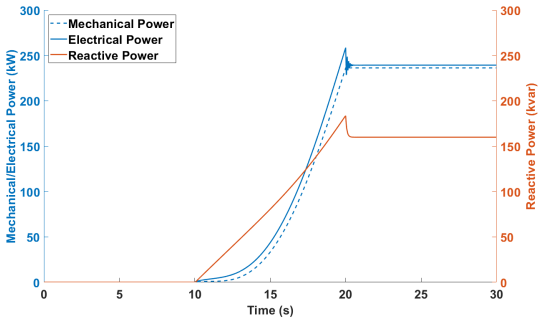

(b) Induction Motor Powers

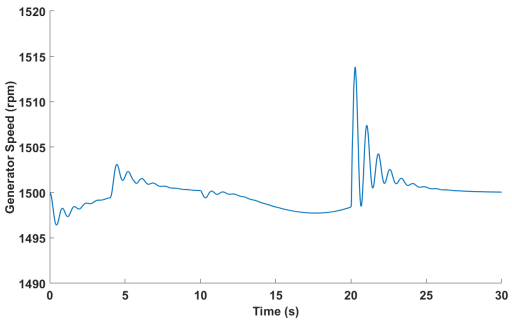

(c) Induction Motor Voltages and Current

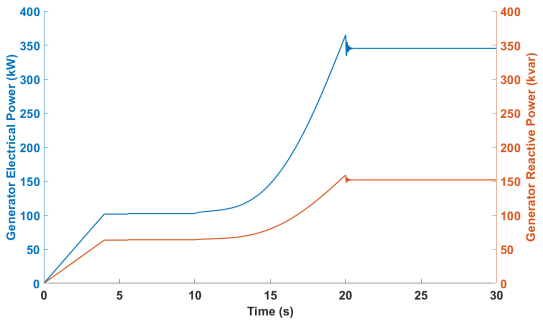

(d) Generator speeds

Figure 5.2: Simulation results for the motor starting simulation

5.5. Short-circuit calculations

The components that will be contributing to the short-circuit current on the DC bus are the battery and the converters. The short-circuit current that the battery will provide is given by the battery manufacturer, but how much the capacitors in the converters will contribute is not known. As discussed in section 3.3.1, the current from a capacitor can be calculated according to the IEC 61660 norm. To get an idea of the peak current and time constant of a capacitor short-circuit, the formulas from section 3.3.1 are used to calculate the short-circuit current of a 2400μF capacitor with a 54.7mΩ series resistance and a 5.5μH series inductance. This graph is shown in figure 5.3. The peak current reached is 6.95kA in 0.134ms. For comparison, the short-circuit current of the battery is specified as 14.9kA with an L/R of 0.16ms.

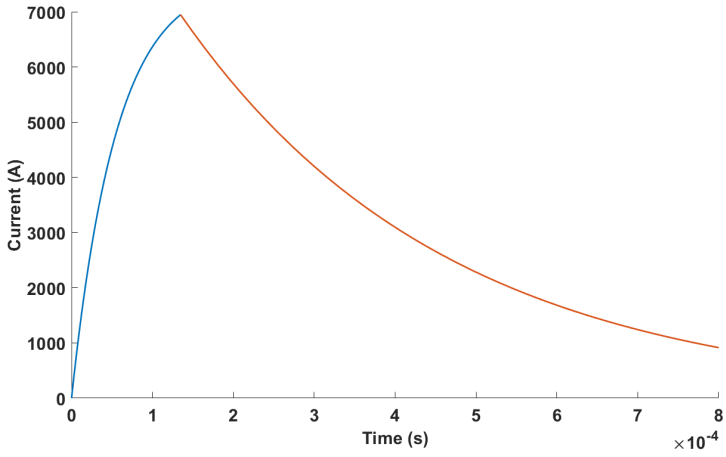

Figure 5.3: Capacitor short-circuit current

Like section 4.5, the short-circuit current of the generators can be calculated according to the AC IEC 61363 standard. Then, the short-circuit current is also simulated using the IEC 61363 calculation tool in ETAP. The result of both is shown in table 5.8.

Table 5.8: Generator short-circuit current

Method	$\mathbf{I_{ac}(t)}$	$\mathbf{I_{dc}(t)}$	$\mathbf{I_p(t)}$
Calculation	7.035 kA	7.689 kA	17.638 kA
Simulation	6.648 kA	7.352 kA	16.648 kA

Similar to the result in section 4.5, there is a slight difference between the calculated and simulated values of the generator short-circuit current. All values that are used for the theoretical calculation are taken from the datasheet, just like the values for the simulation, with one exception. The datasheet did provide an open-circuit transient time constant for the simulation, but not an open-circuit subtransient time constant. This difference between the calculated and simulated value is 5.9%, which is actually one percent less than generator DG#05 from section 4.5.

As mentioned before, the size of the capacitors in the converters in not known and ETAP also does not take them into account. For the charger element, ETAP considers a DC fault current of 150% of the full load current and the inverter elements have no contribution to the DC fault current at all. It is also not possible to manually add a capacitor to the DC grid as DC capacitors are not included in the current version. This means that, in ETAP, the total fault current, in case of a fault on the port side DC bus, would be the sum of the battery fault current and the 1.275kA provided by the charger element connecting the generator to the DC bus.

5.6. Protection & coordination study

The protection and coordination study is much different for the DC bus system, compared to the AC system. The main challenge for selectivity will be on the 400V AC distribution level. For the DC busbar, it will be the challenge to find the right fuse that can sustain the full load of a converter, but also disconnect very quickly in case of a short-circuit. In this system it will be an advantage that the battery is directly connected to the DC busbar as the short-circuit level of the battery should stay close to the value from the datasheet, regardless of the state of charge. This is because the internal resistance of the battery is very low and will only significantly increase at a very low state of charge. Since the battery state of charge is predicted to approach 25% as the lowest value, this should not be an issue.

The goal of the fuses is to disconnect the fault current before the converter gets damaged. The datasheet of a fuse will provide the Total Clearing I^2t, which indicates the thermal energy through the fuse until the current is completely interrupted. Using figure 5.3, the I^2t of the short-circuit current and the time at which the I^2t of the fuse is reached can be calculated. If figure 5.3 is paired with a Eaton Bussmann 170M1790 with an I^2t of 9350, the I^2t of the short-circuit current is equal to that of the fuse at t=0.351ms. The I^2t over time is shown in figure 5.4a and the I^2t value of the fuse should intercept this curve, otherwise it will not clear the fault. The A/μs rise of the short-circuit can also be calculated and is shown in figure 5.4b.

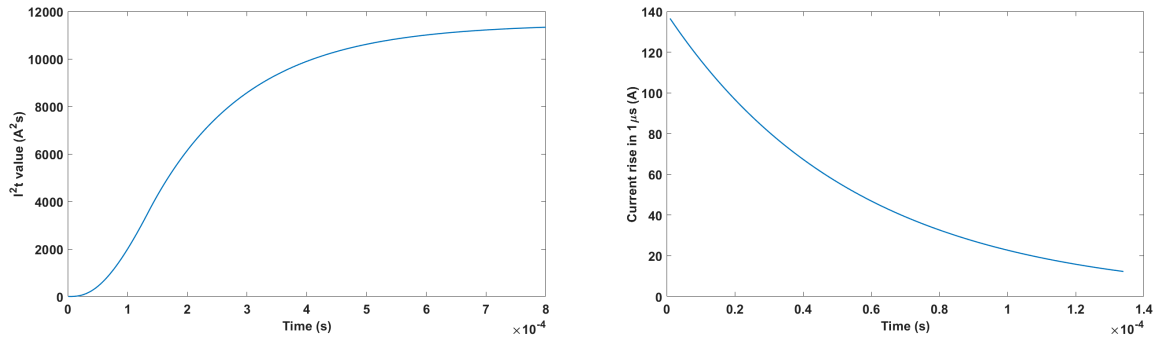

(a) Short-circuit current I^2t curve over time

(b) Short-circuit current rise

Figure 5.4: Short-circuit current plots

In case of a short-circuit at the DC busbar when the port side and starboard side busbar are connected, the DC breaker has to open before any fuses on the non-faulted side reach their I^2t. When this is the case, there is selectivity between the port and starboard side and the non-faulted side will keep operating and the fuses there don't get damaged.

In case of a short-circuit at one of the generator terminals, there is no need for lock-signals between generator breakers. In case of a fault current, the circuit breaker needs to clear the fault as soon as possible as other generators do not directly contribute to the fault current.

In case of a short-circuit fault at the 400V busbar, the situation will depend on if the two 400V busbars are connected and which transformer from the DC side is supplying the 400V busbar. If the 400V busbars are connected and the port side transformer is supplying the fault for example, when the fault is on the starboard side, the circuit breaker connecting the two busbars will detect this and send a lock-signal to the transformer circuit breaker on the 400V side. If the fault is on the port side, the circuit breaker connecting the two busbars will still open, but it will not send a lock-signal to the transformer circuit breaker. As the circuit breaker did not receive a lock signal, it will then clear the fault.

6

Conclusion

This thesis presents the analysis and modeling of the hybrid vessel's electrical power system. In the first part, a study on power quality, short-circuit current and protection & coordination is performed with the goal to get a good fundamental understanding of the vessel's electrical power system and to answer the following research questions:

- What are the rules and standards related to power quality, harmonics and short-circuit calculations in hybrid AC and DC grids?
- What is the theoretical harmonic influence of various electrical components?
- What is the theoretical short-circuit contribution of various electrical components?
- What is the best approach for achieving selectivity in hybrid AC and DC grids?

It was found that as the standard for harmonic control in electrical power systems, the IEEE 1159 describes the recommended practice for monitoring electrical power quality. The IEC 61000 classifies electromagnetic phenomena that are related to power quality. Other norms related to power quality, harmonics and voltage quality are the IEEE 519, IEC 60533 and EN 50160. Classifiers such as DNV, Bureau Veritas and Lloyd's Registrar each have their own requirements related to harmonics and voltage quality, but these requirements are often based on the various standards.

The harmonic influence of various electrical components from the typical maritime electrical power system has been discussed as well as different filters that can improve the harmonic distortion. Big sources for harmonic distortion were found to be the battery energy store system, HVAC and converters without an active front-end. Proper filter design is important and installation of an active harmonic filter can sometimes be a necessity.

For calculating AC short-circuit currents, there are two main IEC standards, the IEC 60909 and the IEC 61363. The IEC 61363 outlines procedures for calculating short-circuit currents that may occur on a marine or offshore AC electrical installation and is the standard that is followed in this thesis. Generators are the major contributors to the short-circuit current. The transformer short-circuit impedance will determine the fault current on the distribution as there is typically no generation there. Asynchronous motors are almost always connected through a Variable Frequency Drive (VFD) so they don't contribute as much as they would when connected directly. The short-circuit current of VFDs will depend on the specific design, but is generally taken as 150% of the full-load current.

For calculating DC short-circuit currents, there is only one IEC standard, the IEC 61660. The standard outlines typical DC short-circuit current diagrams and a standard approximation function to describe the currents as a function of time. A battery or capacitor bank connected directly to the DC busbar is the biggest contributor to the short-circuit current. The IEC 61660 is lacking in the fact that it dates from 1997 and does not provide any calculations for Lithium-Ion batteries and modern converters. There is currently no standard that clearly describes the contribution of all modern day components and educated guesses have to be made instead.

Selectivity in AC grids is achieved through time-current selectivity combined with zone selectivity. Measuring the direction of the fault current and communication between breakers is critical for optimal selectivity and to have redundancy within the system. In DC grids, the I^2t rating of the fuses and fault current is very important for protection. Semiconductor based DC circuit breakers are important for optimal selectivity, but it is not economically viable to use these breakers everywhere.

For the second part of the thesis, two hybrid system models have been created in ETAP's simulation software. The first model is based on an AC bus and various studies have been successfully simulated. These studies include a load flow study, transient stability study including peak shaving and virtual generator simulations for the battery, short-circuit calculation, a protection & coordination study and a harmonic study. In the transient stability study also the critical clearing time of the generators has been analyzed and the protection & coordination study discussed a strategy that can clear a fault before the critical clearing time of the generators.

The second model is based on a DC bus and again, various studies have been successfully simulated. Some challenges with ETAP regarding DC grid simulations have been discussed as well. Furthermore, the formulas and standard approximation function of the IEC 61660 have been used to calculate the short-circuit current and I^2t of a capacitor. Finally, a protection strategy has been discussed to protect the system in case of a short-circuit fault.

A manual for ETAP has also been created as part of this thesis, as well as a draft for a conference paper based on this thesis. These are attached in appendix C and D respectively.

Limitations and recommendations

While the author has tried to implement as much actual data and realistic situations as possible, there are some limitations to the presented work. Informational limitations are the lack of exact specifications of the synchronous generator exciter and governor system and the exact short-circuit and harmonic contribution of converters and drives. Software limitations are some missing features in ETAP that would have improved the simulation results. These include not being able to implement the circuit breaker 'lock' signals in the simulation, the lack of any DC capacitors and the limited Battery Management System of the included battery. The author urges ETAP to look into adding these features and especially the missing objects.

For future work, it is recommended to try and get hold of the informational limitations mentioned previously to increase the accuracy of the results and to work towards a digital twin model that can be used to help engineers verify their designs and to troubleshoot any problems that may arise when the vessel is doing actual work. It is also recommended to create a second DC bus system where the battery is not connected to the busbar directly, but through a DC/DC converter instead. Reference [39] describes a protection strategy for this case, but it will be interesting to implement this for a vessel. Finally, it is recommended that Alewijnse look into the harmonic study results and compare them to their internal tool for components of which the harmonic spectrum is provided by the manufacturer.

Bibliography

[1] Global Maritime Forum. *Getting to Zero Coalition*. 2019. URL: https://www.globalmaritimeforum.org/getting-to-zero-coalition (visited on 01/02/2023).

[2] CF Matt et al. “Optimization of the operation of isolated industrial diesel stations”. In: *6th World Congress on Structural and Multidisciplinary Optimization*. 2005.

[3] Daniel L. Gerber et al. “Energy and power quality measurement for electrical distribution in AC and DC microgrid buildings”. In: *Applied Energy* 308 (2022), p. 118308. ISSN: 0306-2619. DOI: https://doi.org/10.1016/j.apenergy.2021.118308. URL: https://www.sciencedirect.com/science/article/pii/S0306261921015658.

[4] O. Salor et al. “Electrical Power Quality of Iron and Steel Industry in Turkey”. In: *IEEE Transactions on Industry Applications* 46.1 (2010), pp. 60–80. DOI: 10.1109/TIA.2009.2036547.

[5] Pedro E. Issouribehere et al. “Power quality measurements in a steel industry with electric arc furnaces”. In: *2008 IEEE Power and Energy Society General Meeting - Conversion and Delivery of Electrical Energy in the 21st Century*. 2008, pp. 1–8. DOI: 10.1109/PES.2008.4596177.

[6] Dinesh Kumar and Firuz Zare. “A Comprehensive Review of Maritime Microgrids: System Architectures, Energy Efficiency, Power Quality, and Regulations”. In: *IEEE Access* 7 (2019), pp. 67249–67277. DOI: 10.1109/ACCESS.2019.2917082.

[7] Tomasz Tarasiuk et al. “Review of Power Quality Issues in Maritime Microgrids”. In: *IEEE Access* 9 (2021), pp. 81798–81817. DOI: 10.1109/ACCESS.2021.3086000.

[8] Volker Staudt, Roman Bartelt, and Carsten Heising. “Short-circuit protection issues in DC ship grids”. In: *2013 IEEE Electric Ship Technologies Symposium (ESTS)*. 2013, pp. 475–479. DOI: 10.1109/ESTS.2013.6523779.

[9] Peixiao Sun, Zaibin Jiao, and Hanwen Gu. “Calculation of short-circuit current in dc distribution system based on mmc linearization”. In: *Frontiers in Energy Research* 9 (2021), p. 634232.

[10] Espen Haugan et al. “Discrimination in offshore and marine dc distribution systems”. In: *2016 IEEE 17th Workshop on Control and Modeling for Power Electronics (COMPEL)*. 2016, pp. 1–7. DOI: 10.1109/COMPEL.2016.7556731.

[11] ABB. “Onboard DC Grid–The Step Forward in Power Generation and Propulsion”. In: *Technical Brochure* (2011), p. 1.

[12] “IEEE Recommended Practice for Monitoring Electric Power Quality”. In: *IEEE Std 1159-2019 (Revision of IEEE Std 1159-2009)* (2019), pp. 1–98. DOI: 10.1109/IEEESTD.2019.8796486.

[13] Leon M Tolbert, Harold D Hollis, and Peyton S Hale. “Survey of harmonics measurements in electrical distribution systems”. In: *IAS’96. Conference Record of the 1996 IEEE Industry Applications Conference Thirty-First IAS Annual Meeting*. Vol. 4. IEEE. 1996, pp. 2333–2339.

[14] Girish Kumar Singh. “Power system harmonics research: a survey”. In: *European Transactions on Electrical Power* 19.2 (2009), pp. 151–172.

[15] Igor Zhezhelenko and Yuri Sayenko. “Analysis methods of interharmonics investigations in power supply systems”. In: *Ninth International Conference on Harmonics and Quality of Power. Proceedings (Cat. No. 00EX441)*. Vol. 1. IEEE. 2000, pp. 61–63.

[16] “IEEE Standard for Harmonic Control in Electric Power Systems”. In: *IEEE Std 519-2022 (Revision of IEEE Std 519-2014)* (2022), pp. 1–31. DOI: 10.1109/IEEESTD.2022.9848440.

[17] Shailendra Jain. “Chapter One - Power Quality: An Introduction”. In: *Modeling and Control of Power Electronics Converter System for Power Quality Improvements*. Ed. by Sanjeet Kumar Dwivedi et al. Academic Press, 2018, pp. 1–29. ISBN: 978-0-12-814568-5. DOI: https://doi.org/10.1016/B978-0-12-814568-5.00001-6. URL: https://www.sciencedirect.com/science/article/pii/B9780128145685000016.

[18] “Rotating electrical machines - Part 1: Rating and performance”. In: *IEC Std 60034-1:2022* (2022), pp. 1–161.

[19] George J Wakileh. “Harmonics in rotating machines”. In: *Electric Power Systems Research* 66.1 (2003), pp. 31–37.

[20] PA Hargreaves, BC Mecrow, and R Hall. “Open circuit voltage distortion in salient pole synchronous generators with damper windings”. In: (2010).

[21] Chang Eob Kim and J.K. Sykulski. “Harmonic analysis of output voltage in synchronous generator using finite-element method taking account of the movement”. In: *IEEE Transactions on Magnetics* 38.2 (2002), pp. 1249–1252. DOI: 10.1109/20.996319.

[22] Dr. Jawad Al-Tayie, Chris Whitworth, and Dr. Andreas Biebighaeuser. “AC Generators with 2/3rd and 5/6th winding pitch”. In: *Technical Information from Cummins Generator Technologies* (2013).

[23] Vacon. “Active front end unit (AFE) user manual”. In: *Vacon NX AC Drives* (2018).

[24] Joable Andrade Alves, P Torri, and G da Cunha. “Medium voltage industrial variable speed drives”. In: *Pulse* 6.7.0 (2009), pp. 8–.

[25] Admin. *How to choose a medium voltage VFD: Line side connection and power quality*. May 2019. URL: https://mb-drive-services.com/how-to-choose-mv-vfd-line-conn/.

[26] Danielle Collins. *Construction and benefits of an active front end (AFE) drive*. Aug. 2018. URL: https://www.motioncontroltips.com/what-are-the-benefits-of-an-active-front-end-afe-drive/.

[27] Marco Liserre, Frede Blaabjerg, and Steffan Hansen. “Design and control of an LCL-filter-based three-phase active rectifier”. In: *IEEE Transactions on industry applications* 41.5 (2005), pp. 1281–1291.

[28] Aleksandr Reznik et al. “LCL filter design and performance analysis for grid-interconnected systems”. In: *IEEE transactions on industry applications* 50.2 (2013), pp. 1225–1232.

[29] Muhammed H. Rashid, S. Mark Halpin, and Angela Card. “Power Electronics Handbook 3rd edition”. In: Elsevier, 2011. Chap. 40.

[30] Janitza Electronics. *Voltage dips and interruptions*. 2023. URL: https://www.janitza.com/voltage-dips-and-interruptions.html (visited on 08/14/2023).

[31] “Electrical installations of ships and mobile and fixed offshore units - Part 1: Procedures for calculating short-circuit currents in three-phase a.c.” In: *IEC Std 61363-1:1998* (1998), pp. 1–81.

[32] Eaton. “Protecting semiconductors with high speed fuses”. In: *Application Guide 10507* (2016).

[33] “Short-circuit currents in d.c. auxiliary installations in power plants and substations Part 1: Calculation of short-circuit currents”. In: *IEC Std 61660-1:1997* (1997), pp. 1–84.

[34] Salvatore Favuzza et al. “A General Methodology for Short-circuit Calculations in Hybrid AC/DC Microgrids”. In: *IEEE Transactions on Industry Applications* (2023).

[35] Sim Sang-Bo. “Study on the explosion and fire risks of lithium batteries due to high temperature and short circuit current”. In: *Fire Science and engineering* 30.2 (2016), pp. 114–122.

[36] ABB. “Low voltage selectivity with ABB circuit-breakers”. In: *Technical Application Papers* (2008).

[37] Alstom. “Network Protection & Automation Guide”. In: Alstom Grid, 2011. Chap. 9.

[38] David Paul. “Understanding Time Current Curves”. In: (2019).

[39] Simon Ravyts et al. “Fuse-based short-circuit protection of converter controlled low-voltage DC grids”. In: *IEEE Transactions on Power Electronics* 35.11 (2020), pp. 11694–11706.

[40] Prabha Kundur. “Power system stability and control”. In: McGraw-Hill, 1993. Chap. 3,4.

[41] Las Vegas University of Nevada. *Synchronous Generators I, EE 340*. 2011. URL: http://www.egr.unlv.edu/~eebag/Synchronous%5C%20Generator%5C%20I.pdf (visited on 12/19/2022).

[42] “IEEE Guide for Test Procedures for Synchronous Machines Including Acceptance and Performance Testing and Parameter Determination for Dynamic Analysis”. In: *IEEE Std 115-2019 (Revision of IEEE Std 115-2009)* (2020), pp. 1–246. DOI: 10.1109/IEEESTD.2020.9050934.

[43] “IEEE Guide for Synchronous Generator Modeling Practices and Parameter Verification with Applications in Power System Stability Analyses”. In: *IEEE Std 1110-2019 (Revision of IEEE Std 1110-2002)* (2020), pp. 1–92. DOI: 10.1109/IEEESTD.2020.9020274.

[44] R. E. Doherty and O. E. Shirley. “Reactance of Synchronous Machines and its Applications”. In: *Transactions of the American Institute of Electrical Engineers* XXXVII.2 (1918), pp. 1209–1340. DOI: 10.1109/T-AIEE.1918.4765572.

[45] Gurakuq Dajaku and Dieter Gerling. “The correct analytical expression for the phase inductance of salient pole machines”. In: *2007 IEEE International Electric Machines & Drives Conference*. Vol. 2. 2007, pp. 992–996. DOI: 10.1109/IEMDC.2007.382811.

[46] P. L. Dandeno. “Supplementary Definitions & Associated Test Methods for Obtaining Parameters for Synchronous Machine Stability Study Simulations”. In: *IEEE Transactions on Power Apparatus and Systems* PAS-99.4 (1980), pp. 1625–1633. DOI: 10.1109/TPAS.1980.319588.

[47] S. Ghodratollah Seifossadat, Mohsen Saniei, and A. Raeszadeh. “Reactive Power Pricing in Competitive Electric Markets Using a Sequential Linear Programming with Considered Investment Cost of Capacitor Banks”. In: (Jan. 2009).

A

Simulation parameters

A.1. AC grid generators

DG#01, DG#04			
direct-axis synchronous reactance	Xd	1.400	p.u.
direct-axis transient reactance	Xd’	0.320	p.u.
direct-axis subtransient reactance	Xd”	0.162	p.u.
quadrature-axis subtransient reactance	Xq”	0.192	p.u.
negative-sequence reactance	X2	0.177	p.u.
zero-sequence reactance	X0	0.045	p.u.
transient open-circuit time constant	Td0’	3.20	s
transient short-circuit time constant	Td’	740	ms
subtransient short-circuit time constant	Td”	47	ms
armature winding short-circuit time constant	Ta	86	ms
asymmetric short-circuit current (peak c.)	Is	31.50	kA
asymmetric short-circuit alternating c. (eff.)	Ik”	12.40	kA
sustained short-circuit current (eff.)	Ikd	7.50	kA

Table A.1: Parameters of DG#01 and DG#04

DG#02, DG#03			
direct-axis synchronous reactance	Xd	1.400	p.u.
direct-axis transient reactance	Xd’	0.320	p.u.
direct-axis subtransient reactance	Xd”	0.168	p.u.
quadrature-axis subtransient reactance	Xq”	0.162	p.u.
negative-sequence reactance	X2	0.165	p.u.
zero-sequence reactance	X0	0.047	p.u.
transient open-circuit time constant	Td0’	3.30	s
transient short-circuit time constant	Td’	785	ms
subtransient short-circuit time constant	Td”	48	ms
armature winding short-circuit time constant	Ta	87	ms
asymmetric short-circuit current (peak c.)	Is	40.60	kA
asymmetric short-circuit alternating c. (eff.)	Ik”	15.90	kA
sustained short-circuit current (eff.)	Ikd	10.70	kA

Table A.2: Parameters of DG#02 and DG#03

DG#05												
Reactances		Unsaturated, (rated kVA): (%)								Time constants:			
SCR		Xd	Xq	X’d	X’q	X”d	X”q	X2	Xo	T’do	T’d	T”d	Ta
0.45		277	141	24.7	141	12.9	16.1	14.5	9.0	2.660	0.238	0.022	0.041
		Saturated, (rated kVA): (%)								Seconds			
Ra (%)	X/R	Xds	Xqs	X’ds	X’qs	X”ds	X”qs	X2s	Xo	T”do	T’q	T”q	T”q0
0.9	11.7	220	112	21.0	112	11.0	13.7	12.3	9.0	0.042	NA	0.020	0.174

Table A.3: Parameters of DG#05

A.2. Exciter and governor parameters

Exciter parameter	Value
T_R	0
VI_{max}	10
VI_{min}	-10
T_C	1
T_B	10
VR_{max}	5.64
VR_{min}	-4.53
K_A	200
T_A	0.015

Table A.4: Parameters of the exciter

Governor parameter	Value
K	20
$T1$	0.25
$T2$	0.019
$T3$	0.005
$T4$	1.99
$T5$	0.7
$T6$	0.4
P_{max}	2, 2.6
P_{min}	0
Td	0.02
$T8$	0.1

Table A.5: Parameters of the governor

A.3. DC grid generators

Xd Synchronous reactance	2.0593	p.u.
X'd Transient reactance	0.1700	p.u.
X"d Sub Transient reactance	0.1164	p.u.
Xq Quad axis reactance	1.2355	p.u.
X"q Quad axis subtransient	0.1342	p.u.
XL Leakage reactance	0.0626	p.u.
X2 Negative sequence	0.1431	p.u.
X0 Zero sequence	0.0178	p.u.
T'd Transient time constant	0.185	s
T"d Sub-transient time constant	0.025	s
T'do OC field time constant	2.35	s
Ta Armature time constant	0.04	s
Short circuit ratio	1/Xd	
Stator Winding resistance L-N	0.0034	Ω
Rotor Winding resistance	1.75	Ω
Number of winding leads	6	

Table A.6: Parameters of the generators used in the DC simulation

B

Synchronous machine

Synchronous machines are very often used in power systems of ships and vessels and are fundamental to the stability of the power system. A schematic of a synchronous machine can be seen in figure B.1. The stator or armature is stationary and has longitudinal slots that contain the armature windings. The rotor is mounted on the shaft and rotates within the stator. The winding on the rotor is called the field winding.

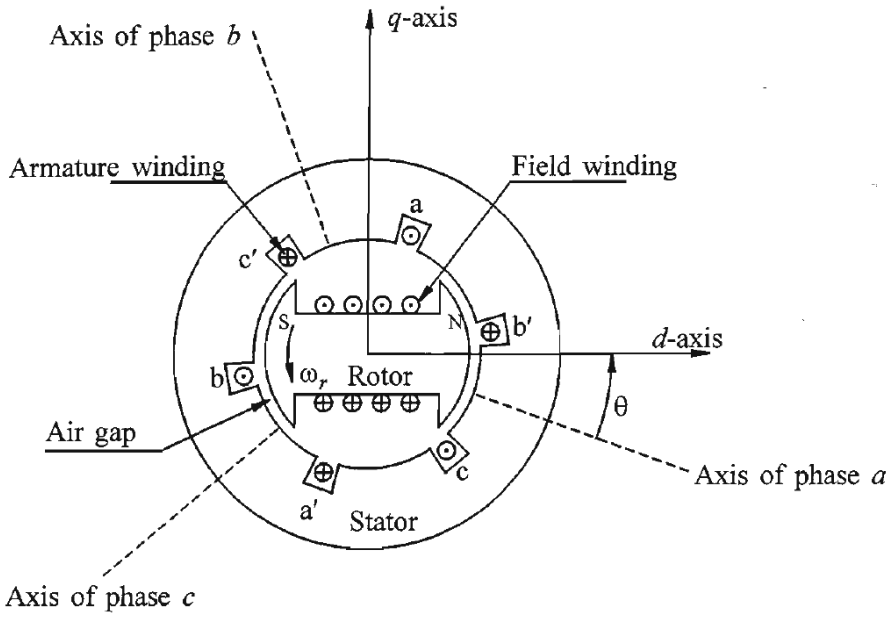

Figure B.1: Schematic of a three-phase synchronous machine [40]

B.1. Basics

The synchronous machine in figure B.1 has two field poles or one pair of field poles. Depending on the speed of the machine, two basic rotor structures are used. A round-rotor machine works at high speeds and has a round or cylindrical rotor made up of solid steel forgings and have either two or four field poles. Salient-pole machines work at low speeds and have a relatively large number of poles and have damper wingdings or amortisseurs. Damper windings consist of connected/shorted copper bars that pass through the poles of the rotor and provide eddy current damping to damp out oscillations that occur on a sudden load change or short circuit. The synchronous speed of a synchronous machine is determined by the number of poles of the machine and the frequency of the system according to

$$f_e = \frac{P}{2}\frac{N_s}{60}\text{Hz} \tag{B.1}$$

Where f_e is the electrical frequency, P is the number of poles and N_s is the synchronous rotor speed in rpm. From this, f_m can be defined as the mechanical frequency, and is equal to $\frac{N}{60}$.

When the machine is used as a generator, a DC current is applied to the rotor windings. This is done either via an external DC source by the means of slips rings and brushes, or via a DC power source mounted directly on the shaft of the machine. Slip rings are metal rings that completely encircle the shaft and they make contact with a graphite or metal brush that rubs the outside diameter of the ring. Through this, DC voltage is supplied to the field windings.

On large generators and motors, brushless exciters are used. A brushless exciter is a small AC generator whose field circuits are mounted on the stator and whose armature circuits are mounted on the rotor shaft. The exciter generator's 3-phase output is rectified to DC through a 3-phase rectifier that is mounted on the shaft and is fed into the main DC field circuit. Through this, it is possible to adjust the field current of the synchronous machine by controlling the small DC field current of the exciter. [41]

In its simplest form, a synchronous machine can be represented by a circuit as shown in figure B.2. In this figure, E_f is the excitation voltage, X_s is the synchronous reactance, R_a is the stator winding resistance and V_t is the terminal voltage. E_a is the internally generated voltage in a single phase of the machine. E_a is equal to V_t when the machine is unloaded. This circuit can be used to study the steady-state behaviour and represents one of the three phases. X_s accounts for all the flux, magnetizing as well as leakage, produced by the armature current.

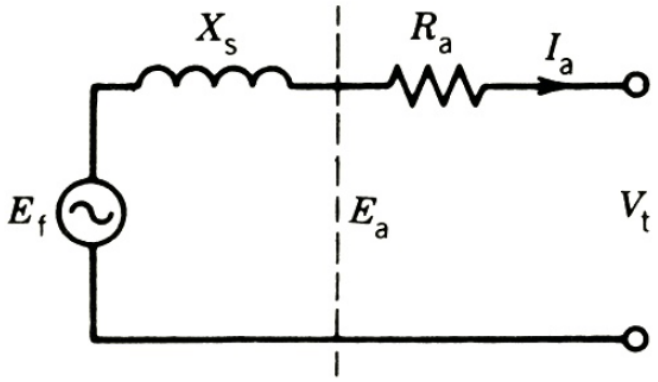

Figure B.2: Synchronous machine simple equivalent circuit

B.2. Dynamic models

In more accurate models it is not possible to describe a synchronous machine with only one resistor and reactance, and there are actually many parameters to consider. Both the stator and rotor have self-inductances ($L_{aa}, L_{ff}, \ldots$) and there are mutual inductances between the phases ($L_{ab}, L_{ac}, \ldots$) and between the phases and the rotor ($L_{af}, L_{bf}, \ldots$). Most of these inductances are dependent on the rotor position as well.

Equations using these inductances to describe flux linkages for example, can be expressed in a simple form by transforming the three-phase a, b and c variables of the stator into three new sets of variables called the direct-axis, quadrature-axis and zero-sequence quantities. These are distinguished by the subscripts d, q, and 0, respectively. The transformation is given in equations B.2 and B.3. Here, the a-axis is aligned to the d-axis through angle Θ. The 0-coil is stationary and the d- and q-coil rotate in synchronism with the rotor.

$$P = \frac{2}{3}\begin{bmatrix} cos\,\theta & cos(\theta - \frac{2\pi}{3}) & cos(\theta + \frac{2\pi}{3}) \\ -sin\,\theta & -sin(\theta - \frac{2\pi}{3}) & -sin(\theta + \frac{2\pi}{3}) \\ \frac{1}{2} & \frac{1}{2} & \frac{1}{2} \end{bmatrix} \tag{B.2}$$

$$\begin{bmatrix} i_d \\ i_q \\ i_0 \end{bmatrix} = \mathbf{P}\begin{bmatrix} i_a \\ i_b \\ i_c \end{bmatrix} \qquad \begin{bmatrix} v_d \\ v_q \\ v_0 \end{bmatrix} = \mathbf{P}\begin{bmatrix} v_a \\ v_b \\ v_c \end{bmatrix} \qquad \begin{bmatrix} \lambda_d \\ \lambda_q \\ \lambda_0 \end{bmatrix} = \mathbf{P}\begin{bmatrix} \lambda_a \\ \lambda_b \\ \lambda_c \end{bmatrix} \tag{B.3}$$

The transformation in equation B.2 is a power variant transformation. There is also a power invariant

version that has $\sqrt{\frac{2}{3}}$ instead of $\frac{2}{3}$ in front of the matrix and replaces the zero-sequence $\frac{1}{2}$ with $\frac{1}{\sqrt{2}}$. It is an advantage that this second version is power invariant, however it removes the unit-to-unit relationship between the abc and dq0 variables. Also, using the first transformation, the inductances in the resulting equivalent circuits correspond to those normally calculated by machine designers.[40]

Figure B.3 shows the stator and rotor circuits of a synchronous machine. It also shows the d- and q-axis and the definition of angle θ. It describes the stator phase windings (a, b, c) and its voltages (e_a, e_b, e_c), currents (i_a, i_b, i_c) and the various flux linkages (Ψ_a, Ψ_b, Ψ_c). The rotor circuit shows the field voltage e_{fd} and current i_{fd}, the d-axis amortisseur current i_{kd} and the q-axis amortisseur current i_{kq}.

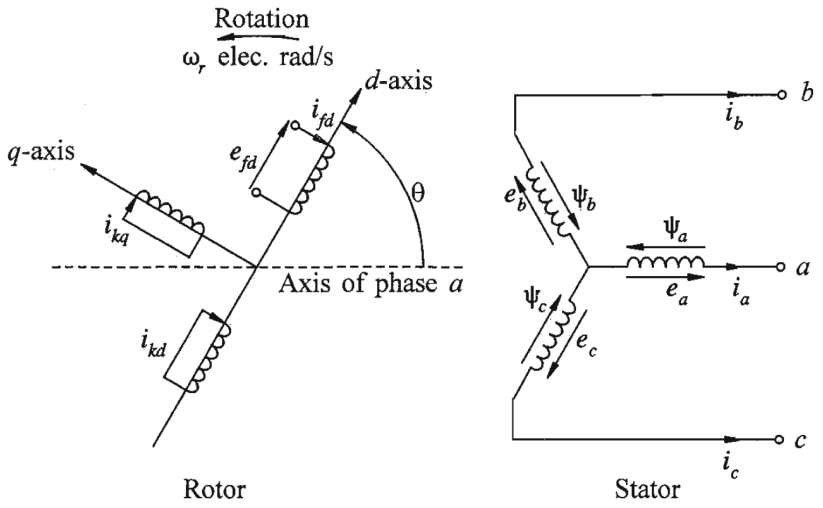

Figure B.3: Stator and rotor circuits of a synchronous machine [40]

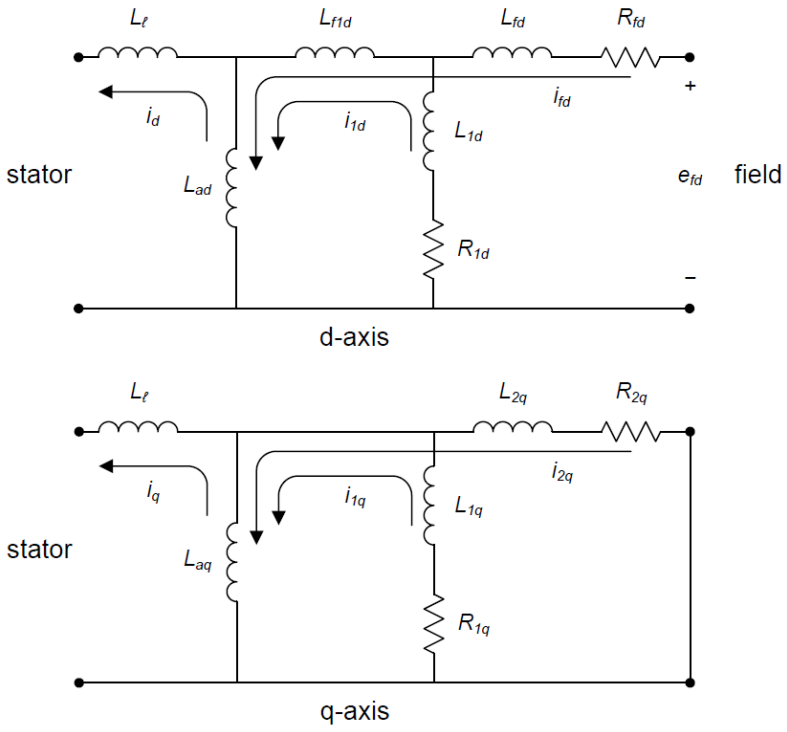

Figure B.4: Synchronous machine equivalent circuit [42]

The IEEE Std 1110 [43] describes various equivalent circuits depending on the number of damper circuits on the d- and q-axis. A commonly used model is one with one amortisseur on the d-axis and two amortisseurs on the q-axis. This equivalent circuit is also used in IEEE Std 115 [42] and is shown in figure B.4. In the stator circuit, L_l is the leakage inductance and L_{f1d} is the differential leakage inductance. L_{ad} is the d-axis mutual inductance between the stator and rotor, L_{1d} and R_{1d} are the d-axis amortisseur inductance and resistance and L_{fd} and R_{fd} are the field inductance and resistance. For the stator, L_{aq} represents the q-axis mutual inductance between the stator and rotor, L_{1q} and R_{1q} are the inductance and resistance of the first q-axis amortisseur and L_{2q} and R_{2q} are the inductance and resistance of the second q-axis amortisseur.

B.3. Transient and subtransient characteristics

Traditionally, the transient and subtransient effects of have been studied by performing short-circuit tests. By analyzing these tests, transient and subtransient parameters have been defined [44], and test methods have been standardized to determine these parameters. These parameters such as reactances and time constants were originally used to give both machine designers and users of synchronous machines first-hand knowledge of short-circuit current magnitudes and their rate of change or decay. These magnitudes are important for establishing switchgear fault ratings and the time constants are used to configure protective schemes.[42]

In total, 10 parameters have been defined: the d- and q-axis synchronous reactances X_d and X_q, the d- and q-axis transient reactances X'_d and X'_q and their time constants T'_d and T'_q and the d- and q-axis subtransient reactances X''_d and X''_q and their time constants T''_d and T''_q. Furthermore, 4 open-circuit time constants T'_{do}, T'_{qo}, T''_{do} and T''_{qo} have been defined.

Apart from determining these parameters through tests, they can also be defined using the parameters discussed in section B.2. L_d, L_q and L_0 can be defined according to equation B.4. L_0 here is the zero-sequence reactance and for all inductances, $X = \omega L$. L_{aa0} is the stator self-inductance and L_{ab0} is the stator mutual inductance. L_{aa2} is the variation in self-inductance as a function of Θ, as defined in figure B.5a. L_{aa2} is equal to L_{ab2} from figure B.5b. The open-circuit time constants are constants that characterize the initial decay of transients in the d- or q-axis variables with the stator windings open-circuited.

$$L_d = L_{aa0} + L_{ab0} + \frac{3}{2}L_{aa2} \qquad L_q = L_{aa0} + L_{ab0} - \frac{3}{2}L_{aa2} \qquad L_0 = L_{aa0} - 2L_{ab0} \tag{B.4}$$

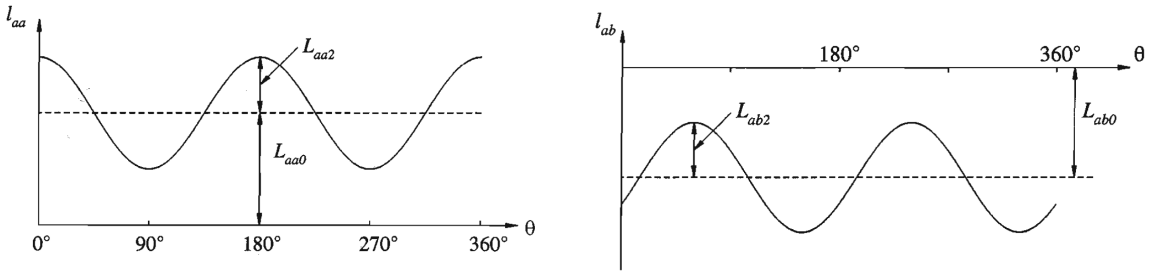

(a) Variation of self-inductance of a stator phase

(b) Variation of mutual inductance between stator windings

Figure B.5: Stator self- and mutual-inductance variance [40] [45]

L_d and L_q can also be written as a sum of the leakage inductance due to flex that does not link any rotor circuit (L_l), and the mutual inductance due to flux that links the rotor circuits (L_{ad}, L_{aq}). This is written out in equation B.5. T'_d and T'_q are the periods over which L'_d and L'_q are defined. L'_d and L'_q are defined by equation B.6 where L_l and L_{fd} are the same as in figure B.4. T''_d and T''_q are the periods over which L''_d and L''_q are defined. L''_d and L''_q are defined by equation B.7.

$$L_d = L_l + L_{ad} \qquad L_q = L_l + L_{aq} \tag{B.5}$$

$$L'_d = L_l + \frac{1}{\frac{1}{L_{ad}} + \frac{1}{L_{fd}}} \qquad L'_q = L_l + \frac{1}{\frac{1}{L_{aq}} + \frac{1}{L_{1q}}} \tag{B.6}$$

$$L''_d = L_l + \frac{1}{\frac{1}{L_{ad}} + \frac{1}{L_{fd}} + \frac{1}{1d}} \qquad L''_q = L_l + \frac{1}{\frac{1}{L_{aq}} + \frac{1}{L_{1q}} + \frac{1}{2q}} \tag{B.7}$$

The L'_q term in equation B.6 and the $\frac{1}{L_{2q}}$ term in equation B.7 are only defined for round rotor synchronous machines and not for salient-pole synchronous machines. Also, in the definitions of equations B.6 and B.7, assumptions have been made that $R_{1d} = R_{2q} = \infty$ during the transient period and that $R_{fd} = R_{1q} = 0$ during the subtransient period. These assumptions have also been made in the classical theory on synchronous machines, but could lead to significant errors between the calculated and measured values. [46] Expressions that reflect the measurements more closely will not be covered in this document but can be found in reference [40] for example.

B.4. Power angle and control

In order to better understand the voltages and control of the synchronous machine, it's easier to go back to the simplified equivalent circuit of figure B.2 and have a look at its phasor diagram.

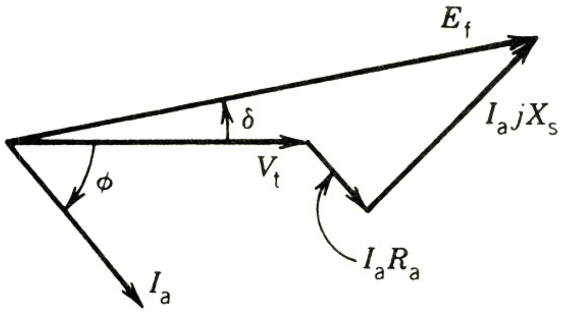

Figure B.6: Phasor diagram of a synchronous machine acting as a generator

In the phasor diagram of figure B.6 is that of a synchronous machine operating in generator mode. The terminal voltage V_t is taken as a reference and all other phasors are drawn accordingly. The angle δ is the angle between V_t and E_f and is called the power angle or rotor angle. E_f can be written as equation B.8.

$$E_f = V_t + I_a R_a + I_a j X_s \tag{B.8}$$

I_a is positive as figure B.2 and B.6 are considering generator mode. In the phasor diagram of figure B.6, the angle δ is positive as well. In motor mode, I_a becomes negative and the angle δ becomes negative as well. The power angle δ can be visualised as is done in figure B.8. The angle Φ is the angle between V_t and I_a and can be used to calculate the power factor according to equation B.9. In figure B.6, the angle Φ is negative, resulting in a *lagging* power factor. If the angle were positive, the power factor is called *leading*.

$$\texttt{power factor} = cos\Phi \tag{B.9}$$

The speed of the synchronous machine can be controlled by controlling the frequency of the applied armature voltage using a variable frequency drive for example. This device is mentioned in section 2.1.3, but the relation between frequency and speed is found in equation B.1. Adjusting the excitation current will change the flux, which in turn changes the excitation voltage. Increasing the excitation voltage E_f of figure B.6 will increase the terminal voltage V_t and decrease the load angle δ. Using this, the terminal voltage can be kept constant in case of a load change. The capability curve shown in figure B.7 is unique for every machine and defines the limits of the synchronous generator and its ability to deliver active and reactive power at a power factor. Point A together with power factor angle Φ indicates the rated power angle of the machine.

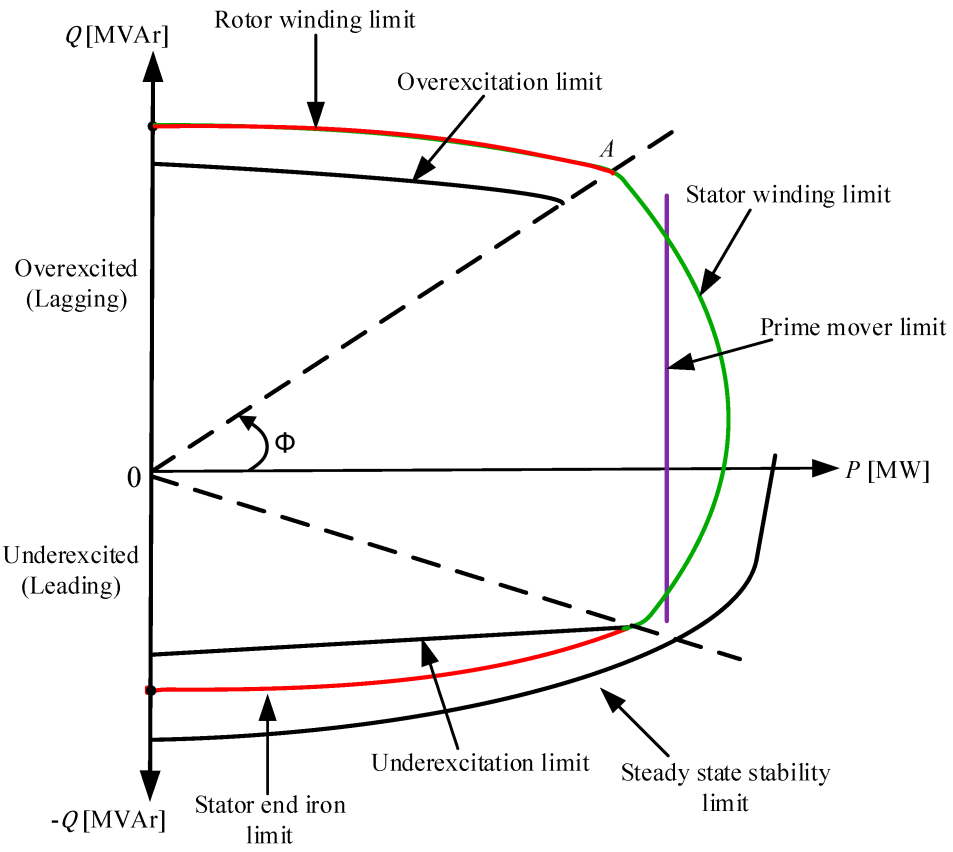

Figure B.7: Capability curve of a synchronous machine acting as a generator [47]

B.5. Stability

Up until this point, only the electrical part of the synchronous machine has been covered. The rotor motion can be described using equation B.10 and is based on the elementary principle in dynamics which states that accelerating torque is the product of the moment of inertia of the rotor times its angular acceleration. In this equation, J is the total moment of inertia of the rotor masses in kg-m^2, Θ_m is the angular displacement of the rotor with respect to a stationary axis, in mechanical radians (rad). T_m is the mechanical or shaft torque and T_e is the net electrical or electromagnetic torque, both in N-m.

$$J\frac{d^2\Theta_m}{dt^t} = T_m - T_e \tag{B.10}$$

The torques T_m and T_e are considered positive for a synchronous generator. When in steady-state operation, T_m and T_e are equal and there is no acceleration or deceleration of the rotor masses. The resulting speed is the synchronous speed N_s from equation B.1.

For stability studies, equation B.10 can be transformed into the so-called swing equation. When the swing equation is solved, an expression of δ as a function of time is obtained, and a graph of the solution can show whether the machine remains in synchronism after a disturbance. To get the swing equation, Θ_m is replaced with δ_m, making it the angular displacement with respect to the synchronously rotating reference axis instead of the stationary axis. The torques T_m and T_e are replaced with P_m and P_e by multiplying the equation with ω_m, and finally $J\omega_m$ can be replaced with $\frac{2H}{\omega_s}$ where H is the stored kinetic energy at synchronous speed divided by the machine rating in MJ/MVA, and ω_s is the synchronous speed in electrical units ($2\pi f$).

$$\frac{2H}{\omega_s}\frac{d^2\delta}{dt^2} = P_m - P_e \tag{B.11}$$

Looking at figure B.8, in case of a sudden load change, the load angle will change from δ_0 to $\delta_0 + \Delta\delta$. The resulting acceleration of the rotor can be calculated using equation B.11. If The load change causes the load angle to increase above $90°$, the synchronous machine may lose synchronism.

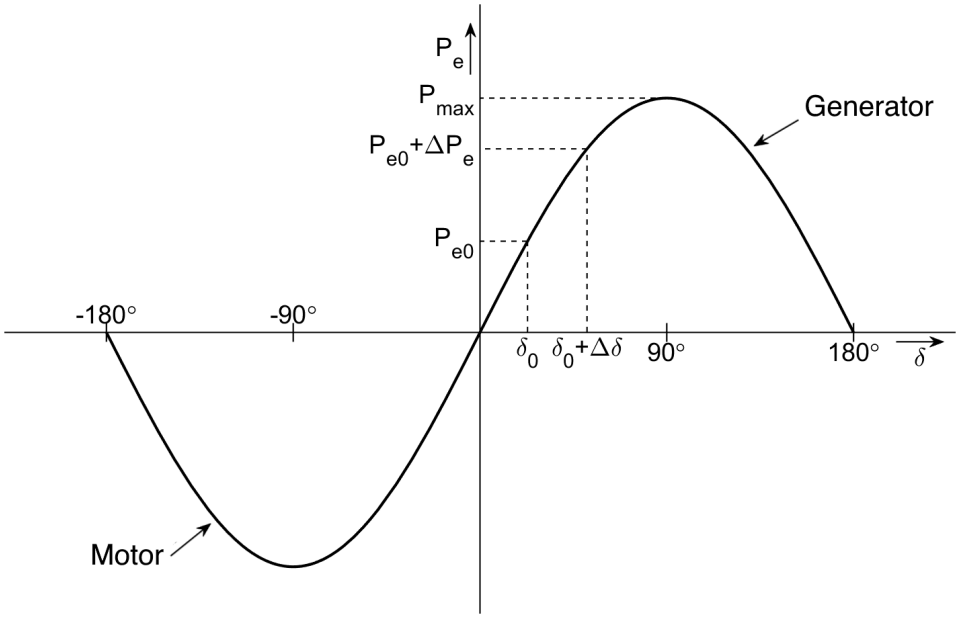

Figure B.8: Power angle curve of a synchronous machine

C

ETAP manual

ETAP manual

Matthijs Mosselaar

August 22, 2023

Introduction

ETAP is an electrical network modeling and simulation software tool that can be used to model and simulate advanced power systems. This document will provide a manual on how to use the software to model, analyze and export results from a power system.

1 Building a model

After starting the software, click on *Create a New Project* to get started. Give it a name, choose the unit system and click *OK*. After this, you can click *OK* two more times until you end up at the following screen:

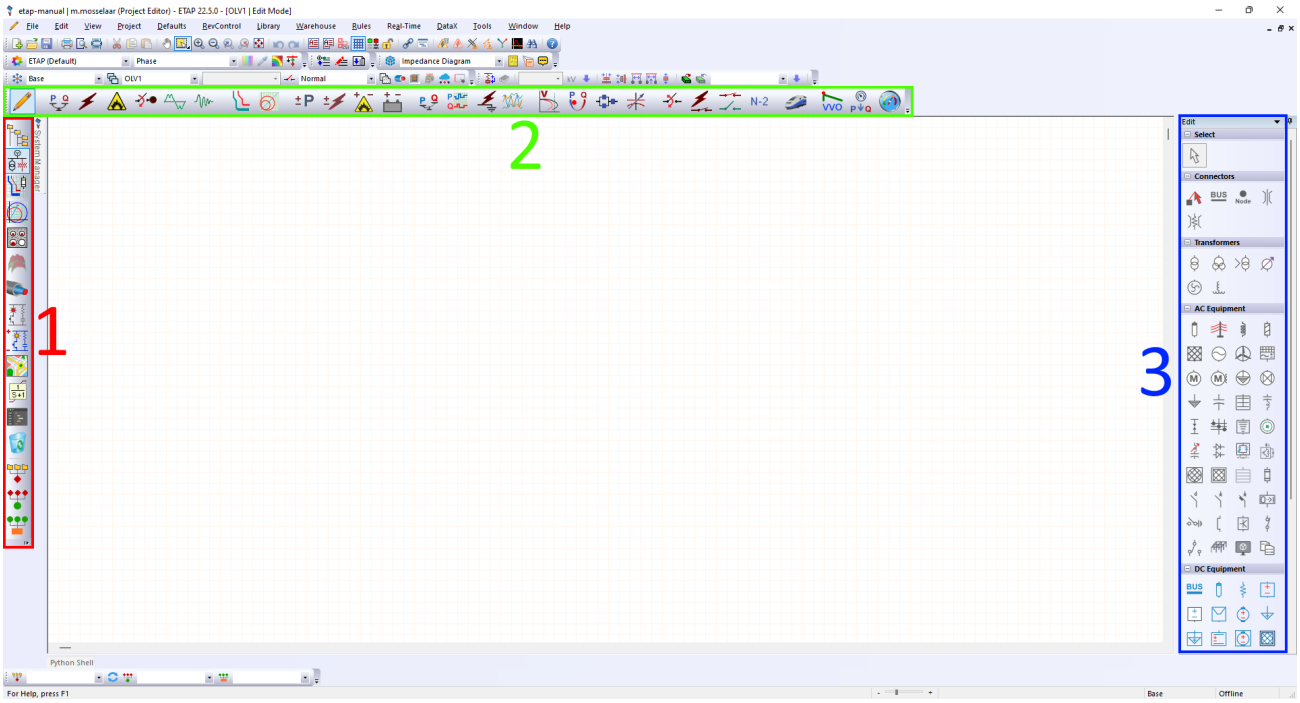

Figure 1: ETAP's One-Line View

In figure 1, 1 switches between various system overviews, the standard *One-Line Diagrams* overview is the most useful one. 2 switches between various studies that can be done, like load flow, short-circuit and protection & coordination. 3 shows the various components that can be used to create the one-line diagram of the system. An example system is shown in figure 2.

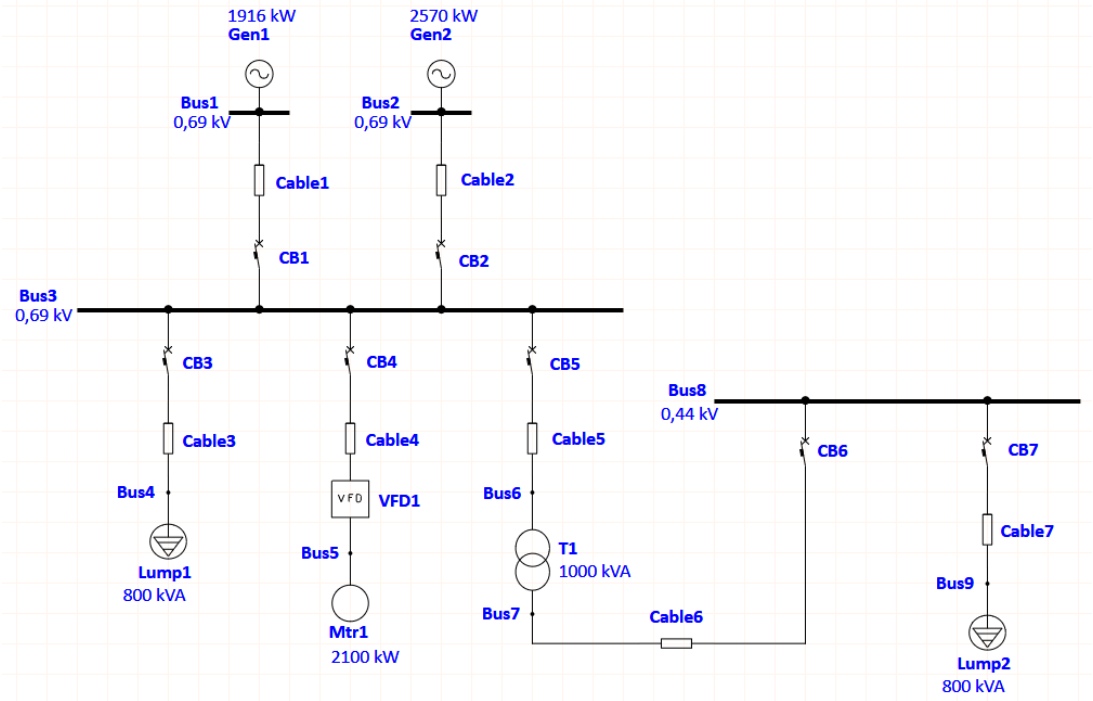

Figure 2: Example system

1.1 Generator data

When double-clicking a component, the relevant data can be inserted. For a generator, the most important data is the following:

- Info page: Operation Mode
- Rating page: The ratings at the top and *Mvar Limits*
- Capability page: Capability curve of the generator
- Imp/Model page: All reactances and time constants of the generator. If unavailable, click *Typical Data* to get started
- Inertia page: the WR^2 or H of the generator
- Exciter page: AC4 with Sample Data is a good one to get started
- Governor page: 2301 with Sample Data and Isoch mode is a good one to get started

1.2 Cable data

For the cable data, it's best to pick one from the library on the Info page. In the pop-up, select a cable and size. Then, back on the info page, set the number of conductors per phase and the length.

1.3 Circuit breaker data

Again, it's best to pick a circuit-breaker from the library, but this time from the Rating page. In the pop-up, select the type, manufacturer, model, size and trip device. The Trip Device page is also important.

1.4 Lumped Load data

The Lumped Load element is a variable load that can also be adjusted during a transient stability study. The important data is in the Nameplate page where the rating and load type is specified.

1.5 Variable Frequency Drive data

For the variable frequency drive, the Rating page is important, as well as the Start Dev page, where the frequency control is defined.

1.6 Induction Machine data

For the induction machine:

- Nameplate page: Ratings at the top including the power factor and efficiency at various load conditions
- Model page: choose a motor circuit model from the library
- Inertia page: the WR^2 or H of the motor
- The load torque characteristics of the motor, again it's easiest to pick one from the *Load Model Lib...*
- Start Dev page: The control type and control characteristics of the motor

1.7 Transformer data

The most important transformer data:

- Rating page: Votage Rating and Power Rating
- Impedance page: If details unavailable, click *Typical Z & X/R*
- Tap page: change tap data and voltage regulation

2 Simulation

This example uses the IEC standard, but with a 60Hz frequency. This can be changed in Project -> Standards.

2.1 Used parameters

For the generators, most of the settings are shown in figure 3. Other than that, both generators are set as Swing, typical data is used in the *Imp/Model* page, Gen1 Generator inertia H is 0.38 and Gen2 Generator inertia H is 0.42. Also, for both, the exciter is AC4 type with sample data and the governor is 2301 type with sample data and Isoch mode.

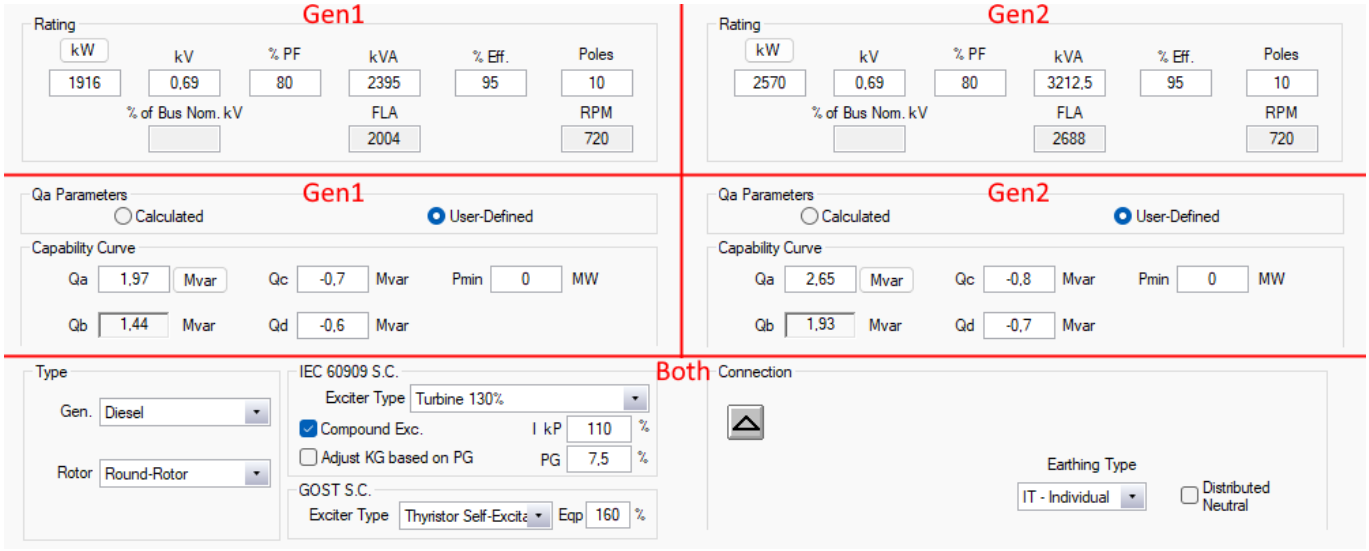

Figure 3: Generator settings

The cable data is shown in table 1. All cables are entry 677 in the ETAP cable library.

Cable name	Size (mm^2)	Conductor #/phase	Length (m)
Cable1	95	14	15
Cable2	95	18	15
Cable3	120	3	115
Cable4	95	6	105
Cable5	120	6	8
Cable6	95	13	12
Cable7	95	6	8

Table 1: Cable settings

Both lumped loads are the same at 800kVA, 90% power factor and 50% motor and 50% static.
The transformer has a 0.69/0.44kV voltage rating and a 1000kVA power rating. Typical Z & X/R is used on the Impedance page.

For the VFD, the main settings are in figure 4.

For the motor, the main settings are in figure 5. When selecting the CKT model, choose the single2 LV-HS-HT, LV200HP2P model and only update short-circuit data and characteristic data, as shown. The motor H is 0.66 in the inertia page and the load model is the pump.

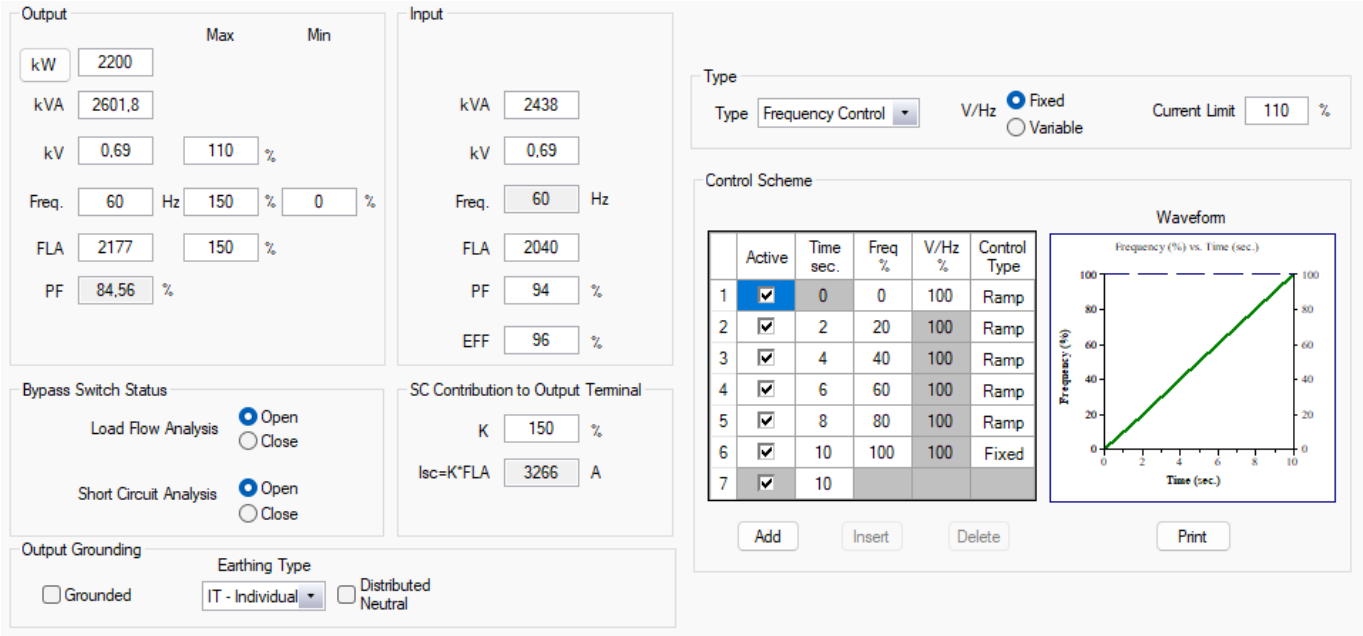

Figure 4: VFD settings

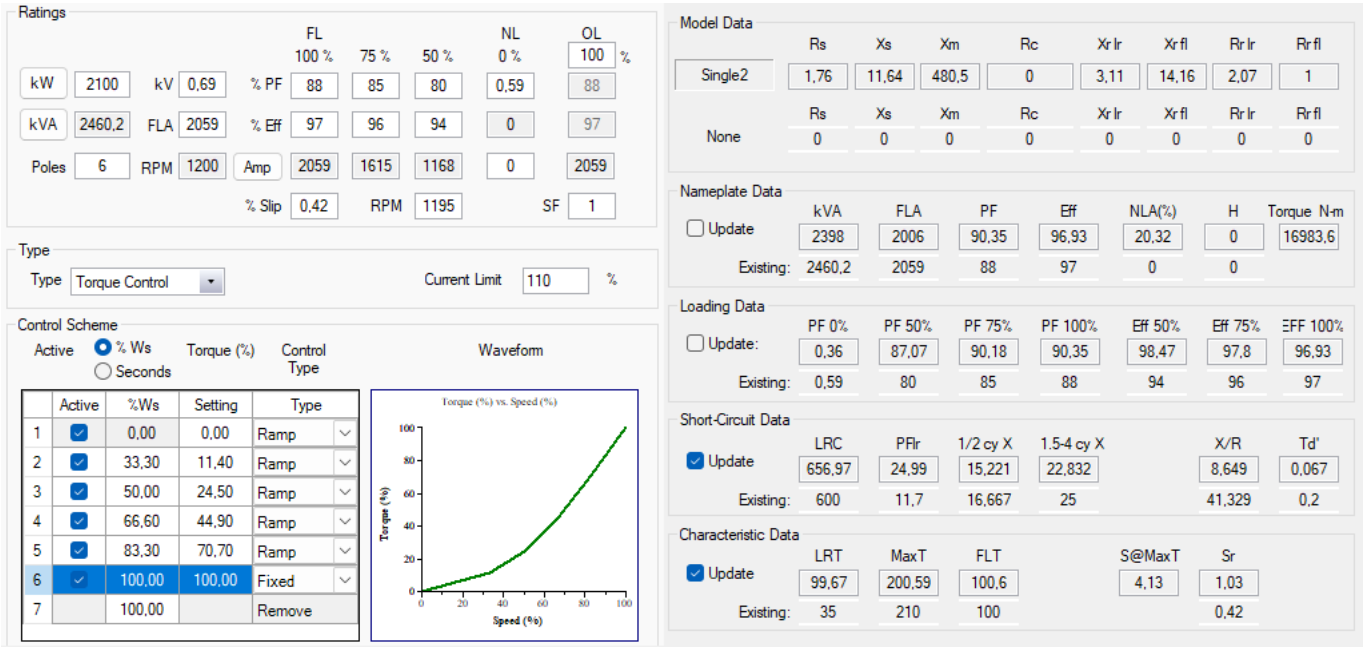

Figure 5: Motor settings

2.2 Load flow simulation

To start a load flow simulation, go to the load flow study, which is the second item in '2' from figure 1. To run the study, click "Run Load Flow", the top-most icon in the bar on the right of the screen. To change the bus voltage from % to volts, click the 9th icon "Display Options" and change the unit. Also select "Show Units" on the bottom of this screen.

The screen should then look like figure 6. The VFD is red and why can be seen in the "Alert View" (4th icon from the top). The 440V bus is colored pink because its voltage dropped below 98%.

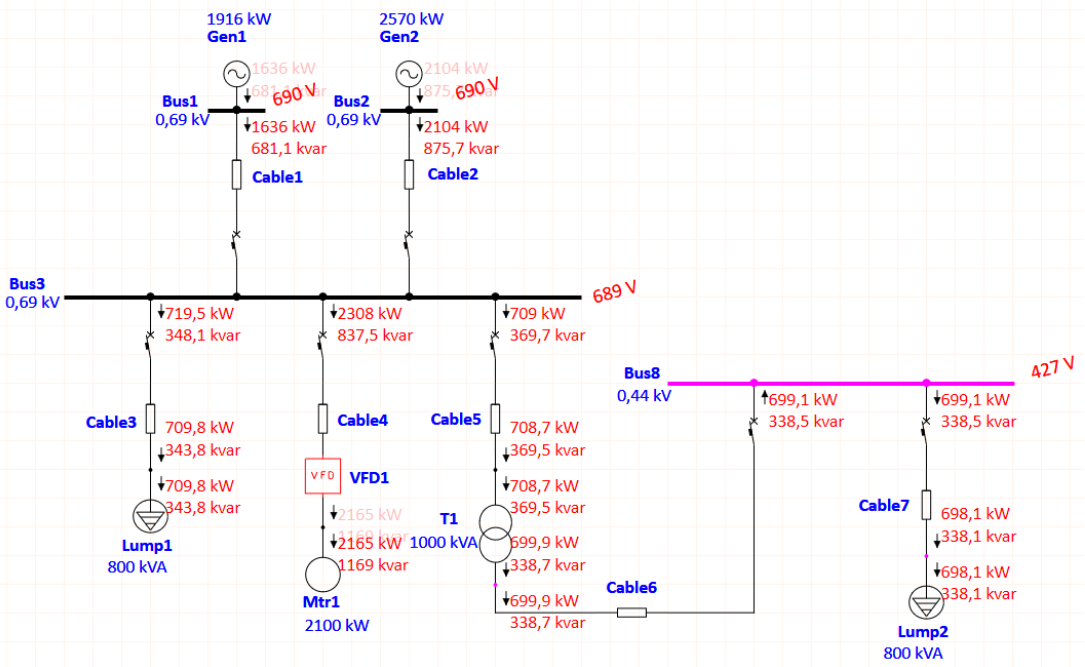

Figure 6: Example system

To edit the study case, click the icon in figure 7. In the Loading page, the loading and generation category can be adjusted. On the Alert page, the marginal and critical percentages can be adjusted.
When adjusting the loading category for example, the simulation will take different loading percentages for the load components. These percentages are usually set in the Nameplate page of the lumped load, motor or other elements.

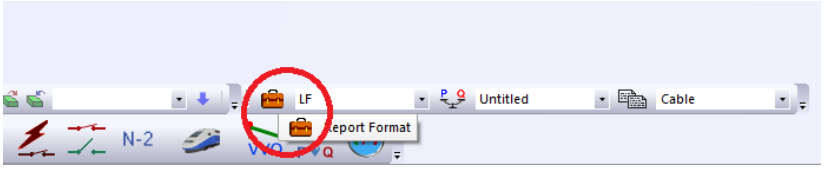

Figure 7: Button to edit the studycase

The results can be displayed in a report by clicking "Report Manager". Then click Result, Load Flow Report and OK.

2.3 Short-circuit simulation

The short-circuit study case is the third item on the study case toolbar. Right click on a bus and select Fault. Then run the 60909 or 61363 simulation in the toolbar on the right. Enable units by clicking "Display Options", and various study case parameters can be adjusted by clicking on the same icon as figure 7.

When running the 61363 simulation, it is also possible to show a plot of the short-circuit current by clicking the "IEC 61363 Short circuit Plots" in the toolbar on the right.

2.4 Transient Stability

For the transient stability study case, some settings in the study case editor have to be adjusted. Open it by clicking on the icon from figure 7. In the Events page, different events with different actions can be set. For this example, create the following according to figure 8 and set the total simulation time to 20 seconds. Furthermore, in the Dyn Model page, click "Ind. Machine, LV" and then "Model Machines Larger or Equal to" right next to it. Do the same for "Lumped Load". Then, in the Plot page, go through all the device types and click "Select All".

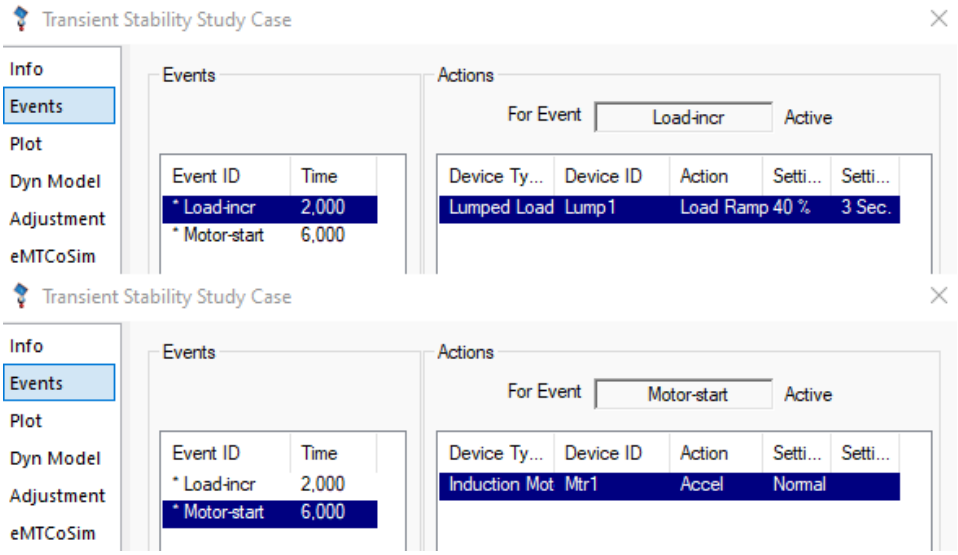

Figure 8: Caption

Now, click on "Run Transient Stability" in the toolbar on the right and ETAP will run the simulation. To show the simulation plots, click on "Transient Stability Plots" in the toolbar on the right. In the menu, the device types and plots can be selected. When viewing the plots for the induction motor, it is clear that something happened around 15.5 seconds into the simulation; the start-up got interrupted. The current graph of the motor shows a transient right around the time the motor stopped starting and this may hint at a current limit of the VFD. In the VFD settings on the Start Dev page, increase the current limit to 120% and the induction motor should now finish its start-up.

The plot data can be exported into excel by clicking on "Export Data" in the top left when viewing the plots. To the right of "Export Data" is "Live-Plot". Click it, minimize the plot window, in the "Start Cat" page of the induction motor set "%Loading" Start and Final both to 80 and run the simulation again. Now go back to the plot window and it has overlaid the new data on top of the old data.

2.5 Protection & Coordination

When in the "Star - Protection & Coordination" study case, select the top half of Bus3 by dragging the mouse. Then, click "Create Star View" in the top of the right toolbar. This switches the view over from "One-Line Diagrams" to "Star Systems" in the toolbar on the left. ETAP now shows the time-current curves of all selected elements in one view. For the generators, it shows automatically generated 'decrement curves'. If a curve is available from the manufacturer, it can be added by clicking "User Curve" in the toolbar on the right.

Because no circuit breakers have been selected yet, these curves aren't shown. Also from the Star Systems view, it is possible to click on the circuit breaker and to select one.
For CB1, select the breaker from figure 9 and set the Rating Plug to 2500 on the Trip Device page. On this same page, disable the instantaneous trip. For CB2, do the same, but select 3200 instead of 2500. The tripping device of the circuit breakers can be adjusted by clicking and dragging the circuit breaker curve. Set CB1 to 0.78 and 3 for the long time and 1.6 and 0.2 for the short time. Set CB2 to 0.83 and 3 for the long time and 1.8 and 0.2 for the short time. Now go back to the One-Line Diagram view on the left toolbar and click "Fault Insertion (PD Sequence-of-Operation)" in the right toolbar. Then click Bus3 and verify that both breakers will trip at 240ms in case of a short-circuit on Bus3.

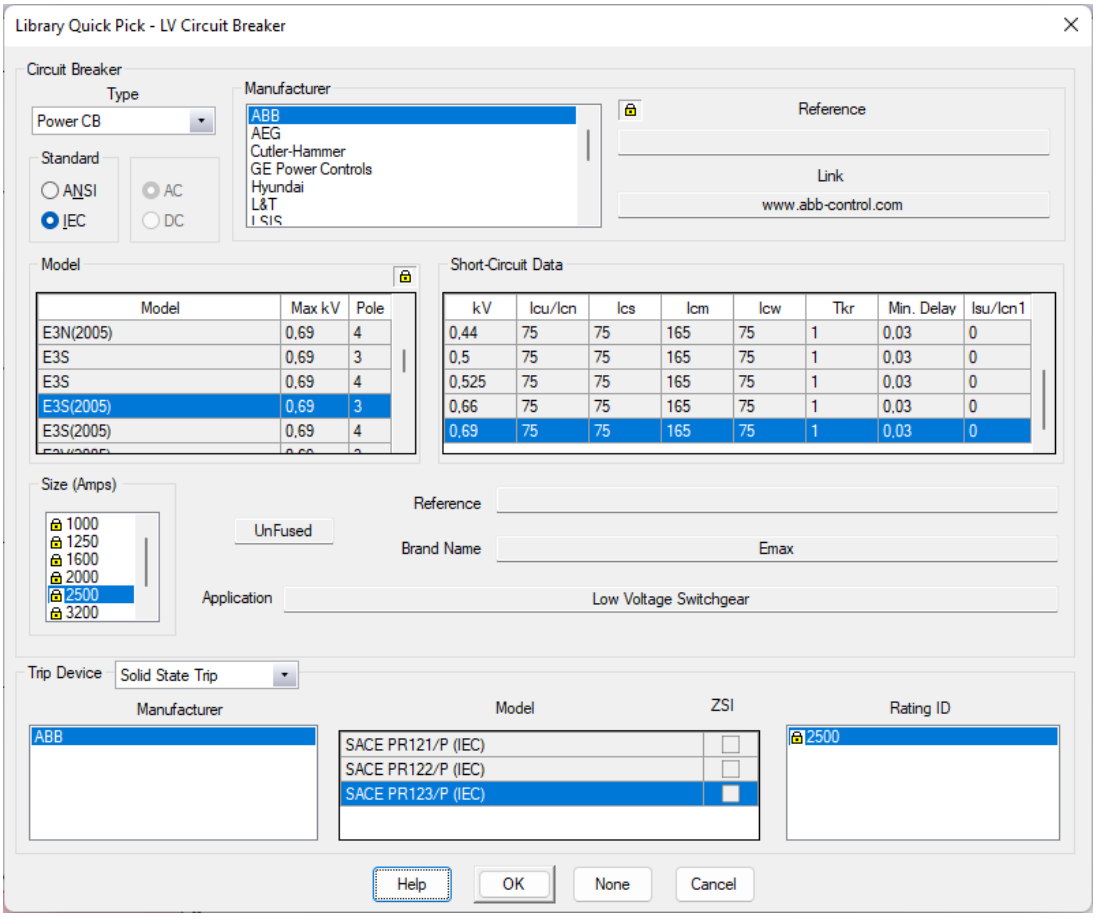

Figure 9: Circuit breaker selection

3 Other elements and studies

Not all capabilities of ETAP are presented in this example, so this section will present more general information about other elements and studies.

3.1 Battery

ETAP has a couple of battery cells in its library, including some Li-Ion cells. In the Rating page, the number of cells, packs and strings can be configured to set the battery voltage and capacity. The BMS of the battery is useful for simulations with renewable sources such as solar or wind.

3.2 Inverter

Important for the inverter is that a DC source must be connected to the inverter DC terminal. If no DC source then the inverter will be automatically considered as not in service. A charger is considered as DC source. If the inverter is set to Voltage control, the "kW ac" on the Generation page can be either positive or negative to allow for battery charging or discharging in the load flow simulation. A UDM model can also be set for the inverter, see next section.

3.3 UDM models

UDM stands for User-Defined Models and it allows for custom dynamic models. These can be added and edited through the UDM Editor. UDM allows for custom exciters, governors, inverters, power system stabilizers and wind turbine generators.

3.4 Time Domain Load Flow simulation

The time domain load flow simulation allows for a simultaneous AC & DC load flow. It also allows for some events to be simulated. Again, there has to be a charger or battery powering the DC bus.

D

Paper draft

Analysis and Modeling of the Hybrid Vessel's Electrical Power System

Matthijs Mosselaar, Zoran Malbašić, Aleksandra Lekić, and M. Popov

***Abstract*—Engineers are always looking to optimize their design strategies and to improve their way of work. This paper presents two electrical hybrid power system models in ETAP simulation software that can be adapted for the engineering of future hybrid vessels. These models are also a step towards a digital twin model that can help in troubleshooting and preventing issues, reducing risk and engineering time. The testing of the models is focused on time domain analysis, short-circuit currents and protection & coordination. The models are based on actual vessels and manufacturer parameters are used where available.**

***Index Terms*—vessel, hybrid, simulation, model, short-circuit current, protection, ETAP**

I. Introduction

The Getting to Zero Coalition is an alliance of over 200 organizations within the maritime, energy, infrastructure and finance sectors. Their goal is to get commercially viable deep sea zero emission vessels powered by zero emission fuels into operation by 2030 for a path towards full decarbonization by 2050. [1] Hybrid ships and vessels play a key role in this transition and it is important to fully understand these hybrid power systems.

Traditionally, a maritime power systems are low voltage, high power systems that are built up from a main busbar to which the main generators and the heavy loads are connected. The voltage level of the systems is usually 690 or 400V and the main busbar may be split in two busbars (port side and starboard side) that can be connected. The frequency is either 50 or 60Hz. From the main busbar, the power can be further distributed on a lower voltage level of 400 or 230V. Often, there is also an emergency generator that can be connected to the main busbar, either directly or through another busbar.

Hybrid systems are not only interesting for newly built vessels, as a battery can be added to older vessels as well. This is typically done during a refit, which happens halfway through the vessel's expected lifetime. A refit can include repairing, fixing, restoring, renewing, mending, and renovating the vessel, depending on its needs. As long as there is space on the vessel to fit the battery and its converter, it should be possible to convert a regular (diesel) vessel to a hybrid vessel. When the vessel has an AC main busbar, the battery can be connected through a bidirectional inverter. When the vessel has a DC main busbar, the battery can be connected either directly or through a DC/DC converter, just like other DC components.

This paper uses ETAP simulation software version 22.5.0 to create two electrical hybrid power system models that can be adapted for the engineering of future hybrid vessels. The first model is based on an AC main busbar and the second system is based on a DC main busbar. Both systems are actual vessels and manufacturer parameters are used where available. The focus of this paper is time domain analysis, short-circuit current calculations and protection & coordination.

II. Hybrid AC grid simulation

The first system is based on an AC bus and is shown in figure 1. The system can be divided in three parts according to the three different sections of the propulsion busbar. The port side (PS) and starboard side (SB) are identical and have two different size 690V generators acting as the main power source. The specifications of the generators can be found in table I. The two inverters connecting the batteries are rated at 1500kW and define the maximum charge and discharge rate of the batteries. The three bow thrusters are rated at 1000kW at 0.85 power factor and the two propulsion thrusters are rated at 2100kW at 0.85 power factor. The cranes are modeled as lumped loads with a 20% static part and 80% motor part with a 0.75 power factor. This results in a 746.7kVA load. The 440 gen. loads are also modeled as lumped loads, but with a 65% static and 35% motor part at 0.90 power factor.

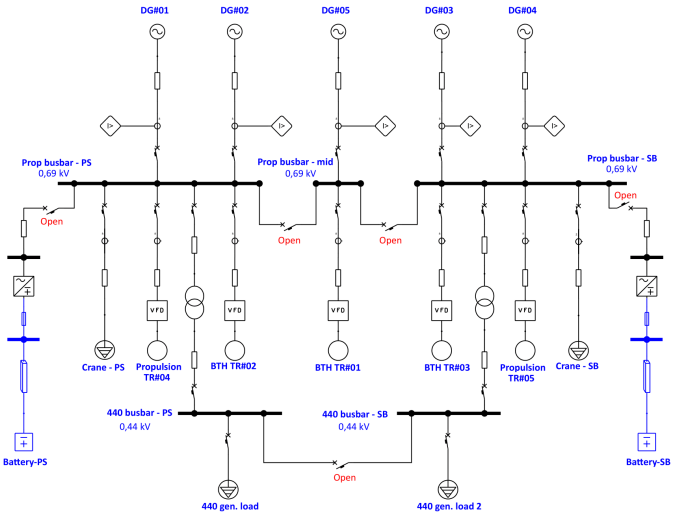

Fig. 1. Single line diagram of the studied AC grid

TABLE I
GENERATOR PARAMETERS

	DG#01 DG#04	DG#02 DG#03	DG#05
Rated power (kVA)	2395	3213	1713
Rated power (kW)	1916	2570	1370
Voltage (V)	690	690	690
Current (A)	2004	2688	1433
Frequency (Hz)	60	60	60
Power factor	0.80	0.80	0.80
Speed (rpm)	720	720	1800
Winding resistance per phase ($m\Omega$)	1.02	0.70	1.46

A. *Time domain analysis*

Two maritime specific time domain simulations are peak shaving and DP mode where the battery may act as a virtual generator. In the peak shaving study case, the goal is to show the peak shaving capability of the inverter. Peak shaving is realized through an ETAP User-Defined Model (UDM) for the inverter that monitors the power of the generators throughout the simulation. If the power were to rise above 80%, the inverter is told to supply the difference, keeping the loading steady at 80%. For DG#01, 80% means 1.5MW and for DG#02, 80% means 2.0MW. The output power of the inverter is limited according to its rating. The inverter is also set to provide reactive power if it were to go above 1Mvar or 1.5Mvar for generator DG#01 and DG#02 respectively.

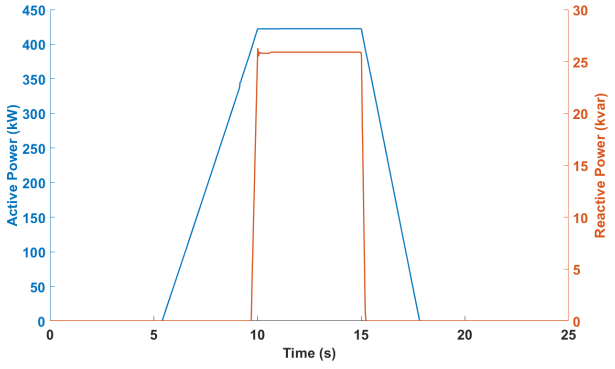

Fig. 2. Inverter active and reactive power

To simulate this, only generator DG#01 is connected and it is loaded slightly under 1.5MW. Then, at $t = 5$s, a lumped load is increased and later decrease, taking the loading of the generator above 1.5MW. Figure 2 shows the inverter during this event. Slightly after $t = 5$s, when the generator power has reached 1.5MW, the inverter starts to provide power according to the increasing load. Only at the very end of the load ramp does the reactive power of the generator go above 1Mvar. Figure 3 shows the mechanical power, electrical power and reactive power of the connected generator. As can be seen, the active power of the generator does not go above 1.5MW and the reactive power does not go above 1Mvar.

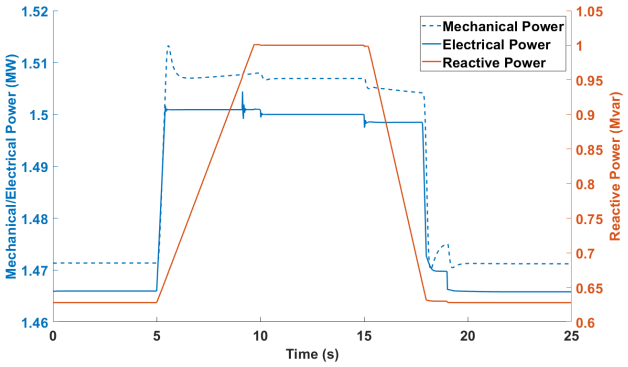

Fig. 3. Generator active and reactive powers

In the DP-mode simulation, a sudden loss of a generator is simulated by opening the circuit breaker that connects the generator to the main busbar. The inverter is then set to provide whatever power the generator that got disconnected was providing, up to its rated limit. This is again done through a UDM that monitors power of the generators and stores a delayed value, such that it can provide that value in case of a sudden loss of power.

In this simulation, both DG#01 and DG#02 are connected, and DG#02 will suddenly disconnect. Figure 4 shows both the inverter and generators active and reactive power. As soon as the generator disconnects at $t = 2$s, the inverter starts providing power. After a short spike in the power request from the unaffected generator, the generator power level goes back to the original level.

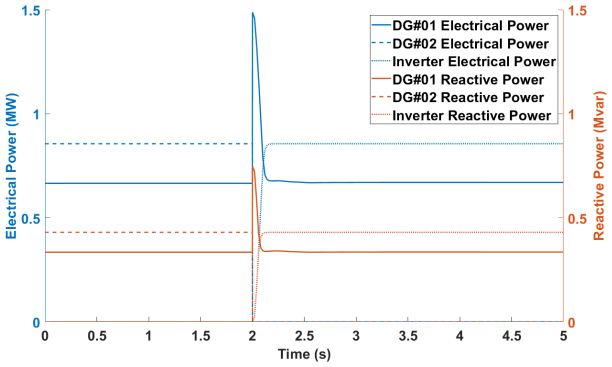

Fig. 4. Inverter and generators active and reactive power

The Critical Clearing Time (CCT) has also been analyzed using ETAP. For all generators, the applied fault is a worst-case fault where the generators are loaded at 90% and the fault is a short-line fault at only 1% cable distance. The CCT of generator DG#01 and DG#04 is 542ms. The CCT of generator DG#02 and DG#03 is 564ms and the CCT of generator DG#05 is 574ms.

B. Short-circuit calculations

Theoretical short-circuit calculations are done according to the IEC 61363 [2], the relevant standard for the maritime industry. Results for the calculated generator short-circuit currents are shown in the top of table II. The results of the simulated short-circuit currents using the IEC 61363 calculation tool in ETAP are shown in the bottom of table II.

TABLE II
CALCULATED (TOP) AND SIMULATED (BOTTOM) GENERATOR SHORT-CIRCUIT CURRENTS

	DG#01 DG#04	**DG#02 DG#03**	**DG#05**
$I_{ac}(t)$	13.759 kA	17.971 kA	12.733 kA
$I_{dc}(t)$	16.311 kA	21.076 kA	15.458 kA
$I_p(t)$	35.769 kA	46.490 kA	33.521 kA
Iac(t)	11.231 kA	14.710 kA	11.662 kA
idc(t)	16.265 kA	21.264 kA	14.867 kA
ip(t)	32.148 kA	42.067 kA	31.359 kA

All values that are used for the theoretical calculation are taken from the datasheets, just like the values for the simulation. The short-circuit currents i_p are a sum of the AC I_{ac} and DC i_{dc} components. When comparing the top and bottom values of table II, there is a distinct difference between the two. One possible explanation for this difference could be that ETAP uses open-circuit time constants in its simulation model and short-circuit time constants are used for the theoretical calculation. The datasheets of generators DG#01 and DG#02 only provide short-circuit time constants and their time constants have been converted for the simulation model. The datasheet of generator DG#05 provides both open-circuit and short-circuit time constants and its simulated short-circuit current is closer to the theoretical value compared to the other two generators. This means a conversion error could be a contributing factor to the difference seen between theoretical and simulated results, but a much larger sample size of generators is needed to prove this.

A second explanation for the difference can possibly be found in the AC part of the short-circuit calculation. Looking at the $I_{ac}(t)$ term specifically, there is the term I_{kd} which represents the steady-state short-circuit current which is generally obtained from the manufacturer. The datasheet value of this current is used in the theoretical calculation, but ETAP calculates this value based on the system impedance at the time of the fault.

Further contribution to the short-circuit current comes from the variable frequency drives and the two lumped loads in the simulation. Specific contribution from the Variable Frequency Drives is not available, but the short-circuit contribution is typically set at 150% of the nominal current. This same short-circuit contribution is also used in the simulation software. The cranes are modeled as lumped loads with a 20% static part and 80% motor part. The motor part of the lumped load will contribute to the short-circuit current. ETAP shows a contribution of 4.831kA and using the IEC 61363 with the same X/R ratio, a contribution of 4.488kA is calculated.

C. Protection & coordination

In the protection and coordination study, it is made sure that the system is able to selectively trip circuit breakers to protect its components during a fault condition. Important aspects for this study are the decrement curves of the generators and the Time Current Curves of the circuit breakers. These are acquired directly from the manufacturer.

In case of a short-circuit fault between the generator and the generator circuit breaker, it is important that the circuit breaker is opened as soon as possible to prevent damage to the generator and instability to the system as discussed in the previous section. However, it also important that only the generator circuit breaker switches off. If the breaker detects a fault, but it's somewhere else in the system, the breaker should wait for another breaker to clear the fault. If another breaker does not clear the fault within a specific time, the breaker should still open.

In practice this means that if a fault occurs between generator DG#01 and its breaker, the breaker will see a fault current in the direction of the generator. The breaker will then send a lock-signal to the other breakers that are contributing to the fault. This will start a delay where, if the fault is not cleared within this time, the breakers that received the lock-signal will open anyway. In the case where the three propulsion busbar sections are connected, if the breaker connecting the port side and the mid busbar receives a lock-signal, it will pass on the lock signal to the other active breakers that are contributing to the fault current.

ETAP's Sequence-of-Operation does not have the ability to implement lock-signals, but it does verify that all breakers detect the fault and are able to switch off quickly. Without implementing the lock signals, ETAP shows that all circuit breakers detecting the fault will open after 216ms, which is within the critical clearing time of all generators. This also shows why no instantaneous tripping is implemented, but only (directional) short- and long-time. Since the fault current will depend on the exact location and the loading of the generators, it would be very difficult to set a current threshold for all breakers for all situations. The protection systems needs a bit of time to send out lock-signals to maintain selectivity and prevent a black-out.

III. HYBRID DC GRID SIMULATION

The second system is based on a DC grid and is shown in figure 5. This system is in many ways similar to the AC grid system, but there are a couple of key differences. In this system, the main busbar is divided in only two sections. The port side and starboard side are not identical as there are only three generators that are all the same size. On the port side, there is one generator and the battery, one propulsion thruster, two smaller thrusters and the connection to the AC 400V distribution board. The port side also has the option to connect a shore connection instead of the generator, but this is not modeled.

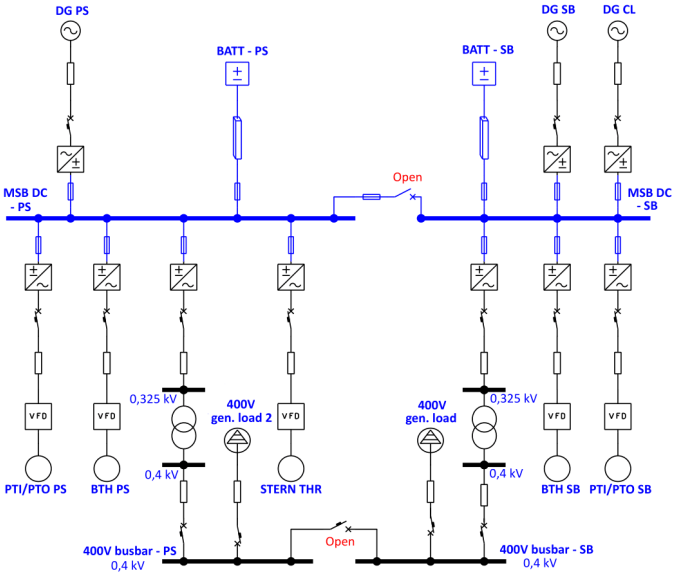

Fig. 5. Single line diagram of the studied DC grid

All three generators shown in figure 5 are identical and their parameteres are listed in table III. The converters are rated at 850A and will be able to cover the full load of the generators. The two batteries are directly connected to the busbar without any converters. The two propulsion PTI/PTO thrusters are rated at 550kW at 0.85 power factor and have an inverter rated at 1150A. The two bow thrusters and the stern thruster are all equal at 200kW at 0.85 power factor and have an inverter rated at 460A. The transformers are rated at 600kVA and have grid inverters rated at 2060A. Finally, the 400 gen. loads are modeled at 400kVA and have a 65% static and 35% motor part at 0.85 power factor.

TABLE III
SPECIFICATION OF DC GRID GENERATORS

	Generators
Rated power (kVA)	582
Rated power (kW)	465.6
Voltage (V)	400
Current (A)	840
Frequency (Hz)	50
Power factor	0.80
Poles	4
Speed (rpm)	1500
Winding resistance per phase ($m\Omega$)	3.4

A. Time domain analysis

In the transient stability study, the system is modeled in time domain, but limitations in ETAP were encountered. It is not possible to properly use the battery in time domain analysis. The integrated BMS can only charge or discharge the battery based on a bus voltage or loading. This is useful in the case of renewable resources, but not for studying peak shaving for example. A second limitation is that it is not possible to study the DC part of the grid. The two AC parts (generators and loads) are two completely separate systems and there is no power balance between the two. To 'solve' this, the generators are connected to inverters instead of charger components. This is because the inverters have the option to create a custom User-Defined Model (UDM), and the chargers do not. The model is programmed to restore the power balance and the DC part is ignored. It takes the power that is provided at the loads by the inverters and sets that as the power required for the generator. In the future, more advanced capabilities can be programmed into the UDM, to show power sharing between the generators or even 'including' the battery, but these functionalities would be difficult to showcase in ETAPs current version and thus don't add much value to this paper. ETAP can't directly showcase the parameters and variables used in the UDM.

B. Short-circuit calculation

The components that will be contributing to the short-circuit current on the DC bus are the battery and the converters. The short-circuit current that the battery will provide is given by the battery manufacturer, but how much the capacitors in the converters will contribute is not known. The IEC 61660 [3] is the standard for DC short-circuit calculations, but it dates from 1997. The standard does not provide any calculations for Lithium-Ion batteries, only for Lead-Acid batteries. The short circuit current curve of a Lithium-Ion battery is similar to that of a capacitor [4], but what if the battery is connected using a DC/DC converter? There is currently no standard that clearly describes the contribution of all modern day components and educated guesses have to be made instead.

The current from a capacitor can be calculated according to the IEC 61660. To get an idea of the peak current and time constant of a capacitor short-circuit, the formulas from the IEC 61660 are used to calculate the short-circuit current of a 2400μF capacitor with a 54.7mΩ series resistance and a 5.5μH series inductance. This graph is shown in figure 6. The peak current reached is 6.95kA in 0.134ms. For comparison, the short-circuit current of the battery is specified as 14.9kA with an L/R of 0.16ms.

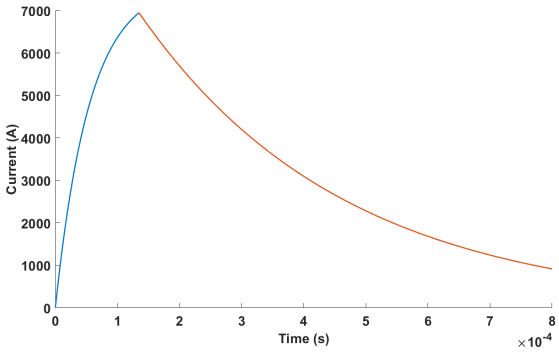

Fig. 6. Capacitor short-circuit current

Similar to the AC grid simulation section, the short-circuit current of the generators can be calculated according to the AC IEC 61363 standard. Then, the short-circuit current is also simulated using the IEC 61363 calculation tool in ETAP. The result of both is shown in table IV.

Again, there is a slight difference between the calculated and simulated values of the generator short-circuit current. All values that are used for the theoretical calculation are taken from the datasheet, just like the values for the simulation, with one exception. The datasheet did provide an open-circuit transient time constant for the simulation, but not an open-circuit subtransient time constant. This difference between the calculated and simulated value is 5.9%, which is actually one percent less than generator DG#05 from the previous section.

TABLE IV
GENERATOR SHORT-CIRCUIT CURRENT

Method	$\mathbf{I_{ac}(t)}$	$\mathbf{I_{dc}(t)}$	$\mathbf{I_p(t)}$
Calculation	7.035 kA	7.689 kA	17.638 kA
Simulation	6.648 kA	7.352 kA	16.648 kA

As mentioned before, the size of the capacitors in the converters in not known and ETAP also does not take them into account. For the charger element, ETAP considers a DC fault current of 150% of the full load current and the inverter elements have no contribution to the DC fault current at all. It is also not possible to manually add a capacitor to the DC grid as DC capacitors are not included in the current version. This means that, in ETAP, the total fault current, in case of a fault on the port side DC bus, would be the sum of the battery fault current and the 1.275kA provided by the charger element connecting the generator to the DC bus.

C. Protection & coordination

The protection and coordination study is much different for the DC bus system, compared to the AC system. The main challenge for selectivity will be on the 400V AC distribution level. For the DC busbar, it will be the challenge to find the right fuse that can sustain the full load of a converter, but also disconnect very quickly in case of a short-circuit. In this system it will be an advantage that the battery is directly connected to the DC busbar as the short-circuit level of the battery should stay close to the value from the datasheet, regardless of the state of charge. This is because the internal resistance of the battery is very low and will only significantly increase at a very low state of charge. Since the battery state of charge is predicted to approach 25% as the lowest value, this should not be an issue.

The goal of the fuses is to disconnect the fault current before the converter gets damaged. The datasheet of a fuse will provide the Total Clearing I^2t, which indicates the thermal energy through the fuse until the current is completely interrupted. Using figure 6, the I^2t of the short-circuit current and the time at which the I^2t of the fuse is reached can be calculated.

If figure 6 is paired with a Eaton Bussmann 170M1790 with an I^2t of 9350, the I^2t of the short-circuit current is equal to that of the fuse at t=0.351ms. The I^2t over time is shown in figure 7 and the I^2t value of the fuse should always intercept this curve, otherwise it will not clear the fault.

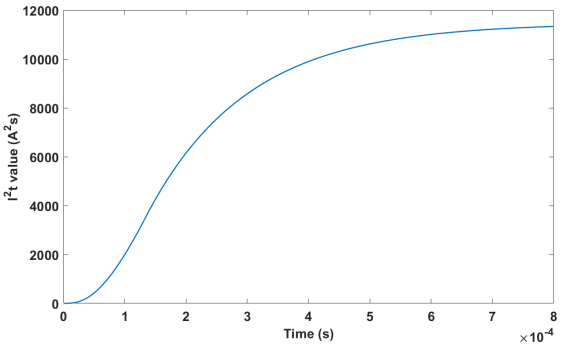

Fig. 7. Short-circuit current I^2t curve over time

IV. CONCLUSION

This paper presents two simulation models in ETAP based on actual vessels that can be adapted for the engineering of future hybrid vessels. For the AC grid simulation, a time domain analysis, short-circuit calculations and a protection & coordination basis have been presented and differences between simulated and calculated results are discussed. For the DC grid simulation, some software limitations were encountered such as missing components and features. Nonetheless, short-circuit calculations and simulations have been presented where possible and a protection strategy based on I^2t has been discussed.

REFERENCES

[1] Global Maritime Forum. *Getting to Zero Coalition*. 2019. URL: https://www.globalmaritimeforum.org/getting-to-zero-coalition (visited on 08/18/2023).

[2] "Electrical installations of ships and mobile and fixed offshore units - Part 1: Procedures for calculating short-circuit currents in three-phase a.c." In: *IEC Std 61363-1:1998* (1998), pp. 1–81.

[3] "Short-circuit currents in d.c. auxiliary installations in power plants and substations Part 1: Calculation of short-circuit currents". In: *IEC Std 61660-1:1997* (1997), pp. 1–84.

[4] Sim Sang-Bo. "Study on the explosion and fire risks of lithium batteries due to high temperature and short circuit current". In: *Fire Science and engineering* 30.2 (2016), pp. 114–122.